

University of Latvia  
Faculty of Physics and Mathematics  
Institute for Mechanics of Materials

**Sergejs Vidinejevs**

**DEVELOPMENT AND CHARACTERISATION OF  
POLYMER COMPOSITE  
MATERIALS WITH BIO-INSPIRED FUNCTIONS**

Doctoral Thesis

Submitted for the degree of Doctor of Physics  
Subfield of Physics of Materials

Riga, 2018

The doctoral thesis was carried out:  
at the Institute for Mechanics of Materials, University of Latvia,  
from 2009 to 2017.

The thesis contains the introduction, 3 chapters, reference list.  
Form of the thesis: dissertation in the field of Physics,  
subfield of Physics of Materials

Supervisor: Dr. Sc. Ing. Andrey Aniskevich, leading researcher, LU MMI

Reviewers:

- 1) Dr. Sc. Ing. Andrejs Krasņikovs, Professor, RTU;
- 2) Dr. Andres Krumme, Professor, Tallinn University of Technology;
- 3) Dr. Phys. Anatolijs Šarakovskis, leading researcher, LU ISSP.

The thesis will be defended at the public session of the Doctoral Committee, University of Latvia, at 12:00 on May 22, 2018 LU PMF Zeļļu iela 25.

The thesis is available at the Library of the University of Latvia, Kalpaka blvd. 4.

This thesis is accepted for the commencement of the degree of Doctor of Physics on February 12, 2018 by the Doctoral Committee of of Physics and Astronomy, University of Latvia.

Chairman of the Doctoral Committee \_\_\_\_\_ / Dr. Phys. Andris Jakovičs

Secretary of the Doctoral Committee \_\_\_\_\_ / Laureta Buševica

## ANOTĀCIJA

Sergeja Vidinejeva promocijas darbs ir izstrādāts disertācijas veidā fizikas nozarē materiālu fizikas apakšnozarē. Promocijas darbs tika veikts Latvijas Universitātes Materiālu mehānikas institūtā. Darba zinātniskais vadītājs ir Dr. sc. ing., vadošais pētnieks Andrejs Aņiskevičs.

Darbs saistīts ar aktuālu un jaunu pētījumu virzienu: bioinspirēto funkciju tālāku attīstīšanu slodzi nesošos kompozītos. Tās ir mehānisku triecienu vizuālās indikācijas un polimēru matricas vaskulārās pašdziedināšanas funkcijas.

Pētījuma laikā pirmo reizi tika izveidots t.s. viedais slānis ar iekapsulētu divkomponentu ķīmisko sastāvu, kas efektīvi vizualizē mehāniska trieciena vietu "ziluma" formā. Šis slānis kopā ar epoksīda pārklājumu – jutības regulatoru, ir iestrādāts kompozītā, izmantojot vakuuma formēšanas metodi. Ir radīta oriģināla digitālo attēlu analīzes metode, lai noteiktu vizuālo reakciju uz pseidotriecienu – iespaidumu. Vizuālās reakcijas sliekšņa slodzes noteikšanai tiek modelēts sprieguma sadalījums pārklājumā. Vizuālās indikācijas ātra aktivizācija un jutības atbilstība tam pseidotrieciena lielumam, kas ir bīstams epoksīda saistvielai, liecina par bioinspirētās funkcijas efektivitāti.

Jaunā tipa viedie slāņi matricas bojājumu vaskulārajai pašdziedināšanai (bojājumu apjomiem lielākiem par  $100 \text{ mm}^3$ ) tika izgatavoti izmantojot dobus kanālus un oglekļa šķiedru plastmasas mikrocaurules. Slāņi tika iestrādāti kompozītā, izmantojot vakuuma formēšanas metodes un divu vai vienkomentu dziedinošo aģentu ķīmiskos sastāvus. Tika piemeklētas dažādas eksperimentu un pārbažu secības (kompozītu saistvielu bojāšana, mehānisko īpašību pārbaudīšana utt.), lai novērtētu funkciju efektivitāti. Augsta dziedināšanas efektivitāte (līdz 52 %) liecināja par bojāto kompozītu mehānisko īpašību ievērojamu atgūšanu.

Veiktais pētījums palīdzēs projektēt slodzi nesošus kompozītus ar pagarinātu mūžu, izmantojot: a) indikācijas slāni ar iepriekš noteiktu jutību vai slāņa pielāgošanu gatavajiem izstrādājumiem, lai agrīni atklātu triecienu, kas izraisa bojājumu; b) vaskulārās pašdziedināšanas funkciju, kas spēj atjaunot saistvielu un atjaunot tā mehāniskās īpašības; c) iebūvētus viedus slāņus, kas pārāk nesamazinātu kompozīta stinguma un izturības īpašības; d) vairākas bioinspirētas funkcijas, lai iegūtu viedas struktūras.

Promocijas darba rezultāti ir publicēti piecos recenzētos rakstos zinātniskajos žurnālos, kas tiek indeksēti Scopus tīmekļa vietnē, kā arī ir ziņoti divpadsmit starptautiskās konferencēs un iekļauti vienā patenta pieteikumā.

**Atslēgvārdi:** vizuālā indikācija, kompozīti ar "zilumiem", pašdziedināšana, mikrocaurules, digitālo attēlu analīze, mehāniskās pārbaudes.

## ANNOTATION

The doctoral thesis of Sergejs Vidinejevs is in the form of dissertation in the field of Physics, subfield of Physics of Materials. The study was conducted at the Institute for Mechanics of Materials, University of Latvia under the supervision of A. Aniskevich, Dr. Sc. Ing., leading researcher.

The work relates to topical and novel direction of research: development of additional bio-inspired functions for the load-bearing composites, such as visual indication of mechanical impacts and polymer matrix vascular self-healing.

For the first time, effective visual indication in a form of "bruise" became available by developing smart layer on the base of encapsulated two-component chemistry in the research. The layer was built into the composites using the vacuum moulding method together with the epoxy coating to adjust the sensitivity. The original method of digital image analysis was developed to identify quantitatively the visual response after pseudo-impact indentation. The model of the stress distribution in the coating was designed to determine a threshold load of this visual response. A proof of function efficiency was a capability of indication to be activated within seconds and a sensitivity correspondence to the values of pseudo-impacts endangering the epoxy binder.

New types of smart layers were created for vascular self-healing of composite binder damages with volume of more than 100 mm<sup>3</sup>. The layers were fabricated on the base of either hollow channels or carbon reinforced plastics micro-tubes. Such layers were built into composites using vacuum moulding methods. Two- or one-part chemistry was used as healing agents. The sequences of tests (damages of the binder of composites, testing of mechanical characteristics etc.) were found to evaluate the efficiency of the functions. The high healing efficiency (up to 52 %) was evaluated as an assurance for appreciable recovery of the mechanical properties of damaged composites.

Performed study will help to design load-bearing and life-time-expanded composites using: a) indication layer with predetermined sensitivity including adaptation of the layer to the finished products for early detection of damages caused by impacts; b) vascular self-healing function that is capable to restore the binder and recover its mechanical properties; c) built-in smart layers, which would not lead to a significant reduction in composite stiffness and strength characteristics; d) multiple bio-inspired functions to get smart structures.

The results of the thesis were published in five peer-reviewed scientific papers in journals indexed by Scopus and one patent application as well as presented at twelve international conferences.

**Keywords:** visual indication, bruisable composites, self-healing, micro-tubes, digital image analysis, mechanical testing.

## **ABBREVIATION**

BVID – barely visible impact damage  
CFRP – carbon-fibre-reinforced polymer/plastic  
CNT – carbon nanotube  
CVL – crystal violet lactone  
DCB – double-cantilever beam  
FRP – fibre-reinforced polymer/plastic  
HA – healing agent  
HE – healing efficiency  
NDT/I – non-destructive testing/inspection  
PMF – poly (melamine-formaldehyde)  
RGB – red-blue-green (primary colours)  
SH – self-healing  
SHM – structural health monitoring  
TDCB – tapered double-cantilever beam  
UV – ultraviolet  
VARTM – vacuum assisted resin transfer moulding

## LIST OF FIGURES

Fig. 1.1. Sketches illustrate BVID in laminated composites .....	17
Fig. 1.2. Reliability improvement of engineered materials by implementation of self-healing principle [14].....	19
Fig. 1.3. The bio-inspired concepts for improving reliability of FRP composites .....	20
Fig. 2.1. UV/visible transmission spectra of the elastomeric opal film at different strains [66].....	25
Fig. 2.2. Coloured crack sign appeared from broken microencapsulated dye particle [91] .....	27
Fig. 2.3. Schematic cross-section of the synthesized microcapsules with main constituents and shell formation scheme [75].....	27
Fig. 2.4. The concept of fluorescence microcrack probing [72].....	28
Fig. 2.5. Schematic of autonomous damage indication concept: upon mechanical damage, the microcapsules rupture and the released core materials react with the coating to change locally colour [73].....	29
Fig. 2.6. Transformation between uncoloured and coloured form of CVL dye – halochromism.....	30
Fig. 2.7. Prototypes of bruisable coatings offered by several companies.....	31
Fig. 2.8. Dispersion of an organic liquid in continuous water phase in a form of emulsion, droplets forming core material, and final core-shell microcapsule.....	34
Fig. 2.9. Scanning electron microscope images: CVL microcapsules with average diameter of ca. 10 – 15 $\mu\text{m}$ .....	34
Fig. 2.10. SEM photo of fabric fibres with Microcapsules 500 black copy and Colour developer particles of the developer .....	35
Fig. 2.11. Components of the indication layer preform: nylon fabric fibres (1), microcapsules of a leuco dye (2), particles of a developer (3), and a binder — epoxy-modified polyurethane-acrylate (4).....	36
Fig. 2.12. A ‘bruise’ in the preform of the indication layer.....	36
Fig. 2.13. Composite manufacture process: impregnation of the indication layer preform with an epoxy binder (a); lay-up of the unidirectional glass yarns (b); vacuum bagging moulding process (c); a plane composite specimen with the function of indication of impact (d).....	37
Fig. 2.14. The side view of composite with the indication layer and epoxy layer of varied thickness more than 1 mm against the background of the ruler .....	38
Fig. 2.15. A specimen of the load-bearing composite with indication layer and thin epoxy coating after indentation .....	38
Fig. 2.16. A safety helmet with indication layer strips glued on .....	39

Fig. 2.17. Scheme of indentation loading of the FRP composite with a built-in indication layer: the transparent epoxy layer (1), visual indication layer (2), load-bearing layers of the composite (3), and visual response (4); maximum normal pressure $p_0$ , and radius $a$ of the contact zone.....	40
Fig. 2.18. The two types of the palettes (bottom): $B_{ij}$ rises due to illuminance and $\beta_{ij}$ is constant (left column); $B_{ij}$ rises at constant illuminance and $\beta_{ij}$ is rising too (right column).....	42
Fig. 2.19. An example of digital image analysis of the bruise spots images in three indication coatings .....	43
Fig. 2.20. The typical relation $B$ vs. $P$ ; the arrows connect experimental points with the corresponding painted maps of the $\beta_{ij}$ and bruise images .....	44
Fig. 2.21. Experimental points of relation $z$ vs. $P^*$ and solid line of analytical approximation (2.9).....	45
Fig. 3.1. Self-healing approaches: intrinsic (a), capsule-based (b), and vascular (c) [40].....	50
Fig. 3.2. Performance map for self-healing approaches [40].....	53
Fig. 3.3. TDCB specimen [159] (all dimensions in mm).....	57
Fig. 3.4. The scheme of tensile loading and the main dimensions of the sample for interlaminar shear testing ( $F$ is the area of the shear zone) [171].....	59
Fig. 3.5. Epoxy TDCB specimen with a crack and transmitted light microscopy images made in several places along the crack .....	61
Fig. 3.6. Epoxy TDCB specimen with a crack filled by green dyed alcohol.....	62
Fig. 3.7. Crack injected alcohol mass $m$ vs. time $t$ for a TDCB specimen .....	62
Fig. 3.8. Representative load $P$ vs. displacement $h$ curves of a TDCB specimen manually healed using ethyl cyanoacrylate glue .....	63
Fig. 3.9. Representative load $P$ vs. displacement $h$ curves of a TDCB specimen manually healed using resin and hardener stoichiometric mixture.....	64
Fig. 3.10. TDCB specimen with 5 channels filled with two-part HA system .....	65
Fig. 3.11. TDCB specimen after self-healing: the channels in the upper part A are empty since the HA flowed out into the cracked region while the cannels in zone B remain filled .....	66
Fig. 3.12. Representative load vs. displacement curves of the virgin (dotted line), once healed (solid line), twice healed (dashed line) TDCB specimen.....	66
Fig. 3.13. Views of manual stacking of a plate preform with PTFE tubes (left) and VARTM process of plate manufacture (right).....	68
Fig. 3.14. Multiple damages in the specimens by three-point flexure loading with a short span .....	70
Fig. 3.15. A CFRP micro-tube embedded into GFRP releases liquid dye after indentation .....	73
Fig. 3.16. The scheme of specimen for shear test with the CFRP micro-tube layer transversely positioned in the middle zone between notches .....	75
Fig. 3.17. A flowchart of the experimental study of laminated composite.....	75

Fig. 3.18. The scheme of damage of the specimens with self-healing vascular channels .....	77
Fig. 3.19. Tensile tests of specimen with two notches.....	78
Fig. 3.20. Deformation diagrams of the virgin V-specimens .....	79
Fig. 3.21. Shear fracture of the virgin V-specimens: the crack deflects around the micro-tubes .....	80
Fig. 3.22. Shear fracture of the damaged D-specimens: the crack propagates through the micro-tubes .....	80
Fig. 3.23. Typical deformation diagrams of the virgin (V), damaged (D), manually healed (MH), self-healed with two-part HA (AH), and healed under pressure (PH) specimens.....	81
Fig. 3.24. Comparison of the interlaminar shear strength of virgin (V), damaged (D), manually healed (MH), self-healed with two-part HA (AH), and healed under pressure (PH) specimens (error bars reflect one standard deviation of data).....	82

## LIST OF TABLES

Table 3.1. Vascular self-healing of fibre-reinforced polymer composites and HE values $\eta$ achieved (also, the data of this research are included).....	55
Table 3.2. Experimental data of TDCB specimens.....	67
Table 3.3. Stages of sequence of experiments .....	69
Table 3.4. Elastic modulus and healing efficiency of flat specimens determined in static (numerators) and dynamic (denominators) flexural tests .....	70
Table 3.5. Physical and mechanical properties of DPP <sup>TM</sup> high performance micro-tubes [178].....	74

## TABLE OF CONTENTS

ANOTĂCIJA .....	3
ANNOTATION .....	4
ABBREVIATION.....	5
LIST OF FIGURES .....	6
LIST OF TABLES .....	9
TABLE OF CONTENTS.....	10
INTRODUCTION .....	11
Topicality and novelty of the research.....	11
Aim and tasks.....	12
Proposed theses.....	12
Methodology.....	13
Approbation of results.....	13
1. Bio-Inspired Concepts for Improving Reliability .....	16
2. Visual Indication of Mechanical Impact .....	22
2.1. Current Trends.....	22
2.1.1. Indicating, sensing, and probing layers or coatings for visual inspection of bulk material .....	22
2.1.2. Visual indication using microencapsulated dye.....	26
2.1.3. Impact-sensitive coatings for FRP composites.....	30
2.2. Function of Visual Indication of Mechanical Impact in Composites.....	33
2.2.1. Preparation of indication layer.....	33
2.2.2. Embedment of indication layer into FRP composites.....	37
2.2.3. Mechanical testing, visual response quantification, and stress modelling.....	39
2.2.4. Visual indication efficiency .....	47
2.3. Conclusions of the Section .....	47
3. Vascular Self-Healing .....	49
3.1. Current Trends.....	49
3.1.1. Self-healing approaches for low-sized damages in thermoset polymers and composites.....	49
3.1.2. Vascular approach for self-healing polymers and FRP .....	54
3.1.3. Healing efficiency evaluation and mechanical tests of self-healing materials.....	56
3.2. Function of Autonomous Self-Healing.....	60
3.2.1. Self-healing of epoxy binder: preparation and experimental verification .....	60
3.2.2. Self-healing of FRP composite: development and experimental verification .....	67
3.3. Function of Self-Healing under Pressure.....	72
3.3.1. Preparation of carbon FRP micro-tube layer .....	73
3.3.2. Experimental determination of self-healing efficiency.....	78
3.4. Conclusions of the Section .....	83
GENERAL CONCLUSIONS.....	85
REFERENCES .....	86
ACKNOWLEDGEMENTS.....	98

# INTRODUCTION

## Topicality and novelty of the research

The advancement of fibre reinforced polymer (FRP) composites and structures is restrained by dependence of their performance on sudden and adverse external mechanical influences. Often foreign object impacts do not show themselves on the surface, but lead to damages and complications inside the material. Promptly undetected residual damage can lead to a failure with catastrophic consequences. Non-destructive testing/inspection (NDT/I) methods that were traditionally used for damage detection and failure prevention are complex and expensive. Continuous structural health monitoring is an alternative to periodic testing. In this case, the monitoring is implemented by micro sensors or optical fibres placed into the composite [1]. This additional element installation is often technologically complicated task [2], which affects the integrity of the structure and can shorten the product life cycle thereby. Forced dismantling of damaged structural members for repair or replacement is costly too.

Therefore, finding new alternative techniques for reliability improvement of FRP composites is an important challenge. Creation of smart materials with inherent bio-inspired functions is attributed to them. Smart materials can change their physical properties in a unique way, responding to the selected specific stimulus in a controlled and predetermined manner [3]. This ability can be exhibited in the presence of some additional functions for the load-bearing composite.

The human body gives two examples for inspiration. The bruise on the skin informs about impact and possible injury of inner tissues. This response helps to timely limit the consequences of the impact on health. The substances delivered through the blood and lymphatic vasculatures provide post-injury self-healing of tissues in the wound.

In a comparable way, the inanimate composites with similar functions will improve reliability due to their ability to recover mechanical properties timely after the impact. However, such reinforced composites with bio-inspired functions have not gone beyond the laboratory and become commercial yet. Owing to that, the methods of implementation the function of visual indication of mechanical impact and self-healing function in composites are important and topical.

The main scientific novelties of the work presented are:

1. For the first time (European patent application was published), an effective indication layer with controllable sensitivity to impart FRP composites visual indication function of impacts in a form of "bruise" was implemented. The indication layer can be integrated within the composite at the manufacturing stage or adhered to the finished products.

2. A digital image analysis method was developed to quantify the visual response in the indication coatings and layers of different compositions and designs, by using the local intensity of dominant colour.
3. The analytical approach of the contact mechanics of elastic bodies was used to determine the stress in the indication layer at the threshold load. Impacts that can damage the binder confirmed the efficiency of the developed visual indication.
4. New methods of the creation of self-healing layers with vascular systems were developed for FRP composites. These methods use removable flexible tubes as moulds for hollow channels embedment or industrial carbon FRP micro-tubes as vessels for healing agent (HA). Two-part or one-part chemistry of HA was proposed for these types of layers and high healing efficiency of the layers was confirmed experimentally.

### **Aim and tasks**

**The aim of the research** is to improve the reliability of load-bearing FRP composites by providing them with the additional bio-inspired functions of visual indication of impacts and polymer matrix vascular self-healing.

For this purpose, the following tasks have been formulated:

- Preparation of layers for the effective visual indication of impacts and vascular self-healing of binder damages;
- Development of embedment methods of these layers into the load-bearing epoxy FRP composites;
- Finding of appropriate sequences of tests, developing quantification methods and a mechanical model for evaluation of the efficiency of additional functions in the composites;
- Evaluation of the efficiency of additional functions of the composites.

### **Proposed theses**

1. Smart layers increase the reliability of FRP composites by means of early detection and timely healing of mechanical damages.
2. The smart layers built into the composite do not lead to a significant reduction in composite load-bearing capacity.
3. Active components of the indication layer are shielded from alkali chemistry of the epoxy binder by protective polymeric coating.
4. Impact sensitivity of the indication layer is adjusted by a transparent coating of different stiffness and thickness.
5. The vascular system self-heals damages with large voids.

## Methodology

The doctoral thesis is based on results of interdisciplinary research involving the use of material science, polymer and composite mechanics, physics, optics, and chemical methods, which can be combined in the following groups:

- Methods of manufacture of polymers and composites, including composites with functional features;
- Experimental methods for simulation of damage to composite materials;
- Experimental methods for determination of fracture toughness of polymers, elastic and strength properties of composites;
- Analytical modelling of a stress state;
- Methods for digital processing and analysis of coloured images.

## Approbation of results

The summarised information in Scopus Author Identifier (ID: 55313602200) on 12.09.2017: Documents – 7; Citations – 16 total citations by 13 documents; *h*-index – 2; Co-authors – 8.

### Scientific papers

1. S. Vidinejevs and A. Aniskevich, "The system of carbon fibre-reinforced plastics micro-tubes for self-healing of glass fibre-reinforced plastics laminates," *Journal of Composite Materials*, Vol. 51, no. 12, pp. 1717-1727, 2017.
2. O. Bulderberga, A. Aniskevich, and S. Vidinejevs, "A Glass-Fiber-Reinforced Composite with a Damage Indication Function," *Mechanics of Composite Materials*, Vol. 52, no. 2, pp. 155-162, 2016.
3. A. Aniskevich, S. Vidinejevs, V. Kulakov, and O. Strekalova, "Development of Composites with a Self-Healing Function," *Materials Science (Medžiagotyra)*, Vol. 21, no. 1, pp. 32-37, 2015.
4. S. Vidinejevs, O. Strekalova, A. Aniskevich, and S. Gaidukov, "Development of a composite with an inherent function of visualization of a mechanical action," *Mechanics of Composite Materials*, Vol. 49, no. 1, pp. 77-84, 2013.
5. S. Vidinejevs, A. N. Aniskevich, A. Gregor, M. Sjöberg, and G. Alvarez, "Smart polymeric coatings for damage visualization in substrate materials," *Journal of Intelligent Material Systems and Structures*, Vol. 23, no. 12, pp. 1371-1377, 2012.

### International conference proceedings

(speaker is underlined)

1. O. Strekalova, A. Aniskevich, and S. Vidinejevs. "GFRP composite with damage indicating layer". *Baltic Polymer Symposium 2014*, September 24–26, 2014, Laulasmaa, Estonia, *Proceedings of the Estonian Academy of Sciences*, 64 (1 S), pp. 79, 2015.

2. S. Vidinejevs and A. Aniskevich. "Self-healing of GFR/ epoxy composite with binary vascular system". *Proceedings of the Fourth International Conference on Self-Healing Materials—ICSHM2013*, Ghent, Belgium, June 16–20, 2013, pp. 264-267, 2013, ISBN: 9789082073713.
3. O. Strekalova, S. Vidinejevs, and A. Aniskevich. "Polymer composite layer with damage indication ability". *Proceedings of the Fourth International Conference on Self-Healing Materials—ICSHM2013*, Ghent, Belgium, June 16–20, 2013, pp. 713-716, 2013, ISBN: 9789082073713.

Presentations in international conferences

1. O. Bulderberga, A. Aniskevich, and S. Vidinejevs. "GFRP Composite with Damage Visualization Capability". *ECCM17-17th European Conference on Composite Materials*, 26-30th June, 2016, Munich, Germany, Excerpt from ISBN 978-3-00-053387-7, PO-6-06.
2. S. Vidinejevs and A. Aniskevich. "CFRP vessels for self-healing of laminated GFRP". *EuroNanoForum 2015*, June 10–12, 2015, Riga, Latvia, Excerpt from <http://euronanoforum2015.eu/poster-sessions/> (accessed 06.01.2017), 1B-62.
3. A. Aniskevich, O. Bulderberga, and S. Vidinejevs. "Polymer composites with ability of visual damage indication". *EuroNanoForum 2015*, June 10–12, 2015, Riga, Latvia, Excerpt from <http://euronanoforum2015.eu/poster-sessions/> (accessed 06.01.2017), 1B-61.
4. O. Bulderberga, A. Aniskevich, and S. Vidinejevs. "Visual indication of mechanical damages in polymer composites". *Open Readings 2015*, March 24–27, 2015, Vilnius, Lithuania, Book of abstracts, p. 155.
5. S. Vidinejevs and A. Aniskevich. "Shear strength recovery of GFRP laminate using carbon-fibre tubes as self-healing vasculature". *XVIII International Conference on Mechanics of Composite Material*, June 2–6, 2014, Riga, Latvia, Book of abstracts, p. 190.
6. O. Strekalova, S. Vidinejevs, and A. Aniskevich. "GFRP composite with integrated damage indication layer". *XVIII International Conference on Mechanics of Composite Material*, June 2–6, 2014, Riga, Latvia, Book of abstracts, p. 177.
7. O. Strekalova, S. Vidinejevs, and A. Aniskevich. "Self-monitoring fibre reinforced composites: visual response to the external indentation". *XVII International Conference on Mechanics of Composite Material*, May 28–June 1, 2012, Riga, Latvia, Book of abstracts, p. 208.
8. O. Strekalova, S. Vidinejevs, and A. Aniskevich. "Critical loading visualization capability in glass fibre reinforced epoxy composite". *Baltic Polymer Symposium 2011*, September 21–24, 2011, Pärnu, Estonia, Book of abstracts, p. 95.

9. S. Vidinejevs, O. Strekalova, and A. Aniskevich. "Biomimetic fibre reinforced composite with damage visualization capability". *Third International Conference Self-Healing Materials*, June 27–29, 2011 Bath, United Kingdom, Book of abstracts, p. 153.
10. S. Vidinejevs and A. Aniskevich. "Binary vascular system in self-healing epoxy matrix". *Third International Conference on Self-Healing Materials*, June 27–29, 2011 Bath, United Kingdom, Book of abstracts, p. 139.
11. S. Vidinejevs, A. Aniskevich, A. Gregor, M. Sjöberg, and A. Picot. "Manual healing and damage sensitive coatings towards bio-inspired solutions in epoxy based composites using microcapsules approach". in *DURACOSYS 2010, Patras, Greece, September 12–15, 2010*, CD of Book of abstracts, p.70.
12. A. Gregor, A. Aniskevich, M. Sjöberg, A. Picot, and S. Vidineev. "Self- healing and damage indicating composites using microcapsules approach". *European Conference on Composite Materials, ECCM 14*, June 7–10, 2010, Budapest, Hungary, CD, No. 725.
13. S. Vidinejevs, A. Aniskevich, A. Gregor, and J. Kers. "Manual healing of cracks in epoxy matrix". *XVI International Conference Mechanics of Composite Materials*, May 24–28, 2010, Riga, Latvia, Book of abstracts, p. 204.

#### Patent application

1. S. Vidinejevs, A. Aniskevics, and O. Strekalova. "Method of making an impact-indicating coating on a surface of an article made of composite materials" (EP 2 537 666 A1, 26.12.2012).

#### Scientific projects

1. "Development of nano-modified polyolefin multilayer extrusion products with enhanced operational properties", European Regional Development Fund project No. 1.1.1./16/A/141 LU reg. No. ESS2017/202.
2. "Multifunctional materials and composites, photonics and nanotechnology IMIS2", NRP, 2014-2017.
3. "Support for international cooperation projects in the polymer composite physical-mechanical research", European Regional Development Fund project No. 2010/0201/2DP/2.1.1.2.0/10/APIA/VIAA/005, 2012-2013.
4. "New mounting system from pultruded composite materials: the development and application in structural parts with high load-bearing capacity", European Regional Development Fund Project No. 2010/0296/2DP/2.1.1.1.0/10/APIA/VIAA/049, 2010–2013.
5. "Involvement of human resources to complex investigation of modern composite materials". European Social Fund Project No. 2009/0209/1DP/1.1.1.2.0/09/APIA/VIAA/114, 2009–2012.

# 1. Bio-Inspired Concepts for Improving Reliability

A rapid uptake of composite materials is being observed in high-performing industries. The high strength- and modulus-to-weight ratios in the reinforcement direction as well as corrosion resistance are key factors of this uptake. An important factor is the possible performance period expansion against traditional metal materials especially in view of cost savings. Nevertheless, lack of damage tolerance of the traditional composites is a restraining factor in the trend of substitution for metals in different applications due to the inherent anisotropy and low transversally-shear strength of composites. For example, epoxy resins are often used as a matrix of the fibre-reinforced plastics (FRP) composites to achieve high structural strength and stiffness of the lightweight structures. However, epoxy-based composites are brittle and unable to deform plastically. Sudden and adverse external mechanical influences such as impacts of foreign objects often result in energy absorption via creation of defects and damages. The damage often manifests itself internally within the material as matrix cracks and delaminating of a variety of sizes and complexities and do not manifest themselves on the surface thus can be difficult to detect visually [4] (e.g. barely visible impact damage – BVID) [5] (Fig. 1.1). Not promptly detected and eliminated residual damage can lead to both performance period reduction and a failure with catastrophic consequences. The essence of the problem is vividly transmitted in the following quotation from [1]: „Aircraft maintenance crews use the BVID criterion: if you can't see any damage under typical lighting conditions from a distance of five feet, the structure is still good to fly. Fine for metal structures, but not for composites”. Accordingly, the health monitoring of structures made of composite materials is more important than in the case of the traditional metal structures [6].

Constructions made from composite materials have the most advanced safe design and maintenance in the aircraft industry because of the high cost and catastrophic consequences of a possible failure. The concept of the limits of acceptable damage or concept of damage tolerance is a basis, which consists in the design of composite structures with a high margin of safety and requiring periodic inspection of products operated. Practically, the limits of acceptable damage establish the sizes of potential damage, which reduces the structure residual strength from ultimate load level to maximum allowed limit load if any damage is discovered and repaired in scheduled maintenance. The damage beyond these sizes that occurs in flight is immediately obvious to the flight crew but residual strength is sufficient for safe flight continuation [7-11]. If the carbon fibre, for example, may lose up to 50 % of its initial compressive strength as a result of impact damage such energy when the dent on the surface is not yet appeared, the structure thereof must be designed under the assumption that the fault in the material may already exist. The increased weight is a payment for it [12, 13]. In the damage tolerance strategy, the over-designing approach (leads to higher cost and weight) is a traditional

tendency to implement safety requirements, mitigate probability of costly forced dismounting of damaged structural elements for repair or replacement, and get improved reliability.

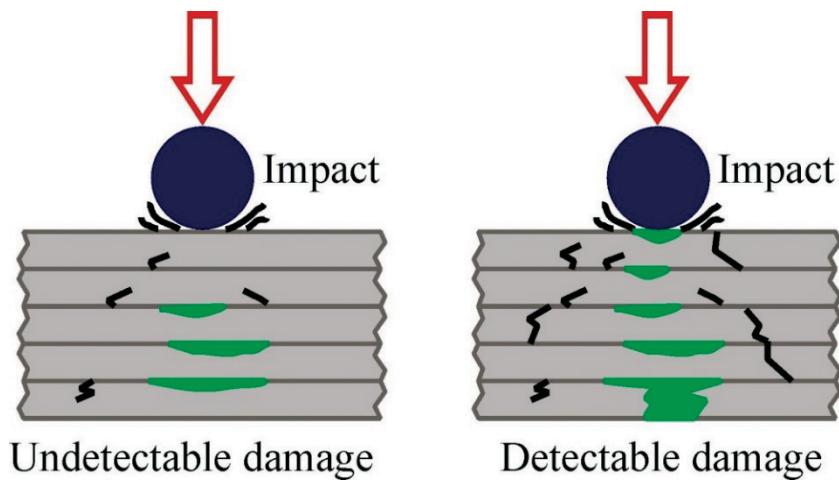


Fig. 1.1. Sketches illustrate BVID in laminated composites

In the case of other polymer composite structures, the same conservative way is traditional in the design with a high margin of safety accompanied with higher cost and weight. In addition in the traditional damage tolerance strategy, another approach is the designing of more impact-damage resistant and better materials with enhanced performance than the original ones. This performance is achieved by modifying the polymer architecture itself (e.g. crosslinking density, aromatic chains, crystallinity) or by introducing external agents such as exfoliated clays or graphene plates [14]. Unfortunately, the strategy of improving the initial properties leads to small developments in the performance and, as a result, to only a small extension in the service life due to the big advances achieved so far.

The maintenance works of the structures designed in damage tolerance strategy are important aspect in providing reliability of them. The works consist in periodical non-destructive testing/ inspection (NDT/I) which includes visual inspection; optical methods; eddy-current (electro-magnetic testing); ultrasonic inspection; laser ultrasonics; acoustic emission; vibration analysis; radiography; thermography, and Lamb waves [15]. This number is supplemented by relatively new methods for monitoring carbon fibre reinforced plastic (CFRP) and polymer/carbon nanotube (CNT) composites via electrical resistance and potential change [16, 17], ohmic heating and thermographic imaging of the response [18]. The problem with these techniques is that they often require removal or detachment of the component from the structure to be evaluated. Additional problems are the prolonged inspection of large structures using scanning methods and expensive response analysis using spectral methods apparatus. All these tests need qualified staff. The economic aspect of the matter is indicative in load-bearing aircraft structures. The

cost of inspection is approximately one-third of acquiring and operating composite structures [15].

One approach unlike the aforementioned conservative way is to produce multifunctional engineering material. Multifunctionality can be defined here as imparting the ability for the material to perform some useful secondary function as well as achieving the primary, usually structural, requirement [19]. The example of such secondary function is ability of continuous (in situ and in real time) structural health monitoring (SHM). Almost all of these techniques follow the same general procedure: the structure is excited using actuators, and the dynamical response is sensed at different locations throughout the structure. Any damage will change this vibrational response [20]. The state of the structure is diagnosed by means of the processing of these data. The additional element installations/embedment (actuators, microsensors, optical fibre, etc.) into composites are often technologically complicated tasks that affect the integrity and thereby can influence the member life cycle. To compete with or supplement SHM in the increasingly demanding area of polymer composite structures, noninstrumental inspection techniques based on visual indication of impact damage could be developed. The impact visual indication function on a level with other efficient methods for the rapid and regular, ideally, – continuous inspection of composite products can objectively help to reduce both the requirements for resistance to accidental impact and the necessary safety margin. Additionally, the material will provide lower maintenance costs both in terms of inspection and repair [21-23].

Another advanced approach is to produce multifunctional engineering material with self-healing (-repair) mechanisms. Self-healing (SH) concepts offer an alternative strategy based on damage management rather than damage tolerance [14]. Composites with SH function recover residual strength level after moments of real damage up to acceptable level. In the ideal SH case, the composites enable continued operability without reduction in performance and prevent further degradation to catastrophic failure (e.g. in the case of an aircraft). Thus, if strength is maintained sufficiently less material can be used as per durability and damage tolerance, yielding a lighter structure [24]. This new approach already led to very significant results despite the young age of the field. The relation between performance (e.g. residual strength) and service lifetime is depicted in Fig. 1.2 [14]. The compared curves demonstrate the advantages in lifetime extension of advanced approaches (including ideal SH with multiple healing events) against traditional approaches.

The above-mentioned multifunctional material could be defined as a smart structure. A smart structure is that assembly, which has the ability to respond adaptively in a pre-designed useful and efficient manner to changes in environmental conditions, including any changes in its own condition [25]. Biological structures or systems are the smartest and most economical in terms of energy consumption. They serve for bio-

inspiration and mimicking design of the smartest artificial structures. Biological structures have several characteristics: sensing; actuation; adaptability; self-repair; self-replication or reproduction, etc. At last, they have the ability of diverse and in a controlled manner to respond to external stimuli. Several latest publications and reviews [26-29] allow to make representation about advanced bio-inspired solutions in different fields of coatings, solid materials, and structures. An example of successfully developed approach is continuously SHM system using embedded sensor networks reacting to stress, deformation, and the structural integrity of load-bearing structures. Such system copies principles of functioning of the nervous system and the animal receptors [30].

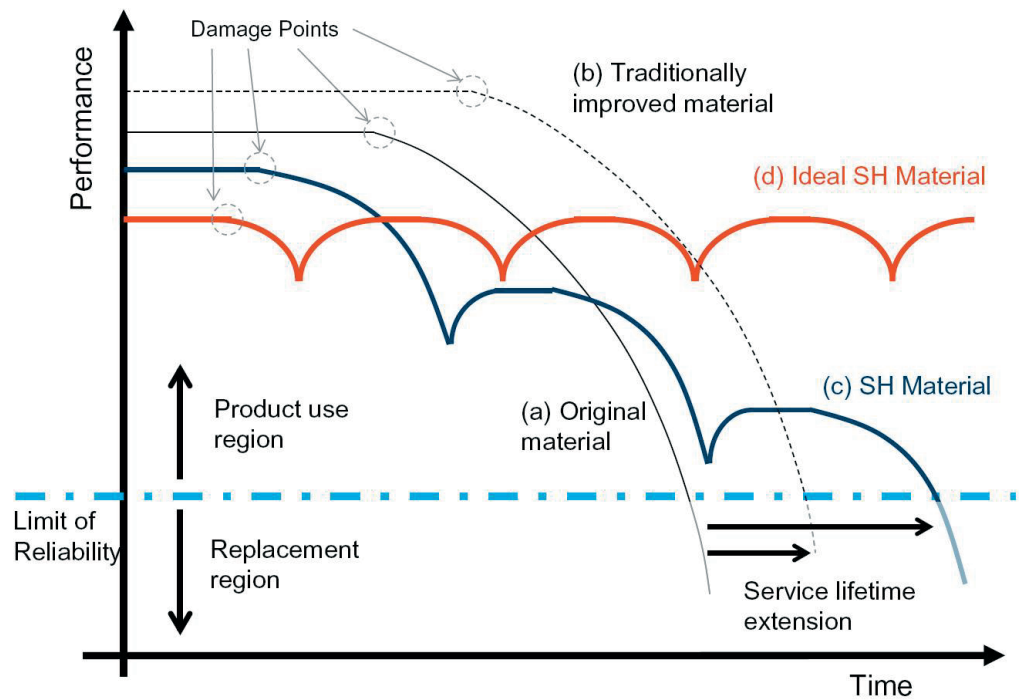


Fig. 1.2. Reliability improvement of engineered materials by implementation of self-healing principle [14]

This study is based on other concepts which mimic two known functions of blood circulation in human body: a) bruise formation on the skin after injury (impact indication); b) blood release from vasculature at site of injury, further haemostasis process, and tissue recovery (self-healing) (Fig. 1.3).

The concept of visual indication of mechanical impact ('bruisable' composites [31, 32]) involves incorporating dye-filled microcapsules within the binder or coating layer. The capsules rupture under impact or excessive strain leaving a coloured stain or 'bruise' on the surface of the structure. The physical size and intensity of the bruise are an indication of the degree of damage to the structure. By the latter is meant that the composite material has a sensitive to mechanical stress layer that can generate a visually observed response. The observable response should appear only after impact that could

cause mechanical damage in interior of the material. There must be a way to adjust the sensitivity of the visual indication function. The ability to indicate actions that cause barely visible impact damage can help to reduce the allowed margin of safety. Composite materials, which show a bruise like a person's skin when damaged, will simplify and cut the costs of inspecting and evaluating structures due to the use of the most cost-effective, and almost always available visual inspection. The ability to identify the location and magnitude of impact loads would enable small, focused inspections of potentially damaged areas of the structure rather than inspections of the entire area of the structure at specified intervals [33]. The principal benefit for engineers or technicians will be quickly scanning large or small external surfaces of composite structures, which are critical for the safety. The benefit will be to identification of areas, which have been damaged due to mechanical impact, lightning strike etc. especially on surfaces, or in areas, which are not normally accessible by other inspection techniques (e.g. wind turbine blades, boat hulls, aerospace fuselages etc.).

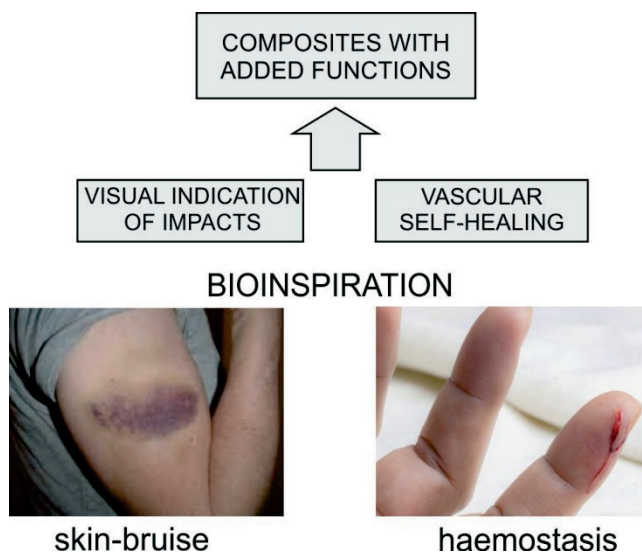


Fig. 1.3. The bio-inspired concepts for improving reliability of FRP composites

In turn, the vascular self-healing (-repairing) concept is based on the use of system of hollow channels or hollow glass fibres/micro-tubes, which are able to deliver a necessary amount of a liquid HA into the damaged place after impact to recover composite binder. This concept starts from the pioneering works of Dry et al. [34, 35]. The advances in this and other two main self-healing approaches (intrinsic, capsule based) for polymer materials and structures on their base are represented in series of recent reviews [36-40]. The vascular concept is the most promising for the creation of self-healing layer and placing it in the most vulnerable site of the layered FRP composite or structure. The concept has advantages: 1) unlimited release a HA when the structure is damaged after impact, so that the HA will fill delaminations, voids, and cracks (including large-scale damages); 2) possibility to feed repeatedly healing process thus reacting on

multiple impacts. The advantages become apparent especially if an outer reservoir is used for HA. A system of extended capillaries or hollow channels, which may be interconnected or branched as vasculature, may be used in this self-healing layer.

In mostly layered FRP composites, the sources of added bio-inspired functions can be concentrated in certain areas, forming definite layers. The smart bio-inspired layers together with load-bearing layers can form the structure of the composites with potentially improved reliability. The bio-inspired layers can serve for both impact indication and self-healing together or separately adding multifunctional nature to composites and structures.

The analysis of literary data presented in this section confirms the objectivity and attainability of the aim set before the study. The following two sections of the thesis relate to the implementation of formulated tasks separately for each of the selected bio-inspired concepts.

## 2. Visual Indication of Mechanical Impact

### 2.1. Current Trends

#### 2.1.1. *Indicating, sensing, and probing layers or coatings for visual inspection of bulk material*

The search for optimal ways of visualising of mechanical action and damages caused by them is an actual problem. Initially, there have been two different approaches to the visual inspection: 1) the instrumental monitoring of structures *in situ* and in the way as they are; 2) using the presence of the smart (self-sensing) layer or coating over bulk material of member or construction.

Optical Deformation and Strain Measurement System is an example of successfully developing instrumental approach. In this approach, an optical technique used to measure the deformation and strain of the surface of an object before and after loading. Global deformation and strain can be here readily visualised by the measurement system, which is able to indicate the damage location and its geometrical features in terms of strain concentrations [41]. Another one instrumental method uses Digital Image Correlation. This method enables the measurement of full field 3D displacements and 2D strains on a specimen surface by tracking a random speckle pattern. The method has allowed identify the failure modes and sequence of events leading to ultimate failure for sandwich specimens subjected to in-plane compression loading [42]. Image processing and pattern recognition techniques [43, 44] are attributes of these methods. These instrumental monitoring methods are complex and expensive as other NDT/I methods. The methods nullify the intuitive idea of non-instrumental visual inspection, which is expected to be more rapid, enough efficient, and cheap. A prerequisite of this visual inspection is the presence of the smart (self-sensing) layer/coating over composite that can show defects in the visible range directly (visual indication) or indirectly by means of appropriate instruments.

Development of smart layers for the visual inspection can review from the point of view of object for visualisation. This view deals mostly with smart layers, which behaviour as smart sensors with *colour* responses (including visible colour change, fluorescence, or phosphorescence). The responses are results of a variety of stimuli: a) of chemical nature (e.g. pH change, redox reactions, presence of heavy metals, sorption of chemicals); b) physical nature (e.g. radiation, temperature changes, electrical current); c) mechanical action. Review [3] gives a complete picture from position of development of this smart sensors and corresponding structural materials, which were stimulated. Since visual response formation to the chemical and physical action has its own specific focus, only progress in the visualisation of mechanical action and stress-strain state will be reviewed.

Significant efforts have been focused on the development of a variety of smart indicating, sensing, and probing layers of damages and stress-strain concentrations inside the materials. These layers are based on the principles of electric resistance or electrical signal generation. Operation principles are based on the change of definite properties. Charge transport properties due to damage or strain were used both inside of electrically conductive materials (aluminium, CFRP plate) [45-47] and through percolation networks in CFRP composites or polymers with dispersed electroconductive micro-/nanoparticles [16, 48-52]. The electrical capacity was utilised in sensor layer built with a soft, stretchable dielectric polymer [53]. The piezoelectric signal in smart sensing paints/layers was used in [54-56]. If a smart layer was generating a response to mechanical influence in the form of an electrical signal, there was not usually further development in the direction of visualisation of this influence. The exceptions were the results in [45] where hue-saturation-intensity colour model was proposed for crack existence probability or results in [51, 52] where a two-dimensional mapping method, based on resistance change measured by surface electrodes, was developed.

The smart surface layers generating electrical signal are used mostly for SHM, and surface crack detection and investigation of effects of cycle stress. The inconvenience of such sensors is that damage detection is possible only there where the sensor is localized and when the optimal configuration of electrodes is ensured.

An example of a smart surface layer serving to visualise an important for aerodynamic testing mechanical impact of air pressure is air pressure-sensitive paint. Luminescence intensity ratio as a function of pressure ratio of is used in this paint for the complete pressure mapping with high spatial resolution [57-60]. Unfortunately, this technique successfully exploits particular chemical feature i.e. presence of oxygen in the air because there are oxygen-sensitive luminescent molecules dispersed in an oxygen-permeable polymer binder in pressure-sensitive paint. This technique cannot be directly transferred to visualise mechanical impacts.

Optically mechanoresponsive materials seem to be the most promising for visualisation purposes of mechanical effects. Such chromogenic effects are exceedingly useful for sensing and in particular material failure monitoring in situ due to stress fracture or fatigue [61]. Mechanochromic materials which change their absorption colour (emission or reflection colour are also included) upon deformation [62] represent prominent class of mechanoresponsive materials. Following Weder [62] usually, three operating entities are distinguished in mechanochromic materials: a) polymers with aggregachromic dyes; b) mechanically responsive photonic crystals; c) mechanochemical stress-indicating polymers. In each area, there are notable achievements in terms of visualisation, but also prominent imperfections or limitations in these approaches are revealed. However, the chemical side of search for new prototypes of mechanochromic materials usually dominates in many researches.

Polymers with aggregachromic dyes rely on the formation of micro-/nanoscale non-covalently incorporated aggregates of these dyes in the polymeric host, which are dispersed irreversibly or reversibly upon deformation of the material, and thus cause a change of the material's optical properties [62]. The authors [63, 64] have concluded that many existing on the market organic dyes and polymers open unlimited possibilities for the development of advanced multiphase materials with chromogenic properties. They have pointed that an optimal combination consists from small and ductile dye aggregates and plastic-type (thermoplastic) matrices for the realisation of highly responsive mechanochromic polymer blends. In practice, it enables the production of flexible or rigid polymeric thin films that show remarkable optical response towards external mechanical stimuli at the addition of very low (less than 2 wt. %) amounts of properly selected aggregachromic dyes. Nevertheless, the approach appears to be unsuitable directly to the thermoset binders of load-bearing FRP. Considering that the luminescent fillers usually do not reinforce the polymer matrix in current materials authors [65] have been able successfully create of stress-monitoring material. The bulk material was photoluminescent and at the same time reinforced elastomeric material with the inorganic tetrapodal ZnO micro-particles (with high aspect ratios in different directions) as fillers.

Mechanically responsive photonic crystals form broad family of structured materials. A spatially periodic variation of the dielectric permittivity in it causes a photonic band gap, i.e. a frequency regime, in which no radiation of the respective frequency can propagate [62]. At least on the laboratory level, the fabrication of photonic crystals is possible through a self-assembly of spherical particles with narrowly defined diameter into colloidal crystals or opals. Fig. 2.1 illustrates efficiency for deformation visualisation of elastomeric polymer opal films, which behave like rubbers or thermoplastic elastomers and exhibit almost fully reversible mechanochromic behaviour. Nevertheless, there are still some obstacles to overcome to arrive at practicable applications and production of large-scale films. Unoccupied sites in the crystals and dislocations result in decreasing colour brilliance. In addition, the films tend to lack mechanical robustness [66].

Mechanochemical stress-indicating polymers in which mechanical stress provides the activation energy to trigger specific pre-programmed chemical reactions e.g. pulling of weak links (mechanophores), which in turn cause a colour change [62]. Obviously, a functional dye is covalently linked to the polymer chains in this case [63]. These mechanochromic polymers can be exploited for damage sensing in glassy solid polymers and as an indicator of plastic deformation occurring ahead of the crack tip. It is achievable by use of colour-changing mechanophores, spiropyrans, which are grafted into the backbone of poly(methyl acrylate) and poly(methyl methacrylate) polymer chain or are employed as cross-linkers [67, 68]. A protein-based mechanical nanosensor for the polymer matrix has been presented in [69]. The UV fluorescence-based microcrack

sensor-films are proposed by [70, 71]. The films employ the crosslinked polymers of dimeric cinnamate and anthracene moieties. It is demonstrated that, upon cracking, the sensors underwent bond cleavage of the dimeric structures followed by regeneration of the monomeric moieties having strong fluorescence [72]. The idea is that guest proteins can be entrapped permanently into the cavities by covalent linker chemistry of host load-bearing material. Unfortunately, submicrometer scale of visualisation impedes yet early detection of damage by these means. Performance of developed mechanochemical systems as damage indicators is limited by low intensity and potential bleaching of fluorescence [73]. Complex synthetic procedures and structural instability upon exposure to external environment are disadvantages of these systems [72].

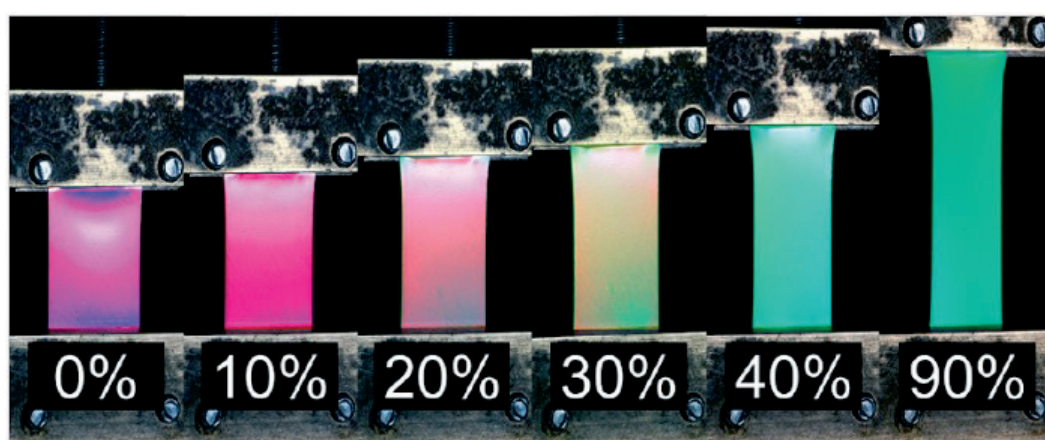


Fig. 2.1. UV/visible transmission spectra of the elastomeric opal film at different strains [66]

The methods discussed are important for solving the problem of visualisation of specific mechanical damages in the specific polymer and composite materials, as well stimulating the search for other approaches. At the same time, disadvantages, or limitations of the application of the methods considered become clearer:

- The instrumental monitoring methods are complex and expensive as other NDT/I methods. The situation is complicated further if an image processing, pattern recognition techniques, multi-dimensional mapping methods, and electronic signal detecting and visualising techniques are used. When using the sensors for damage detection, their localization as well configuration of electrodes affects the result.
- During creation of load-bearing solid materials, a crucial point is the strength of the filler-polymer interaction to achieve reinforcement. A strong filler-polymer interaction can be realized by reduction of filler size, providing a greater filler-polymer interface area. However, nano-sized fillers raise the problem of agglomeration, thus require complicated processing [65].

- In the case of optically mechanoresponsive layers or films, main problems are the complexity and high cost of harmonization of chemical, physical, and mechanical properties of these layers or films with load-bearing composite materials. The damage sensing function of the mechanochromic material is highly dependent on the specific polymeric system used. The techniques using single molecule optical response permit to detect stress-strain state at very small length scales. Connection of molecular and macroscopic levels needs sophisticated formalisms for mechanochemical coupling [74]. It refers to engineering a material response and to understanding possible perturbations of chemical reactions in loaded materials, which could be misleading during analysis of visual response. The sensing systems become again complex and expensive because costly catalysts are often employed in order to achieve mechanochromic functionality in the polymeric system [75]. Instruments are necessary for fluorescence exciting and for weak light signals detecting. Lack of the chemical and thermal resistance, problems with the durability and the large-scale production [29], along with low intensity and potential bleaching of fluorescence, problems with false indications [73] are attributes of mechanochemical systems. The reversible nature of many mechanochemical transformations can be an obstacle to the use it for visual indication of impact or permanent damage detection.

An alternate strategy for damage detection and visualization is to store mechanoresponsive indicators in isolated capsules or hollow fibres [61]. An opportunity appears of long-term stability. It is desirable that the optical response is in the visible range. The next section is dedicated to this approach.

### ***2.1.2. Visual indication using microencapsulated dye***

The idea to store mechanoresponsive indicators in isolated capsules [73, 76, 77] or hollow vasculcs [78, 79] is originated mostly on the experience gained from the development of microcapsule and vascular approach to self-healing. Microcapsules have an advantage of keeping core materials (dye or its precursor) stable for a long time. The ability of the capsules to break down because of damage to the polymer binder and to release HA which flows along the cracks in the binder has been repeatedly demonstrated [40]. It has been shown not only in the bulk material, but also on various types of self-healing coatings. The effective parameters in synthesis of micro/nanocapsules, as well as approaches to fabricate self-healing coatings based on these capsules and challenges of embedding them in coatings matrix have been reflected in [80-88]. At the same time, experimental data on the use of the microcapsules in other smart-coatings has been accumulated. Microcapsules with both film-forming material and corrosion inhibitor as well as microspheres with anti-fouling agent were successfully produced in [89]. In [90],

a self-healing concept for epoxy-based anticorrosive coatings is investigated. The microcapsules filled with reactive agents are incorporated into the coating matrix.

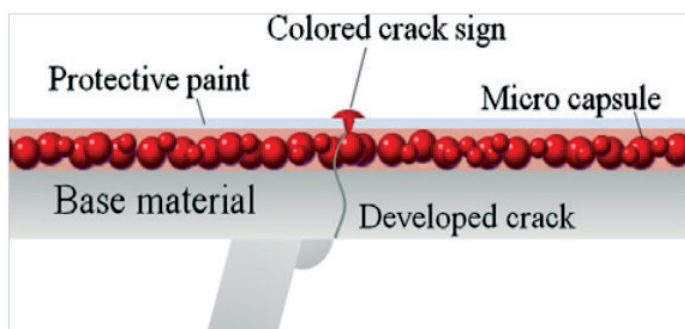


Fig. 2.2. Coloured crack sign appeared from broken microencapsulated dye particle [91]

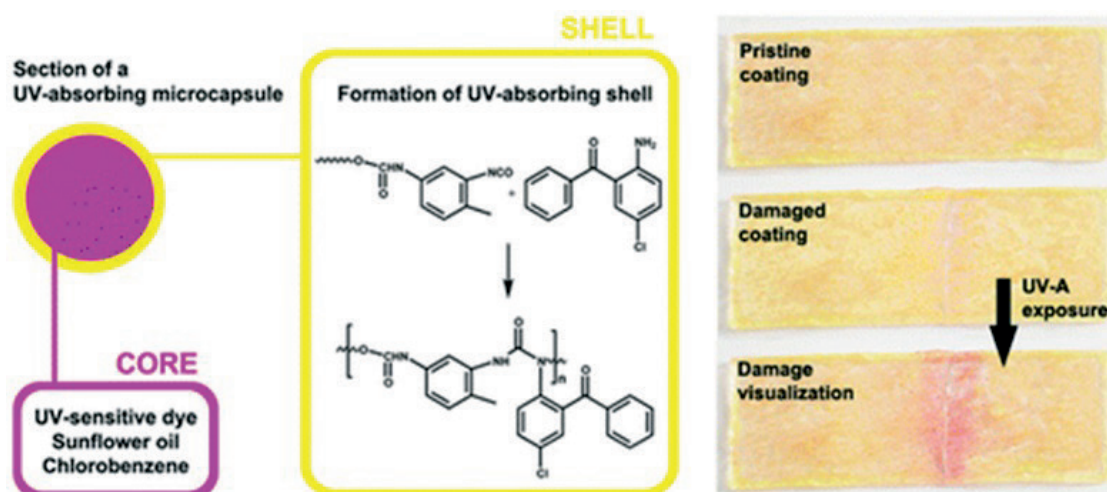


Fig. 2.3. Schematic cross-section of the synthesized microcapsules with main constituents and shell formation scheme [75]

Encapsulated systems in polymer coatings have been proposed in several works for visual indication of scratches and fatigue cracks. In the simplest cases [76, 91], the microcapsules have contained only dye particles. After scratching or cracking the coating, the microcapsules break, and the core material e.g. red dye is released and diffuses into the coating matrix (Fig. 2.2). Unfortunately, the capsule contents shine through their walls. The contrast of the observed crack is reduced in a case of thin protective paint.

Part of that disadvantage can be eliminated by using encapsulation of an ultraviolet-(UV)-responsive photochromic dye (one-component chemistry) [75]. In this case, only broken capsules create the visual response after the UV-exposure under condition of sufficient thickness and robust UV-absorbing shells of capsule (Fig. 2.3). The strength of the approach presented in this work lies in the possibility to convert any type of conventional polymeric coating into a UV-light-sensitive mechanoresponsive smart

coating by simple addition of our new UV-screening microcapsules. A similar easy fabricated microcapsule-type fluorescent microcrack probe system has been developed for the detection of microcracks in cementitious materials [72] (Fig. 2.4). The exact position of microcracks can be effectively detected without any expensive detection instrument due to strong fluorescence emission when the microcapsules are distributed in the adhesion promoter at mass ratio of 1 : 3.

To be independent of UV-exposure, avoid a false response due to a permanently triggered state of the dye in the core and have enough contrast response by colour change, a use of two-component chemistry in a solid polymer film with microcapsules has been demonstrated in [77]. Thus, the core material 1,3,5,7-cyclooctatetraene, which is a conjugated cyclic olefin and a precursor to intensely coloured polyacetylene has released from capsules ruptured in the presence of the Grubbs–Love ruthenium catalyst show immediate colour change from nearly colourless to dark purple over time. The authors [77] have been able to prevent volatile capsule cores from leaching into the surrounding matrix and contacting the catalyst before a damage event, which could cause premature colour change. In the later work, the authors [73] from the same group have managed to improve the scratch visual indication using chemistry without expensive catalyst in which the residual free amines of the coating epoxy matrix react with released core materials to locally change colour (Fig. 2.5).

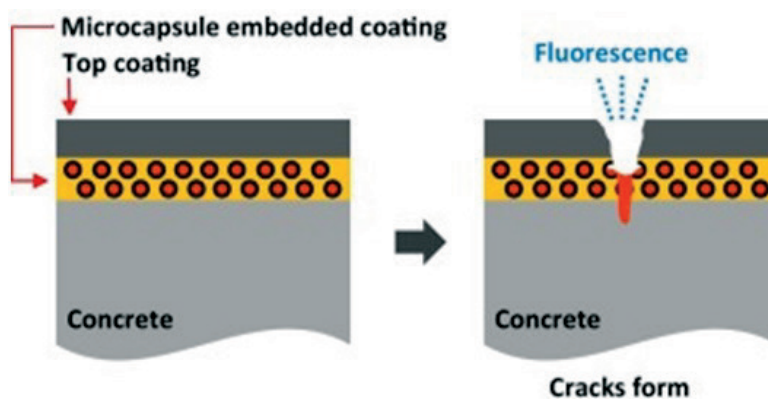


Fig. 2.4. The concept of fluorescence microcrack probing [72]

Another type of microcapsules with two/three-component chemistry has been proposed by the co-authors of the doctor's degree applicant in [92]. The developed damage indication coatings have been organized on water-based acrylic binders that are composed by incorporation of microcapsules into the coating formulation. The microcapsules containing crystal violet lactone (CVL) as leuco dye are embedded into the coating formulation together with colour developers: encapsulated liquid methyl 4-hydroxybenzoate and/ or non-encapsulated solid colour developer – silica gel. The content is released when the microcapsules break during external mechanical stress.

The chemical reaction between dye and colour developer providing acidic environment (Fig. 2.6) leads to appearance of the intensive blue colour in the CVL dye instead colourless and therefore the development of a colour change – halochromism in the surface of damage-sensitive coating. Thereby the external stress able to damage a substrate causes response of the coating in a form of a bruise.

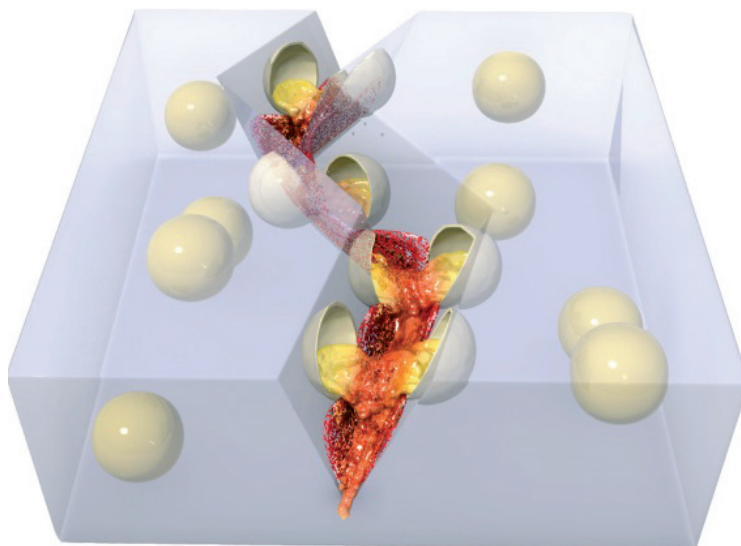


Fig. 2.5. Schematic of autonomous damage indication concept: upon mechanical damage, the microcapsules rupture and the released core materials react with the coating to change locally colour [73]

The development of microcapsules with two-component chemistry eliminates the shortcomings of previous approaches (low-contrast response, the need for UV-exposure), but the matrix chemistry should be adjusted to the desired chemistry of the microcapsule core. That reduces the versatility of the approach. Researchers often pay attention to two opposite points. From one side detecting cracks by colour cannot be generally clearly seen in the case of very fine cracks [72] or it is difficult to find the initiation, characteristics of fatigue cracks (length and propagations) [75]. Here, obviously, we are confronted with a limitation in resolution of the naked eye during inspection. From the other side, the diffusion of the dye sideways of the scratches and cracks increases visualization, but does not speak about the true size of the damage [75]. This in turn reminds the most complete information about the fault can be obtained from the complex NDT/I, if the site of damage has been localised.

The peculiarity of the work [92] has been the fact that the evaluation of the coatings with different formulations of leuco dye and developer occurred in terms of visual indication of mechanical impacts using the quasi-static indentation. The experiments conducted in this study allowed to develop a method of digital image analysis. The method was developed and used for evaluation of coating response to indentation.

However, the level of smart coating achieved in this study has definite shortcomings. The dye system in the coating produces an insufficient contrast response to indentation. The lower threshold of indentation energy absents. The coating has weak adhesion to the substrate and lack of mechanical strength.

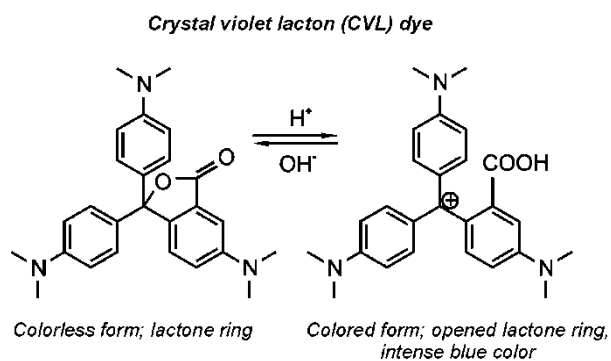


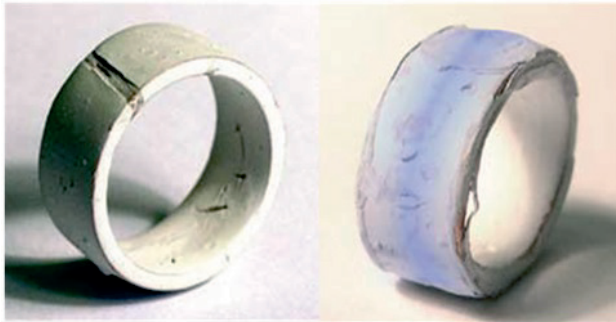
Fig. 2.6. Transformation between uncoloured and coloured form of CVL dye – halochromism

### 2.1.3. *Impact-sensitive coatings for FRP composites*

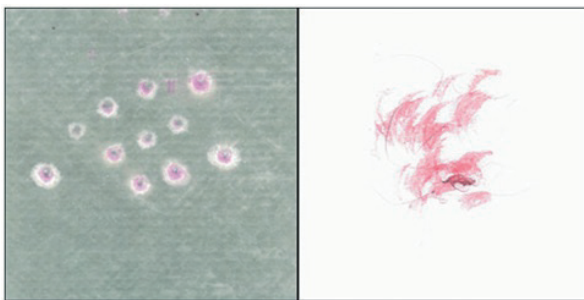
As has been evidenced above the most commonly encountered type of damage to FRP composites is caused by mechanical impacts [15]. Flaw detection and determination of the remaining strength and life of the structure that contain different phases of material (fibres and matrix) remains a challenging task. Correspondingly, a challenging task is the use of scientific background above reviewed for development of bruisable impact-sensitive coatings and visual indication layers for FRP composites. The patent literature data reflect the attempts to propose practical implementation of these scientific ideas on the base of a microencapsulated fluorescing dye [12, 93]; microencapsulated leuco dye and particles of a developer [94, 95]. The encapsulated dye can be in a polymeric matrix [96] and in a matrix, which contains reinforcing elements [97]. Some ways are suggested for calibration of the visual response according to the spot area and for control of the sensitivity of a visualization function by varying the thickness of capsule shells [98]. A perspective application of this concept is using for polymer composite products and structures, from sports and industrial helmets to transport vessel components. This bruisable coatings and layers could not require advanced skills and special electrical equipment, and could allow effective inspection with relatively wide range [94-96, 98, 99]. Nevertheless, additional investigations are required for characterizing the extent and severity of the damage in depth of the composite as well for making a prognosis of the lifespan the member.

The existing scientific background does not demonstrate a successful practical application of visual indication of impacts. Available also concepts of composites with

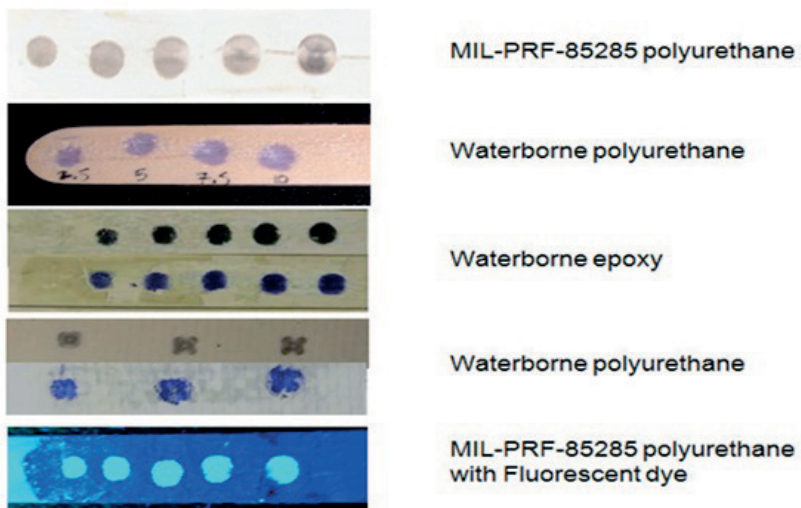
bruises have not led to successful proposals on the world market (Fig. 2.7). Especially, it concerns widespread composites with an epoxy binder. An obstacle for the realisation is the chemical nature of an uncured epoxy resin: the amines of traditional hardeners, which have an alkaline reaction [100], deactivate the developer, which usually has an acidic reaction [101].



Sensor Products Inc.



EPL Composite Solutions Ltd



Luna Innovations Inc.

Fig. 2.7. Prototypes of bruisable coatings offered by several companies

Therefore, there is a need for new techniques of implementation of the function of visual indication of mechanical impacts and formation of bruises in epoxy composites. The successful application of the concept in accordance with the [90] implies the need for the implementation of a few obvious chemical requirements for microcapsules:

- Remain intact during storage, surrounding coating formulation and application;
- Contain sufficient amount of chemicals with fast reaction kinetics;
- Rupture readily when a coating is damaged;
- Exhibit good adhesion with the polymer matrix.

Simultaneously it is desirable that there is no deterioration of the mechanical properties of the host matrix by microcapsules (not compromise mechanical properties of the matrix). The perfect solution with the greater reinforcing effect can be reached, when the inclusions are more robust than the polymeric binder is, as it follows from traditional notions of micromechanics [102]. More likely, the bruisable microcapsules should lead to no stiffening of the host composite but to increasing of its impact performance. For example, in the study [103], a soft rubbery core surrounded by the thick shell made of rigid polymer particles have been dispersed into the ply interfaces of composites prepreg to improve impact performance of the resulting carbon fibre/ epoxy composite laminates. Thus, the capability of the elastic energy absorption has been significantly improved (about 360 %) and less energy has been available for the creation of damage. In accordance with authors' explanation in [103]: "When the impact load is applied, the most of the particles would have deformed compressively due to their soft nature. This deformation would have absorbed large amount of energy. While the remaining undeformed particles would have compelled the crack to take a meandering path and further absorb the fracture energy."

In the research [104], compliant inclusions (up to 50 %) of microcapsules of melamine-formaldehyde resin shell in more rigid host polyvinyl acetate matrix have demonstrated yield strength increase (up to 2 times) in tensile tests. At the same time, numerical simulations have not denied that very small microcapsules at small amounts (~1 %) can cause the increase of plastic strains both in the matrix and in the microcapsules shells. In this case, microcapsules act only as the stress-strain concentrators and can drastic decrease the mechanical properties of composite.

The material of the bruisable microcapsules shell must be compliant enough to avoid deflecting cracks away. The shell thickness and mechanical properties microcapsules must be tuned according to the expected stresses in their environment, which are transferred from the matrix to the capsules for their successful rupture and release of encapsulants. In the study [105], an attempt of such tuning of microcapsules made by microfluidics is demonstrated.

The tendency of the microcapsules to be added directly into the resin to aggregate, which was observed in capsules for self-healing [106], can also affect the mechanical properties of the composite.

In addition, mechanical properties microcapsules must be tuned according to the expected stresses in their environment. They must burst readily when a coating is damaged but without ‘hypersensitivity’ to impact, which does not cause damage. The sensitivity of the coatings, which are quite effective for the detection of scratches and fatigue cracks in adjacent bulk material is necessary to roughen for indication of impacts.

## **2.2. Function of Visual Indication of Mechanical Impact in Composites**

In this research, the strategy of creating smart visual indication layer was chosen instead of the direct admixture of dye microcapsules and developer particles into the epoxy matrix of the composite. It was assumed that the creation of a layer containing microcapsules and developer, which have no direct contact with uncured resin in the formation stage, allows eliminate or minimize some of the previously mentioned negative aspects, specifically:

- Elimination of aggregation of microcapsules and preserving them entire during layer creation since the microcapsules are emulsified and easily withstand mechanical manipulations;
- Overcoming the chemical antagonism of the active substances that cause visual response, and the substances of epoxy binder;
- Ensuring the smart layer formulation to remain intact during storage and to have enough encapsulated chemicals with fast reaction kinetics;
- Minimizing the influence of the smart layer on load-bearing properties of the composite due to its location on the surface of the composite;
- Ensuring the impact sensitivity adjustment of the indication layer using a transparent coating of different thickness.

### **2.2.1. Preparation of indication layer**

The visual indication layer of mechanical impacts involves microcapsules of leuco dye and particles of acidic colour developer as two active components embedded into the layer formulation. Particularly, the layer contains a microencapsulated leuco dye — Microcapsules 500 black copy, and Colour developer (Papierfabrik August Koehler AG). These ingredients are commercial products, details of the production and composition of which are not disclosed. Nevertheless, a general principle of production can be illustrated by the polymerization method of the microcapsules with the common crystal violet

lactone — CVL dye (a lactones' derivate of crystal violet 10B). In pure state, it is a slightly yellowish crystalline powder, soluble in non-polar or polar organic solvents and not soluble in water. Therefore, CVL dye is dissolved in phenyl acetate (PA) and microencapsulated with an in-situ polymerization method. The essence of the method involves the dispersion of the organic liquid – polymeric material in a continuous water phase in the form of initial emulsion droplets – a core material [101]. Then during microencapsulation, the core material is coated or entrapped with some wall material usually a melamine-formaldehyde (MF). The entrapped material is usually a liquid but can also be a solid or a gas. Finally, core-shell particles (microcapsules) are formatted (Fig. 2.8).

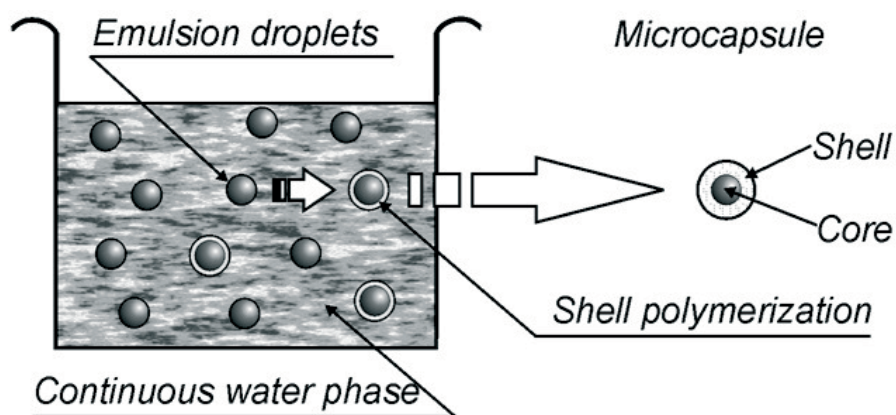


Fig. 2.8. Dispersion of an organic liquid in continuous water phase in a form of emulsion, droplets forming core material, and final core-shell microcapsule

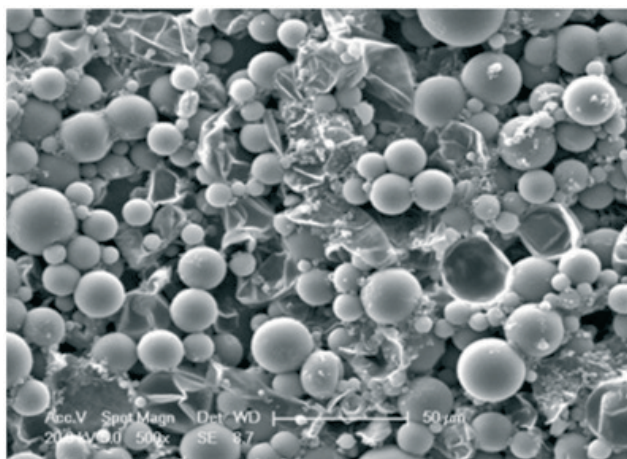


Fig. 2.9. Scanning electron microscope images: CVL microcapsules with average diameter of ca. 10 – 15 µm

Microcapsules with poly (melamine-formaldehyde) (PMF) shell have several advantages compared to traditionally used poly (urea-formaldehyde) microcapsules –

higher water resistance, higher chemical resistance, and improved mechanical stability [107]. The polymerisation of melamine with formaldehyde to produce PMF as a constituent of the shell material of the microcapsules occurs in the continuous phase and at the interface formed by the dispersed core material and the continuous phase [108].

The diameter of the capsules is controlled by changing the size of the initial emulsion droplets and this is changed by varying the stirring speed during emulsion manufacture. The diameter of the microcapsules can be appeared in the range of 0.3 – 100  $\mu\text{m}$ . As example, washed and dried in air microcapsules developed by the co-authors of the doctor's degree applicant in [92] are shown in Fig. 2.9.

In this research, the microcapsules and particles of the developer were supplied in the forms of water dispersion to be used in water-based formulations. These components were added to the commercial epoxy-modified polyurethane-acrylate emulsion — HALWEDROL UV 20/40W (Koninklijke DSM N.V) in a pre-selected, optimal ratio. Due to the hydrophilic nature of the side groups of a cross-linked network of long and flexible chains of polyacrylate, the acrylic component has excellent water dispensability and can maintain stable solutions for up to a year without phase separation. Manipulations in water dispersion form allow preserving microcapsules intact and eliminating their aggregation.



Fig. 2.10. SEM photo of fabric fibres with Microcapsules 500 black copy and Colour developer particles of the developer

The polyamide (nylon) fabric — Stitch Ply A (AIRTECH Europe Sarl) (without a coating; surface density of 88  $\text{g}/\text{m}^2$ ), was used as a basis for the preform of impact indication layer. The fabric was impregnated with the resulting mixture and dried in a suspended state to remove the excess liquid. An electron-microscopic image of the fabric fibres impregnated with capsules and a developer is shown in Fig. 2.10 performed in the

Institute of Solid State Physics of the University of Latvia. The surface of the dried fabric was subjected to UV-irradiation by an SVD-120A mercury-quartz lamp for 30 min from each side. The exposure rate, measured in the range of 280-320 nm, was  $10.5 \text{ W/m}^2$ . The irradiation provided polymerization of the emulsion, which served as a binder for components of the indication layer. The fraction of impregnating composition constituted  $68 \pm 5 \%$  of the initial surface density of the substrate fabric. Thus, the polymerised preform of the layer (Fig. 2.11) consists of fabric fibres (1), microcapsules (2), developer particles (3), and cured modified polyurethane-acrylate as a binder (4).

This preform has advantages over direct admixing of the dye microcapsules and developer into the epoxy. The capsules and their core and developer have additional chemical and mechanical protection. Particularly, the particles of the developer are isolated from the action of alkaline amines of the hardener. The cured preform can be easily wetted and saturated with uncured epoxy resin. The developer particles are reliably protected from uncured epoxy hardener.

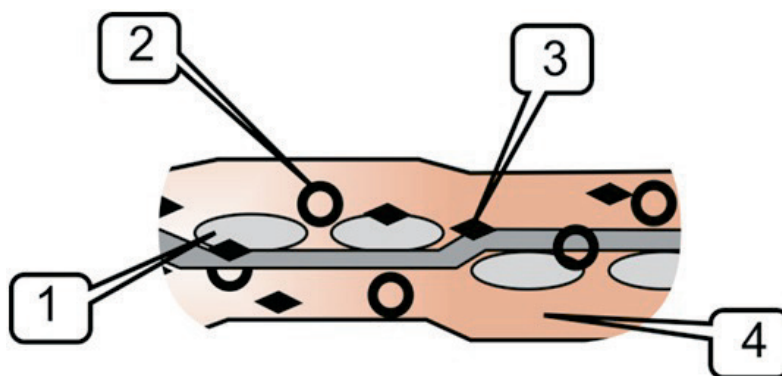


Fig. 2.11. Components of the indication layer preform: nylon fabric fibres (1), microcapsules of a leuco dye (2), particles of a developer (3), and a binder — epoxy-modified polyurethane-acrylate (4)

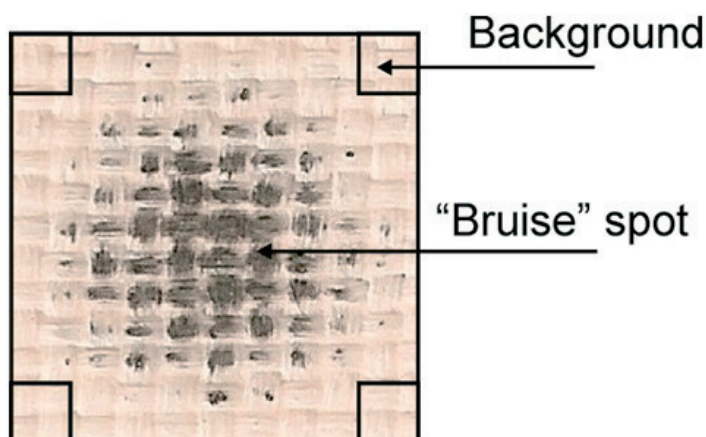


Fig. 2.12. A 'bruise' in the preform of the indication layer

Such indication layer preform can form a clear bruisable visual response to the impact (Fig. 2.12). The dye is released from the capsules and contacts with the developer particles when the layer experiences sufficient mechanical stress. The experimentally estimated external pressure necessary for the appearance of bruise in the preform of the smart layer does not exceed 2 MPa. The contrast and instantaneous response appears as a visible colour change due to a pH change as a stimulus. The halochromic components of the preform keep entire performance for several years. For example, the values of the visual response to equal loads (details of the quantitative assessment see below) of the six-year and freshly prepared indicator layers were identical.

### 2.2.2. *Embedment of indication layer into FRP composites*

It was assumed that a transparent epoxy coating of changeable thickness above the indication layer could serve for the sensitivity adjustment of the function of visual indication of mechanical impact. If the thickness of the coating was increased, then a smaller load would act on unit area of the indication layer. This specific load might become insufficient to rupture the microcapsules.

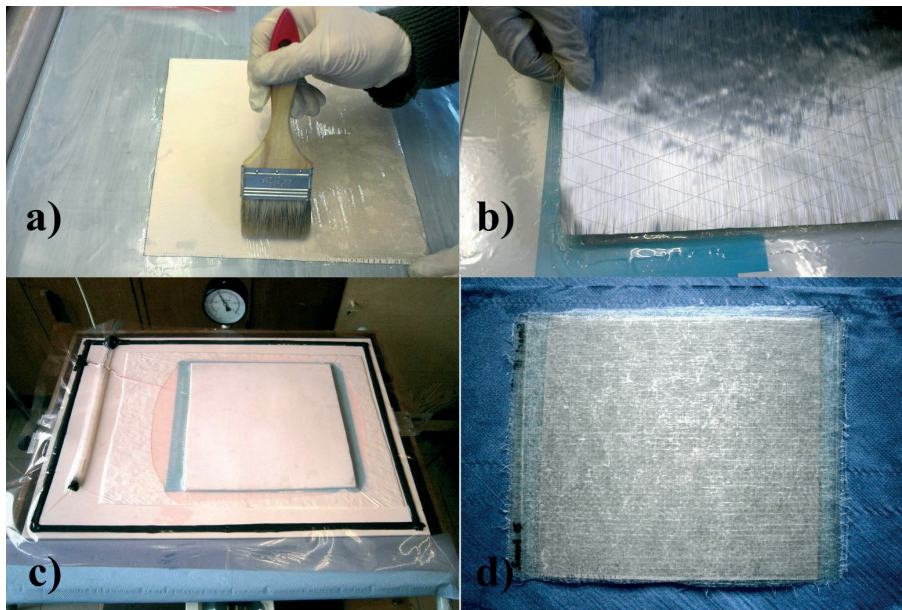


Fig. 2.13. Composite manufacture process: impregnation of the indication layer preform with an epoxy binder (a); lay-up of the unidirectional glass yarns (b); vacuum bagging moulding process (c); a plane composite specimen with the function of indication of impact (d)

In this approach, the indication layer together with epoxy coating of controlled thickness was integrated within the composite using vacuum bag moulding process (Fig. 2.13). The flat surface of a working table was sequentially covered with a layer of

a colourless nylon distributive mesh (for the formation of an epoxy coating), a preform of indication layer, and two load-bearing unidirectional glass yarns connected by network (with the surface density of  $500 \text{ g/m}^2$ , Havel Composites CZ s.r.o. [109]). Both the preform of the indication layer and yarns have been preliminary saturated with an epoxy binder by using a roller or brush (Fig. 2.13.a). Such technology was applied to manufacture composites with an epoxy layer of thickness  $z$  less than 0.5 mm. To obtain composites with an epoxy layer more than 1 mm thick, the same package of layers has been stacked on a preliminary moulded and cured plate of an epoxy binder of thickness varied from 1 to 4.5 mm (Fig. 2.14). The thickness of the coating was determined under a microscope, by measuring the cross section of the specimen around the place of indentation.

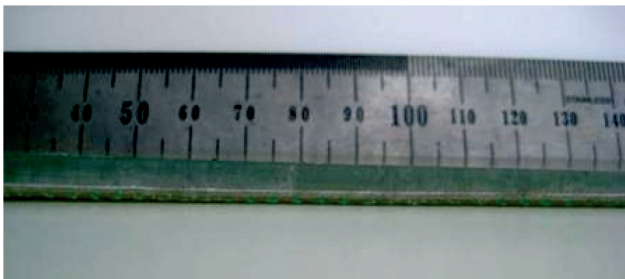


Fig. 2.14. The side view of composite with the indication layer and epoxy layer of varied thickness more than 1 mm against the background of the ruler

The composite was prepared from an LH 289 epoxy resin (based on bisphenol A; viscosity  $500 - 900 \text{ MPa}\cdot\text{s}$  at  $25 \text{ }^\circ\text{C}$ ) and an H 289 hardener (based on cycloaliphatic polyamines) in the ratio of  $100 : 33$  (Havel Composites CZ s.r.o. [109]). In the cured state, the binder possessed an ultimate tensile strength of  $59 \pm 8 \text{ MPa}$ . The moulding (Fig. 2.13.c) and subsequent curing of plane composite specimens were performed in vacuum under 0.4 bars at a temperature of  $40 - 60 \text{ }^\circ\text{C}$  for 20 h.



Fig. 2.15. A specimen of the load-bearing composite with indication layer and thin epoxy coating after indentation

In another example of application, the indication layer preform has been preliminary saturated with an epoxy and glued with it to finished articles or constructive members. The layer can give visual response in the form of bruise indicating a place of possible damage of this substrate material. The articles are possible be inspected continuously. As example, a safety helmet with indication layer strips glued on is shown in Fig. 2.16. The dark bruise is a layer response to the 5-kg rod drop from the 0.5 m height. The indication layer embedment as top layer of the FRP composite will not disturb load-bearing capacity. The members suffered mechanical impacts could be timely repaired or replaced.



Fig. 2.16. A safety helmet with indication layer strips glued on

### ***2.2.3. Mechanical testing, visual response quantification, and stress modelling***

The task was to validate the efficiency of visual indication of mechanical impact. Accidental impacts occurring in service or during maintenance are important sources of damages to composites and structural faults. Impact loading of a laminated composite panel by a hard object results in a high local force causing two forms of deformation: one being indentation (local) and the other bending (global) [110]. Since the energy, rather than force, is the input datum in impact [111], the question arises whether the limit energy resulting in damage can be reliably correlated with appearance of the visual response. In general, this task involves the modelling of complex dynamic phenomena, which cannot be faced by simple analytical tools [111]. Accounting for the vibrational effects is not necessary when low-velocity impact is concerned. In this case, static approaches are often sufficient to model analytically the actual behaviour. Among the analytical models, the Hertzian contact law, spring-mass, energy balance, and several original approaches are used extensively [110-114]. There are many experimental evidences examining a variety

of quasi-isotropic composite laminates in these researches that the use of load–displacement curves determined from quasi-static and low-velocity impact tests are similar where force is examined instead energy. Easy modelling and implementing quasi-static experiments promote the application of this approach in pilot studies of composites with new functions. As example, the quasi-static approach is used to make pseudo-impact damage to self-healing composites via indentation experiments [78, 79]. In this research, quasi-static indentation on a flat foundation has been used as the method of pseudo-impact mechanical testing of composites with a built-in indication layer (Fig. 2.17). An indenter or impactor tip radius could strongly affect the formation of damage (with the larger radius requiring significantly more energy to create damage) [114]. The study of damage formation in the layered load-bearing composite was not a subject of this research. Therefore, the spherical indenter was used of a one radius  $R = 7.0$  mm.

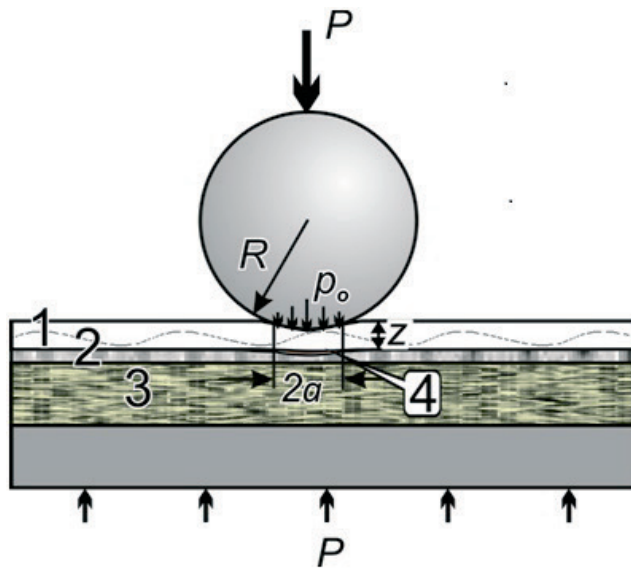


Fig. 2.17. Scheme of indentation loading of the FRP composite with a built-in indication layer: the transparent epoxy layer (1), visual indication layer (2), load-bearing layers of the composite (3), and visual response (4); maximum normal pressure  $p_0$ , and radius  $a$  of the contact zone

The universal electromechanical testing machine Zwick 2.5 was equipped with a spotlight and a camera on a fastening, which ensured constant exposure and position for shooting the same place of indentation on the specimen surface. A series of loading–unloading tests was carried out at the same place of the surface specimen. The tests were carried out with a constant indenter speed of 0.4 mm/min. After each unloading, the value of maximum load  $P$  was increased in the next loading cycle. The possible gradual increase was from 50 to 2000 N of the indentation load  $P$ . The series of tests were conducting until the appearance of a full-grown bruise. Images of the indentation place and arising visual responses were obtained in 3 min. after each unloading. Such series (ca. 10 images) were obtained for each considered thicknesses  $z$  of the epoxy coating. The

series of images obtained after the action of the increasing loading were used to determine the threshold load  $P^*$  of actuation of the function of visual indication of indentation in a composite with a given thickness  $z$  of the surface epoxy layer.

To get quantification method of the visual response to indentation for future evaluation of the efficiency of the function of visual indication in the composites, the original method of digital image analysis was developed. Different monochrome digital image analysis techniques frequently are used with mechanical tests e.g. for identifying size of inclusions [115], or deformation measurements of thin films [116]. The typical image processing and analysis sequence involves the main steps of pre-processing, segmentation (including discrimination by thresholding grey-level intensity), postprocessing, measurement, and data analysis [117]. The method of digital image analysis was worked out during the research of prototypes of bruisable indication coatings upon duralumin substrates developed in [92] by the co-authors.

The series indentations carried out at different places of indication coatings at the stage of working out the method. The images of indentation traces were scanned with HP DeskJet 2180 (optical resolution 1200 dpi) and became the objects of further analysis. It was established firstly in the research of the coatings that active component microencapsulated CVL leuco dye got clear blue colour after halochromic transformation. The bruisable response was coloured upon indentation and consisted mainly of discrete blue dots against the non-white background with some blue inclusions. A colour digital image analysis technique was devised to evaluate impartially this response. The digital image of any response was decomposed into the primary colours. Red (R), green (G), and blue (B) arrays of all image pixels formed three matrices with elements  $R_{i,j}$ ,  $G_{i,j}$ , and  $B_{i,j}$ . It was established, that CVL dye transformation generates only clear blue colour (B) response. Depending on the nature of the halochromic chemistry, other one or two colours can be dominant. Their absolute intensity of the dominant colour depends both on the quantity of ruptured capsules, degree of the halochromic transformation and on illuminance of the place of indentation. Particularly, the rise of illuminance causes the growth of the dominant colour level. Achromatic grey level  $\min(R_{i,j}, G_{i,j}, B_{i,j})$  indicates the illuminance. The excess of the dominant colour over achromatic grey  $B_{i,j} - \min(R_{i,j}, G_{i,j}, B_{i,j})$  is sensitive to the illuminance too. It turned out that the excess divided to this grey level exclude influence of the illuminance magnitude. Thus, the relative value designated as local intensity  $\beta_{i,j}$  of an arbitrary pixel can be calculated using formula:

$$\beta_{i,j} = \frac{B_{i,j} - \min(R_{i,j}, G_{i,j}, B_{i,j})}{\min(R_{i,j}, G_{i,j}, B_{i,j})}. \quad (2.1)$$

To validate above-mentioned assumption, two model palettes of blue colour were examined. The amount of blue dye (colour level  $B_{i,j}$ ) rose due to illuminance at different

places in pixels (px) of the palette in the first case. Alternatively,  $B_{i,j}$  rose due to increase of the blue colourant at a constant illuminance in the second case. As result, a blue response relative local intensity  $\beta_{i,j}$  is constant in the first case but is rising too in the second case (Fig. 2.18).

In this way,  $\beta_{i,j}$  was chosen as a measure of local intensity of the bruise colour response to indentation of the bruisable indication coatings. The digital analysis of image files of the circular bruise spots was replaced with analysis of a representative rectangular strip conformed to the initial image matrixes. In the next step, the  $\beta_{i,j}$  elements were averaged over the stripe  $j$ -th column in vertical direction to minimize noise. In the example of digital image analysis of three indication coatings, the averaged blue local intensity graphs ( $\beta_j$  is designated  $\beta$ ) showed the distribution of the bruise response along the diameter of spot  $d$ . The developed technique also allowed comparing the degrees of total blue colour response i.e. the quality of the responses of different coatings, using an integral blue colourfulness  $\mathcal{B}$  of the indentation trace spot (the shadowed area under  $\beta$  curve and over averaged background level) as an integrated intensity of the response (Fig. 2.19).

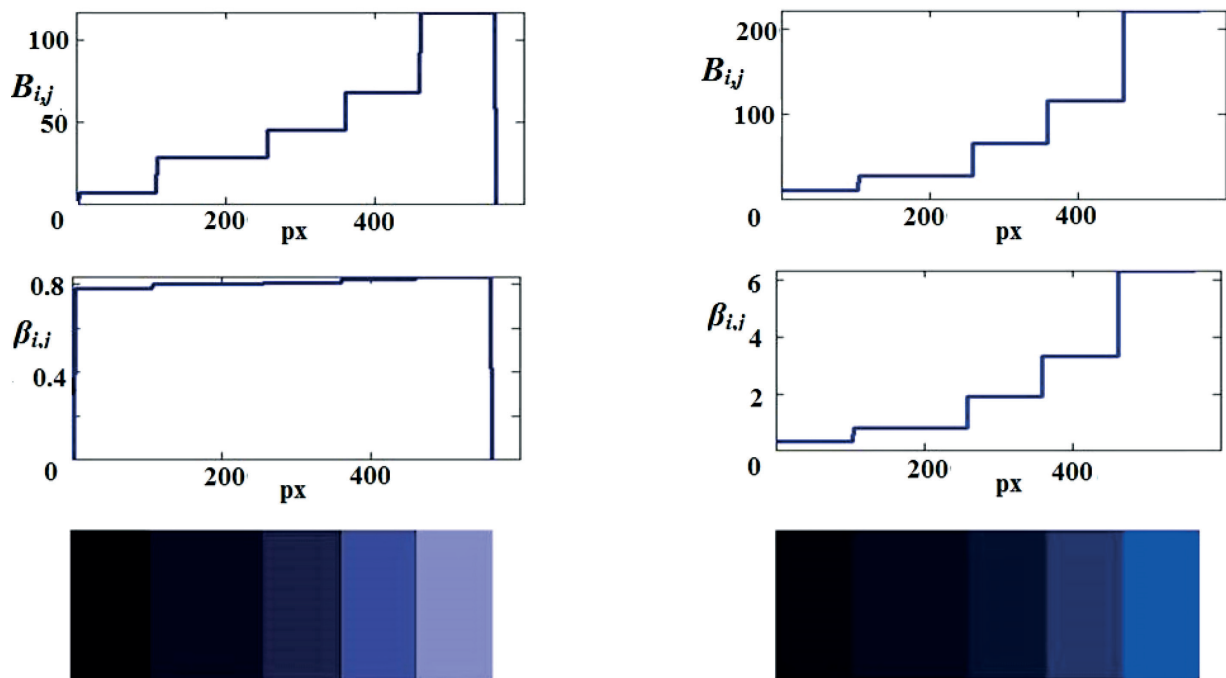


Fig. 2.18. The two types of the palettes (bottom):  $B_{i,j}$  rises due to illuminance and  $\beta_{i,j}$  is constant (left column);  $B_{i,j}$  rises at constant illuminance and  $\beta_{i,j}$  is rising too (right column)

In the composites with the built-in visual indication layer, the red component was chosen as predominated in the visual response since the intensity of the R channel was markedly higher than that of the others. The specific chemical formula of microencapsulated dye differed from above described CVL dye and multi-component composition of the layer play major role in this. The relative value of local intensity  $\beta_{i,j}$  of an arbitrary pixel was calculated using formula (2.2) similar to the previous formula (2.1)

$$\beta_{i,j} = \frac{R_{i,j} - \min(R_{i,j}, G_{i,j}, B_{i,j})}{\min(R_{i,j}, G_{i,j}, B_{i,j})}. \quad (2.2)$$

For a quantitative determination of the total value of response in experiments with indication layers, the variable  $\beta_{i,j}$  was integrated over all pixels of the spot area. For this purpose, the spot of response was first enclosed into a square of obviously greater size (Fig. 2.12). Four angular sections of the square form occurring outside the spot served as background references. They were used to calculate the average value of background intensity  $\beta_{bg}$  and its dispersion  $\sigma^2$ . It was assumed that the spot contained only pixels from the central area, whose values of  $\beta_{i,j}$  exceeded the average background value by more than  $3\sigma$ . Then, over all the selected pixels of the spot, the differences between the local and average background intensities were summed up to determine the integrated intensity of visual response  $B$ :

$$B = \sum_{i,j} (\beta_{i,j} - \overline{\beta_{bg}}). \quad (2.3)$$

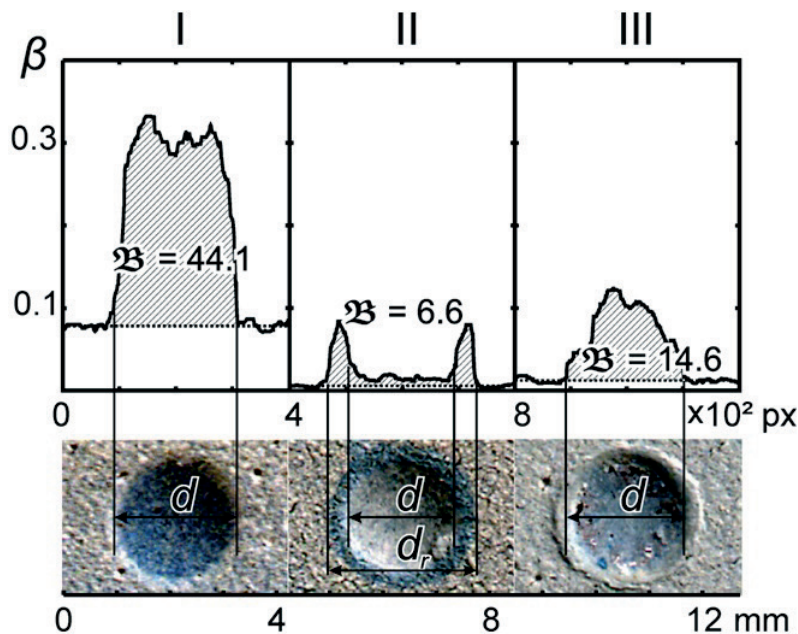


Fig. 2.19. An example of digital image analysis of the bruise spots images in three indication coatings

The quantification of the threshold force for damage initiation is of interest in damage tolerance assessment of load-bearing composites [110]. After this quantification,

the co-ordination of the sensitivity of the visual response in the indication layer embedded to the requirements of a composite designed becomes crucial task. In this research, the value of a threshold of quasi-static indentation load for the visual-response actuation proposed to be adjusted by varying the thickness of the transparent epoxy coating. Relation between the thickness of the epoxy coating and the threshold of a visual response could be determined experimentally.

First of all, a relation was experimentally studied between the integral intensity of response  $B$  and the load  $P$  at a certain thickness of the epoxy coating. The typical relation (at  $z = 1.26 \pm 0.05$  mm) consisted of two parts (Fig. 2.20). At small loads, insufficient to cause any destruction of microcapsules,  $B$  was close to zero. Then, followed a section of practically linear increase when the capsules were destroyed and the spot grew with increasing loading. A visual analysis of the images and a comparison of the maps of local intensity (Fig. 2.20) showed that the intensity of colouring at the spot centre practically did not change. In the load range above the threshold of visualisation, the most of capsules in the centre were broken immediately, and no further bruising was observed with increasing loading. The scatter of the quantities  $B$  was found from several images of the same spot. The point of intersection of the linear growth trend with the abscissa axis was taken as the threshold load  $P^*$  of visual indication, i.e. the smallest load at which a response arose in the specimen. An interval of the error of  $P^*$  was estimated as a scatter of values in constructing the possible linear trends obtained by using different points in the second section and with account of the scatter of  $B$ .

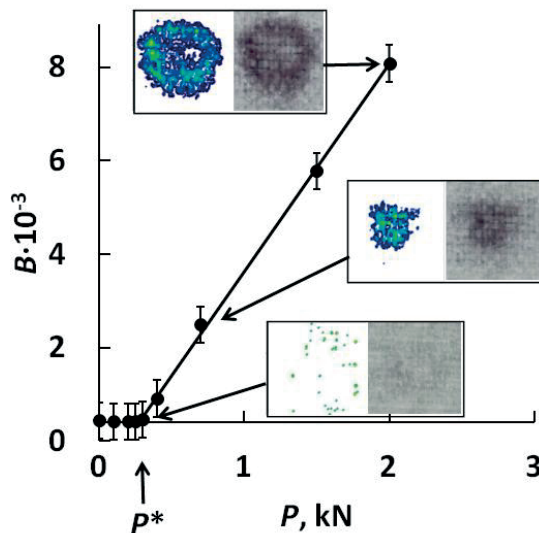


Fig. 2.20. The typical relation  $B$  vs.  $P$ ; the arrows connect experimental points with the corresponding painted maps of the  $\beta_{i,j}$  and bruise images

For different thicknesses, threshold load was established experimentally. The relation  $z$  vs.  $P^*$  (indenter radius  $R = 7.0$  mm) is shown in Fig. 2.21. It was found that

monotonous raising the thickness of epoxy coating from 0.2 to 3 mm was accompanied by the increasing threshold load of visual indication from 0.075 to 1.5 kN. At the thicknesses  $3 < z < 4.5$  mm, the threshold loads exceeded 1.5 kN with further slight increase. In these conditions, the emergence of a visual response was accompanied by a dent remaining on the surface due to viscoelastic and plastic deformations in the coating. Correspondingly, the dashed line at  $z = 3$  mm shows the boundary of elastic behaviour in Fig. 2.21. The variation in experimental results depends primarily on the inhomogeneity of composition of the impregnated indication layer and coating, as well as on the presence of dry spots and small cavities arising as a result of the process of vacuum bag moulding with the use of distribution meshes.

Theoretical estimation of the threshold of response of the indication layer under an epoxy coating because of a mechanical action requires a calculation of the stress–strain state of the coating and the whole composite, with account of their viscoelastic and plastic behaviour. However, of greatest interest for practical applications is the range of small thicknesses of epoxy coatings when no dents were left on the surface of the composite. This means that the action of the indenter looks recoverable but inner damages can exist.

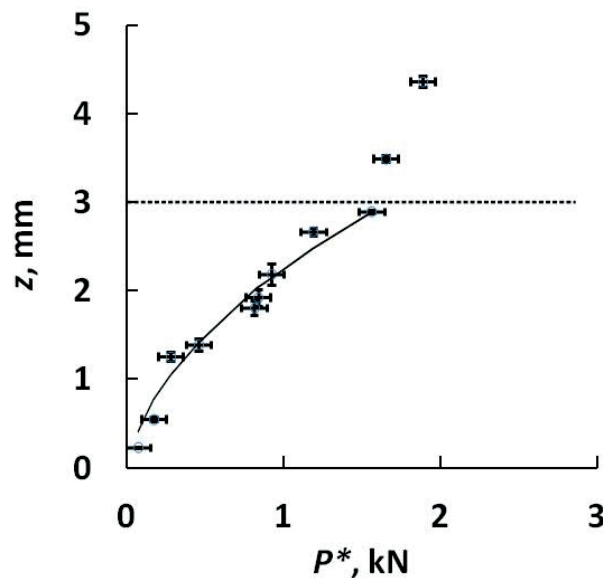


Fig. 2.21. Experimental points of relation  $z$  vs.  $P^*$  and solid line of analytical approximation (2.9)

To model analytically the normal stress arising in the epoxy coating and indication layer interface, the elastic approximation was used. Equation (2.4) from contact mechanics [118] was used to connect the absolute value of normal stress  $|\sigma_z|$  at a depth  $z$  of elastic epoxy semispace with the maximum normal pressure  $p_0$  of indentation:

$$\frac{|\sigma_z|}{p_0} = \left(1 + \frac{z^2}{a^2}\right)^{-1}. \quad (2.4)$$

Here,  $a$  is radius of the contact zone. Further, Hertz's formulae for the frictionless contact of elastic bodies with axial symmetry [118] were used. According to Hertz, the radius of contact zone  $a$  and the maximum normal pressure  $p_0$  arising on contact between an absolutely solid steel sphere of radius  $R$  and an elastic isotropic semispace can be determined as functions of the load value  $P$  according to equations

$$a = \left( \frac{3PR}{4E^*} \right)^{1/3}, \quad (2.5)$$

$$p_0 = \left( \frac{6PE^{*2}}{\pi^3 R^2} \right)^{1/3} \quad (2.6)$$

by using the reduced modulus  $E^*$  of plane strain

$$E^* = \left( \frac{1-\nu_1^2}{E_1} + \frac{1-\nu_2^2}{E_2} \right)^{-1} = 3.7 \text{ GPa}, \quad (2.7)$$

where  $E_1 = 3.1$  GPa and  $E_2 = 200$  GPa are the elastic moduli of an epoxy binder and steel;  $\nu_1 = 0.4$  and  $\nu_2 = 0.3$  are the corresponding Poisson ratios [119, 120]. Thus, formulae allowed eliminating geometric parameter of the contact  $a$  and replacing pressure  $p_0$  by the load value  $P$ . Thus, the dependence  $z = z(P)$  was derived for the depth  $z$ , at which a certain stress  $|\sigma_z|$  arises in the epoxy semispace at an arbitrary load  $P$ . Further, the idealisation of the elastic homogeneous semispace was adopted as an approximation for describing the inhomogeneous in-depth composite with embedded indication layer. The dependence  $z = z(P)$  was transferred to describe the situation when the indication layer is located at different depths of the epoxy. In other words, the layer is covered with the coatings of different thicknesses  $z$ . It was assumed that always the same peculiar normal stress  $|\sigma_z| = |\sigma_z^*|$  arose in the coating on the boundary with the indication layer at the threshold load  $P = P^*$ . The change in thickness of the epoxy coating due to deformation in the contact zone was neglected.

The values of  $a$  and  $p_0$  from (2.5) and (2.6) at  $P = P^*$  were used in (2.4). As a result, we came to an implicit function of the threshold of visualisation of load  $P^*$  relative to the thickness  $z$  of coating:

$$\frac{z^2}{P^{*2/3}} = \frac{3}{2\pi |\sigma_z^*|} P^{*1/3} - \left( \frac{3R}{4E^*} \right)^{2/3}. \quad (2.8)$$

It is obvious that the implicit function has no sense at  $P^* \rightarrow 0$ . Physically, this means that, in this case, there is no reason for actuation of the indication layer. At last, (2.8) obtained explicit final form  $z = z(P^*)$ :

$$z = \sqrt{\frac{3}{2\pi |\sigma_z^*|} P^* - \left( \frac{3R}{4E^*} \right)^{2/3}} P^{*2/3}. \quad (2.9)$$

The value  $|\sigma_z^*|$  was found by fitting the graph of function (2.9) to experimental values of the variables  $P^*$  and  $z$  in the range up to  $z < 3$  mm, where the coating behaved elastically (Fig. 2.21). The minimum sum of squared deviations along the ordinate 0.27 mm and the maximum correlation factor 0.98 were obtained at  $\sigma_z^* = 77 \pm 3$  MPa. The possibility to fit analytical graph to experimental values with high correlation factor indirectly confirmed the admissibility of using the selected analytic approximation. This normal stress magnitude had the order of strength of the epoxy binder and was much higher (more than 30 times) than the pressure of triggering of the pure preform of the indication layer. This can be explained by the fact that only the damage to the epoxy binder, which saturates embedded in composite indicating layer, gives a start to the visual response.

#### **2.2.4. Visual indication efficiency**

The function of visual indication of the mechanical impact is considered efficient for two reasons. The first reason is a highly contrasting visual response that appears rapidly and is easy observable. The second reason is a noticeable shift in stresses of the halochromic transformation – from those causing triggering after capsule shell burst up to the stresses causing damage of the binder in the load-bearing composites. The above interpretation advantageously distinguishes the visual indication function realisation compared to other researches, where the sensitivity to impacts was determined by the strength of microcapsule shells in indication paint. Thus, the problem of potential hypersensitivity of the function is not relevant anymore. The function of visual indication would indicate only those mechanical impacts that can cause the epoxy binder damages. The sensitivity can be adjusted by changing the thickness of the epoxy coating, if necessary. Experiments directly confirmed the efficiency of the function. The thresholds of pseudo-impact load for indication were adjusted from 0.075 to 1.5 kN using the epoxy coating.

### **2.3. Conclusions of the Section**

Load-bearing FRP composites are provided with the additional bio-inspired function of visual indication of impacts for improvement of their reliability. This improvement is achieved through the early detection and subsequent removal of damage caused by the impact.

Analysis of the current problems and trends in the visualisation of mechanical action lead to a development of a new innovative indication layer. The bruisable (with colour response) preform of impact indication layer partly contains the encapsulated two-component chemistry. Together with that, the non-encapsulated active component is

shielded from alkali chemistry of the epoxy binder by protective polymeric coating. The above confirms the corresponding thesis.

A transparent epoxy coating of the indication layer adjusts sensitivity to impacts. The layer with the coating is embedded into composite as an outer layer above load-bearing reinforcement. Manual stacking and vacuum bag moulding process is used for composite manufacture.

The sequence of pseudo-impact indentations is shown on the photographs of visual responses. The original method of digital image analysis is developed to quantify the visual response. Such method allows to exclude an influence of degree of illuminance in a determination of local intensity. One of the research stages includes a modelling of peculiar normal stress that appears in the boundary coating of the indication layer under the threshold load. These activities were carried out to prove the efficiency of the indication function.

A detection of the function sensitivity range that corresponds to the values of the pseudo-impacts is a final evidence of the indication efficiency. It was found that the halochromic transformation starts with the damage of the epoxy binder saturating the built-in indication layer. At that moment, the stress on the indication layer boundary reaches a magnitude of  $77 \pm 3$  MPa. Accordingly, the function of visual indication would indicate only those impacts that can compromise the epoxy binder of load-bearing composite. That confirms a thesis of sensitivity adjustment.

### 3. Vascular Self-Healing

This chapter of the dissertation deals with the second bio-inspired function for reliability improvement of composites – the self-healing (SH) function.

#### 3.1. Current Trends

##### *3.1.1. Self-healing approaches for low-sized damages in thermoset polymers and composites*

Self-healing or self-repairing materials are one of the classes of bioinspired smart materials. These materials possess the ability to change their physical properties in a specific manner in response to a selected specific stimulus in a controlled and predetermined fashion [121]. The self-healing allows to recover physical and mechanical properties thus to prolong useful life of the material. These materials prompted a great interest of the researchers and actively developed in the last 15 – 20 years [122] in leading research centers of the world and Latvia [123]. Significantly, that the term “self-healing” is older and first time has appeared in 1970 in a Latvian journal [124]. A familiar to anybody the first stage of wound healing process (haemostasis), which causes blood bleeding to stop in a case of injury, meaning to keep blood within a damaged blood vessel and which involves coagulation, blood changing from a liquid to a gel is an example of the source of bioinspiration for self-healing materials.

Only a limited number of polymeric materials, for example hard elastic polypropylene, possess the ability to autonomously self-heal in response to damage, while most of other materials require human intervention for repairing damage incurred because of mechanical loads or environment influence. The modern engineering challenge is to understand the principal functional aspects of biological systems that actively react to damage by providing an autonomic healing response at the site of their injury and effectively apply them in designing of synthetic structural materials [125]. Development of composites with self-healing function enable continued operability without reduction in performance due to impacts and prevent further degradation to catastrophic failure. Thus, the lifespan expansion of this materials and structures can be reached.

There exist different manners for self-healing classification in literature. Some experts [126] classify smart materials with self-healing properties into the classes of chemical (reversible) and non-chemical (irreversible) systems. Reversible systems can undergo multiple repair cycles even upon damage at the same site. The systems require an external stimulus, and therefore do not undergo repair autonomously. The representatives of the second class require healing agents to repair damage in the material. Once healed, they cannot be reverted to the appropriate monomers.

The different options for the design of the repair action are the basis for the division of self-healing polymer based systems into stimuli-triggered (assisted) or autonomously healing systems [39, 127]. In this case, vascular systems equally embedded into polymer or composite may be found in different classes depending on whether there is a replenishment agent from an external reservoir or the entire agent stocked in advance.

The common classification is that where the mechanism used to isolate the healing function until triggered by damage is accepted as a basis. SH approaches are often subdivided into three types (Fig. 3.1). The first type is an intrinsic healing achieved by a formation of reversible bond (Fig. 3.1.a). This rebonding requires proximity of the damaged surfaces. Such approach is effective for the damage healing on a molecular scale. The remaining two are capsule-based and vascular types. They are additionally combined into the extrinsic healing by means of triggered release of a pre-added healing system. This system can be embedded within fibre-reinforced composite materials via a liquid healing agent (HA) filled vessels in the form of microcapsules [128, 129] (Fig. 3.1.b) or vascular networks [130, 131] including hollow glass tubes/fibres [35, 79, 132] (Fig. 3.1.c). Capsule-based systems can fill in and heal cavities of damages, the volume of which equals to the volume of broken down capsules. With a common capsule volume fraction, such volumes are ranged from small to moderate (do not exceed usually  $10 \text{ mm}^3$ ) [40].

Vascular systems can deliver a HA to both small and large damaged volumes. Nevertheless, the smallest damage size must be large enough to intersect the vascular network. A liquid HA is usually stored in long channels. The system can deliver a sufficient amount of the HA and heal macroscopic damages. Vascular networks can be replenished by the HA under the pressure, from an external reservoir. In this case, the largest size of healed damage becomes unlimited. These vascular approach capabilities seem to have important advantages over the other approaches.

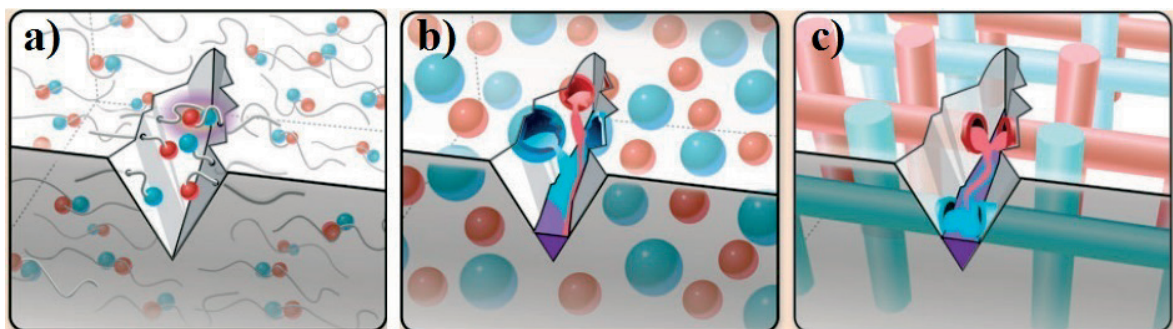


Fig. 3.1. Self-healing approaches: intrinsic (a), capsule-based (b), and vascular (c) [40]

Each approach differs according to the method by which healing function is integrated into the bulk material. Thus, adhering to a review of Blaiszik et al. [40], intrinsic materials contain a latent function that triggers self-healing of damage via:

- a) thermally reversible covalent reactions (e.g. Diels-Alder–retro-Diels-Alder healing system);
- b) hydrogen bonding (e.g. supramolecular elastomeric polymer self-healing materials);
- c) ionomeric arrangements (e.g. poly(ethylene -co-methacrylic acid) self-healing ionomer reversible cross-linking);
- d) dispersed meltable thermoplastic polymers (e.g. linear poly(bisphenol-A-coepichlorohydrin), into an epoxy composite);
- e) molecular diffusion and chain entanglement (e.g. healing of damage in styrene-isoprene-styrene block copolymers and polystyrene).

The most complete and important reviews on intrinsic self-healing which covers various polymer systems synthesis and developments are [37, 38, 40] (mentioned in chapter 1). More modern reviews [126, 127, 133-135] are also noteworthy.

By their nature, intrinsic methods are molecular engineering methods of the polymer in the smallest angstrom- and nanoscale. The repair can occur wherever it is needed without the use of chemical additives and the feed of extra mass. This group of self-healing materials is easier to implement than capsule or hollow fibre/channel based self-healing materials, as the challenges associated with integration and compatibility of healing agent no longer exist [136]. On the other part, as intrinsic self-healing materials do not involve a stored healing agent, it is impossible to recover large-scale damages. At last, the recovery of the bonds and polymer chains requires proximity of the damaged surfaces and needs, as a rule, external energy input usually in the form of thermal energy or photoillumination [40]. The use of high temperatures is required to overcome high viscosity of meltable polymers [135]. The fully autonomous, without the input of external energy intrinsic self-healing succeed relatively readily in soft, rubbery polymers or gels using dynamic bonding [137]. Despite the rapid development of this approach, its application is negligible in structural of polymeric and composite materials. These features stimulate the development of other self-healing approaches.

In capsule-based self-healing materials, the HA is stored in capsules until they are ruptured by damage or dissolved. For self-healing materials, the most common encapsulation techniques are in situ, interfacial, and meltable dispersion [40]. In situ and interfacial encapsulation concept is like that outlined in the previous chapter devoted indication layer development. Since the first successful autonomic self-healing technology in a thermoset epoxy resin [128], multicomponent chemistry is used in this approach. It means that at least one reactive chemical or monomer, usually in a liquid form, is encapsulated and thus sequestered from other chemicals (latent functional

groups, catalysts, and the matrix itself). Thus in [128], dicyclopentadiene (DCPD) was incorporated into capsules and bis(tricyclohexylphosphene)-benzylidene ruthenium dichloride catalyst (Grubbs' catalyst) was housed as a separate phase in the polymer matrix. The microcapsules ruptured by damage release the encapsulated HA microcapsule, the HA flows into the crack plane through capillary action, and then reacts with the catalyst and initiates a polymerization reaction sealing the crack. Depending on the method of placing the second component in the matrix four possible schemes of capsule-based approach are developed. Adhering again to the review of Blaiszik et al. [40], the schemes are divided into capsule-catalyst, multicapsule, latent function, and phase separation schemes. To the latest species, multilayer capsules (all in one type, multi-phase composition) can be included [135].

There are a number, besides above mentioned [37, 38, 40], of modern reviews on capsule-based self-healing achievements [135, 138] as well research articles related such important issues as microencapsulation strategy development or synthesis and characterization new curing agents especially for use in construction polymers and composites [139-141].

The main peculiarity of the self-healing capsules and other additives that are dispersed in a polymeric material is their microscopic scale. Correspondingly they can store and release healing agents to recover damage at this scale (<100  $\mu\text{m}$ ). Particularly, capsule-based approach is effective for retardation of the increase of fatigue cracks as it was demonstrated in a series of works from the University of Illinois [142-145]. Using numerous different healing chemistries and encapsulation techniques, the healing mechanism can be tuned for different matrices and applied to highly crosslinked thermosets [135]. Nevertheless, the microcapsule technique also has several drawbacks:

The volume of the HA is limited by the microcapsule volume fraction. Therefore, it is impossible filling and healing of big cracks with shortage of mass as well multiple healing of the same place of polymer. In turn, the tendency to increase the number of microcapsules in the host polymer gives rise to another group of problems associated with undesirable modification of the polymer. Thus, all microcapsules for polymer self-repair systems use HA and coating material that are alien to the host polymer matrix, resulting often in incompatible ingredients. In any case, the addition of microcapsules and catalysts not only influences the material properties but also the processability (hot pressing, injection or resin transfer moulding, extrusion, lamination, powder coating etc.) of the composites. The severity of these problems has been tested in this study developing the indication layer for damage visualisation. The fracture toughness of the capsule shell wall material should be less than that of the matrix (a crack must rupture the capsules for efficient self-healing), but high enough to withstand the processing conditions. Therefore, the mechanical properties of capsule shells, material, size, and wall thickness need to be considered for each application [135]. The use of popular catalysts (Grubbs' catalyst et

al.) causes additional specific problems. They are very expensive and can be easily poisoned with traditional hardeners based on primary amines [141]. As a result, a concern about the incompatibility of the microcapsules with the resin matrix reduces the potential to be used in industrial applications of capsule-based self-healing [136].

In the vascular approach, the HA is stored in hollow channels or fibres/tubes until damage ruptures the vasculature and releases the HA. Vascular self-healing is organized according to the connectivity of the vascular network. Usually the networks are distinguished among one-dimensional (1D) and multi-dimensional (2D and 3D) [40]. The pioneering work in which the vascular approach was formulated belongs to Dry et al. [34]. In this work, the mechanisms of chemical release from a single millimetre-diameter repair glass-tube embedded in a polymer matrix were investigated using qualitative experimental analyses. Later the development of the vascular systems was based on the use of hollow channels or hollow glass fibres/micro-tubes as vessels to sequester HA.

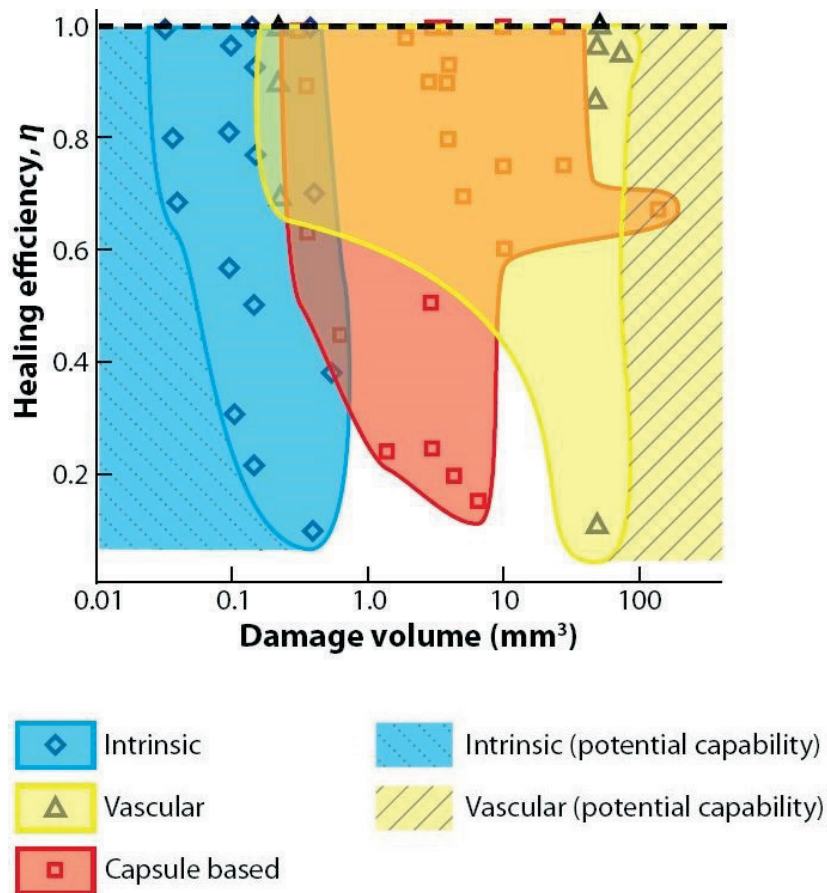


Fig. 3.2. Performance map for self-healing approaches [40]

The main advantage of vascular systems when channels are evenly spread beneath the surface results from the ability to store larger amounts of HA than microcapsules and to heal larger damages of the polymer matrix than with capsule-based and especially intrinsic methods. Blaiszik et al. [40] have submitted a performance maps for self-healing

materials (Fig. 3.2). The data are organized according to the type of self-healing with shaded regions based on data in the literature (plotted as discrete points). Each approach has demonstrated healing for different damage volume regimes. Intrinsic systems are relegated to small damage and can potentially be healed at the molecular scale. Vascular systems have healed much larger damage volumes with shortage of the binder mass and can potentially extend the upper limit for self-healing systems. Capsule-based systems span the gap between intrinsic and vascular approaches.

Since the self-healing of damages of millimetres sizes that can probably be attributed to the macroscopic are in the focus of this research, the more attention will be paid to the vascular approach as the most appropriate for these purposes.

### ***3.1.2. Vascular approach for self-healing polymers and FRP***

Vascular system can deliver an enough liquid HA into the damage place to recover a deficit of composite binder. A system of extended capillaries or hollow channels, which may be interconnected or branched as vasculature, is used for this purpose [40]. The known types of vascular systems use hollow channels [146-153] or hollow glass tubes/fibres [34, 35, 78, 79, 132, 154-157]. The hollow channels are cast along with the polymer or composite. Formative materials then are mechanically removed or decomposed under influence of high temperature and chemical reagents. Channel shaped hollow glass tubes/fibres are also incorporated into a composite at the manufacturing stage, but are not removed later. The HA is often inserted and sealed in the channels at the composite manufacturing stage. Autonomous SH starts by the HA release after a channel rupture in the composite. In this approach, the HA must survive the composite manufacturing process and comply with the terms and conditions of material storage. This restricts the choice of chemical composition of the HA. The restrictions could be overcome if the HA would have been placed into a replaceable or refillable reservoir. The reservoir is attached to the outside of the vascular system after the composite production [40, 151, 153, 155, 157]. The supply of the HA and healing starts after a pump receives definite stimuli. Required amount of HA can be delivered to fill a crack until the maximum possible value. Certainly, in engineering applications, the design of vascular networks includes analysis of the optimum vessel diameter and minimum mass of branching [19]. In addition, the possibility for repeated healing of multiple damages is opened. Although healing cannot occur at the same point for several times, multiple healing events are possible within a certain area, below the surface. The vascular healing network can be refilled from an undamaged but connected region of the vascular system or by an external source. Increased dimensionality of the capillaries adds more reliability, flexibility and increases the number of times healing is initiated, since the damaged area has multiple connectivity to the HA sources [135].

Table 3.1. Vascular self-healing of fibre-reinforced polymer composites and HE values  $\eta$  achieved (also, the data of this research are included)

Composite	Number of HA components	Loading condition	Recovered mechanical characteristic	$\eta$ definition		Ref.
				Maximum $\eta$ (%)		
				Eq. (3.1)	Eq. (3.2)	
Structural, woven glass/epoxy laminate with hollow channels	2	Mode-I DCB fracture	fracture toughness	85-125		[153]
Quasi-isotropic or orthogonal hollow GFR/epoxy laminate	1, 2	impact	compression strength	37	5	[154]
Orthogonal GFR/epoxy laminate with fraction of hollow GFR	2	indentation	flexural strength (4-point bending)	93-97	72-73	[78, 79]
Quasi-isotropic GFR/epoxy laminate with additional hollow GFR self-healing layers	2	indentation	flexural strength	104	130	[132]
Sandwich with GFR/epoxy laminate as vascular core	1, 2	impact	ultimate skin compressive stress	115	150	[155]
Woven GFR/epoxy composite with hollow glass micro-tubes	2	impact	impact property-peak load	95	50	[156]
Woven hollow GFR/epoxy laminate	2	impact	flexural strength/ flexural modulus (3-point bending)	40-73/ 57-89	13-35/ 29-60	[157]
Vascularised quasi-isotropic CFR/epoxy	1	impact	compression strength	94-97	81-91	[158]
UD glass/epoxy composite with hollow channels	2	3-point flexure (short span)	flexural modulus/ dynamic modulus of elasticity		36/ 52	<b>This work</b>
GFR/epoxy laminate stack with embedded CFRP micro-tubes	1	indentation	interlaminar shear strength	71	52	

There are several major drawbacks in the vascular method. They are associated with a possible disbalance between the HA liquid flow properties and properties the release from channels caused by the capillary forces. It would be especially problematic in the case of micro-tubes/fibres. If the two-part chemistry of HA is used, the drawbacks will be also associated with exclusively diffusive mixing of healant and curing agent. The

sufficient mixing strongly depends on the viscosity of the reactants. Inadequate mixing can reduce mechanical properties of the healed matrix [135]. Particularly noteworthy are common drawbacks inherent to all approaches. In most systems, there is no guarantee of matching the healing rate to the damage rate. Usually the first rate is lower than the second one. Only a few exceptions have achieved a balance between healing and damage rates and thus the desired material stasis [40]. The production of SH systems is usually very expensive due to embedment micro-vessels into matrix and chemistry of HA/inherent functional groups and is very complex due to the multistep fabrication.

Analysis of the literature data on types of healed composites, number of HA components, recovered mechanical characteristics, and healing efficiency (HE)  $\eta$  of the vascular systems is presented in Table 3.1. The analysis also shows that insufficient attention has been paid to creation practically available meso-vascular systems for SH of large damage volumes  $\geq 100 \text{ mm}^3$ . These systems can potentially extend the upper limit for SH [40].

### 3.1.3. *Healing efficiency evaluation and mechanical tests of self-healing materials*

One of the first and easiest ways to check the phenomenon of self-healing consists of controlled cracking of a single repair fibre, subsequent release of repair chemical into matrix cracks, and verification using optical microscopy [35].

To date, researchers have proposed several definitions of HE for quantification of the SH [40]. The HE  $\eta$  could be defined as the ratio of a recovered mechanical characteristic in healed specimens  $F_H$  to the same characteristic in virgin specimens  $F_V$  [153]:

$$\eta = \frac{F_H}{F_V}. \quad (3.1)$$

Other definition uses the ratio of changes in a mechanical characteristic of healed after damage relative to a change in this characteristic of virgin in comparison with that of damaged specimen  $F_D$  [40]:

$$\eta = \frac{F_H - F_D}{F_V - F_D}. \quad (3.2)$$

The examined characteristics  $F$  must be matrix-sensitive property e.g. residual compression strength after impact [155], flexural strength/modulus [135], etc. The basic literature data about important for this study characteristics  $F$  and experiments to determine the HE are discussed below.

Early work of Brown et al. [159] employed an approach of fracture mechanics particularly Mode I critical fracture toughness  $K_{IC}$  as a mechanical characteristic  $F$  in (3.1) to investigate crack HE by a microencapsulated HA and a catalytic chemical trigger incorporated in an epoxy matrix. Simultaneously the authors [159] were the first who

used compact, side grooved precracked, tapered double-cantilever beam (TDCB) specimens for rigorous experimental quantification of HE (Fig. 3.3). The side grooves were introduced to these specimens to ensure stable crack propagation and for prevention of loading arm breakoff. The advantage of TDCB fracture geometry was that the specimen possessed region of 30 mm along the centreline with a constant stress intensity factor  $K_{IC}$  for a crack growth. This specimen had been designed and constant- $K_{IC}$  crack length range had been first established through finite-element analyses and experimental verification through quantitative fractographic analysis using the striation measurement technique by Beres et al. [160]. In Mode I fracture tests, the crack length independence of the TDCB negates the need to measure the virgin and healed crack lengths [161] and simplifies calculation of HE to the ratio of healed  $P_C^h$  to virgin  $P_C^v$  critical loads:

$$\eta = \frac{K_{IC}^{healed}}{K_{IC}^{virgin}} = \frac{P_C^h}{P_C^v}, \quad (3.3)$$

since

$$K_{IC} = 2P_C \frac{\sqrt{m}}{\beta}, \quad (3.4)$$

where  $m$  and  $\beta$  are geometry parameters of a TDCB specimen [159]. Particularly the parameter  $m$ , relies on the assumption that the specimen compliance changes linearly with crack length, independent of the groove ratio. [162]. The conventional value of  $m$  for the TDCB geometry as in Fig. 3.3 is  $0.6 \text{ mm}^{-1}$  [159-162]. The second parameter,  $\beta$ , accounts for the impact of the side grooves, weighing the influences of specimen thickness and crack width:

$$\beta = b^{1-\alpha} b_n^\alpha. \quad (3.5)$$

As seen from the linear elastic finite element calculations, the  $\alpha$  value depends on which location along the crack front is being evaluated. Thus, values for  $\alpha$  fall within the bounds of 0.51 and 0.60 obtained at the specimen mid-plane and bottom of the groove respectively [162]. Correspondingly the average value is  $\alpha = 0.56$ .

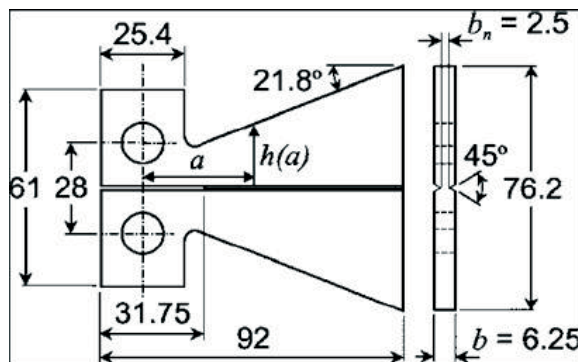


Fig. 3.3. TDCB specimen [159] (all dimensions in mm)

Quasi-static fracture tests using crack opening Mode I of TDCB specimens are widely used for the evaluation of HE of different self-healing systems like that in [100, 128, 159, 163]. Developing microcapsule approach, researchers are forced to seek a balance between quantity of pre-embedded microcapsules and the volume of cracks to be filled by the released-out HA. Usually modified TDCB specimens with a short groove are used to avoid the complete cleaving of a specimen during testing and reduce the crack volume [163-166]. Stiffness of the non-fractured part of a specimen provided closure of faces of the crack after specimen unloading, for the successful self-healing. Kirkby et al. [166] introduced the concept of a fill factor of the crack  $\gamma$ , defined as the relation of the volume of the delivered HA to the volume of the closed crack. Obviously, that effective healing is expected when  $\gamma \geq 1$ . For example, at microcapsule approach the amount of a HA in the damaged area is limited; therefore, one of methods to attain  $\gamma \geq 1$  is the additional constriction of crack's faces in TDCB specimens by shape memory alloy wires [166].

Summarizing the foregoing, we can conclude that the specimens of the TDCB form are very suitable for testing polymers with different self-healing systems in virgin and healed states of the same sample due to specimens provide the controlled and predictable propagation of the crack along the groove. The evaluation of HE needs minimal efforts at that time.

Returning to the question of the HE for vascular self-healing fibre-reinforced polymer composites (see Table 3.1), one can conclude that researchers use of Eq. (3.1) and (3.2) practically equally. Usually, data presented in publications allow additionally calculating both options of the HE. Unfortunately, the more complex structure of the FRP composites and their diversity in comparison with polymers causes profound differences in approaches and makes more difficult to identify preferred embodiments of the self-healing systems using only HE data.

Evaluation of the effectiveness of self-healing system or its elements based on the test results of reinforced composite specimens is a nontrivial task. Quite frequently, compressive residual strength is examined as matrix-dominated property of the material, which is influenced by amount of matrix damage [34]. Thus, compression after impact investigation is used for assessment of structural integrity of developed prototypes of real self-healing structures with hollow glass fibres or internal vascular channels [149, 154, 155, 158]. Since the compression strength is monitored in the plane of stacking during such investigation, the test, in addition to a complex fixture, implies the use of massive and homogeneous in-plane specimens. It is not convenient on the stage of design of architecture of laminated composites and their manufacturing technology [167]. Therefore, some of researchers have used residual flexural strength for evaluation of healing efficiency at the beginning phase of technology development [78, 79, 132]. On the other hand, attempts to use other investigations have not always lead to unequivocal

and convincing estimates of healing efficiency. Thus, the parameters, which have been examined by Zainuddin et al. [156] in the low velocity impact test, indicate the presence of glass vasculature more than the self-healing of a binder. This test does not allow evaluating the effectiveness of the designed self-healing system unambiguously.

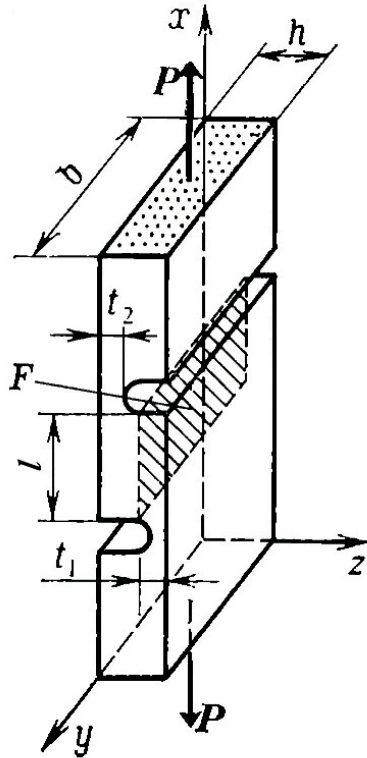


Fig. 3.4. The scheme of tensile loading and the main dimensions of the sample for interlaminar shear testing ( $F$  is the area of the shear zone) [171]

At the stage of novel concept proofing, e.g. concept of using pultruded carbon fibre-reinforced plastics (CFRP) micro-tubes as the vasculature of self-healing layer, a single-layer position of the micro-tubes in GFRP laminate can be chosen. It seems promising to use interlaminar shear strength (between those load-bearing laminae where the layer of vascular channels has been embedded) as the integrity characteristic and the measure of the matrix recovery after self-healing. The tensile test of specimens with two notches fits for this strength monitoring. The method appears as an easy and quick examination of changes of material characteristics in the small area between the notches [168-170] (Fig. 3.4). For a comparative analysis of material strength in the shear zone, inaccuracy of the method [171, 172] caused with a high concentration of stresses near the notches can be neglected. The interlaminar shear strength is determined as an average value of the tangential stress  $\tau_m$ , resulting in the shear zone with length  $l$  and width  $b$  (Fig. 3.4) at a maximum tensile load  $P_{\max}$ :

$$\tau_m = \frac{P_{\max}}{lb}. \quad (3.6)$$

In the case of using this method, self-healing layer placement in laminated composite panel and technology of specimen preparation must be subordinated to the specimen design corresponded to ASTM D 2733 [171].

Selection of the interlaminar shear strength as a characteristic of the integrity of a tested specimen in the area between notches requires testing of specimens up to failure. The strength must be determined experimentally for different specimens in the virgin, damaged, and healed after damage states to evaluate the self-healing efficiency in accordance with (3.2).

### **3.2. Function of Autonomous Self-Healing**

In this research, the strategy of development practically available meso-vascular system for self-healing of large damage volumes  $\geq 100 \text{ mm}^3$  was chosen. A big area layer of one-dimensional system of hollow channels embedded into a laminated composite material can extend the upper limit for self-healing systems. A HA of easily accessible chemistry filled in the meso-channels can be delivered to a place of damage autonomously after triggering of the SH. The chemistry can be polymer resin and appropriate hardener. The components are stored as a two-part healing system in separated channels. The channels form a layer in the most vulnerable places of the binder between load-bearing reinforcement layers of the composite. After rupture, cross-linking of the HA released and rebonding of the cracks is feasible. Thus, the repair of the matrix and restoration of mechanical properties of the composite could be achieved.

The purpose of this study is to test practically the possibility of creating self-healing layer on the base of meso-vascular system in laminated composites and evaluate their self-healing efficiency.

#### ***3.2.1. Self-healing of epoxy binder: preparation and experimental verification***

A preliminary study was conducted to manufacture the meso-vascular system. This study included the choice of the HA, creation of unidirectional SH channels, and evaluation of HE for pure epoxy binder specimens of TDCB geometry. The drawback of traditional TDCB specimens is the complete cleaving during the tests. The joining of the crack faces manually is a routine practice when the capsule-based SH is studied. In this study, the specimen was modified with a hole drilled through the groove at foundation part of the TDCB as a crack propagation limiter. It was an alternative approach instead of accepted use of short groove specimens. After unloading, a crack was not fully closed in such specimen. The residual separation of the crack faces was the consequence of

viscoelastic and plastic behaviour of the polymer. If self-healing of the crack occurs without additional mechanical action for the compression of the faces, which is more realistic scenario, the knowledge about crack volume and correspondingly about amount of necessary healing agent becomes important. Considering, that crack length is approximately equal to the groove and the groove thickness is known in the TDCB specimens the task of actual crack volume determination could be reduced from direct measurement to the crack width measurement. Estimation of crack face separation directly was made by transmitted light microscopy technique in different places along the crack (Fig. 3.5). There was revealed that average face separation was  $5 \pm 2 \mu\text{m}$  and corresponding crack volume was  $0.5 \pm 0.2 \text{ mm}^3$  for different TDCB specimens manufactured from several room-temperature hardened bisphenol-A-(epichlorhydrin) epoxy resin types. Values of stiffness of the non-fractured part of these specimens were in the range 50 – 150 N/mm.

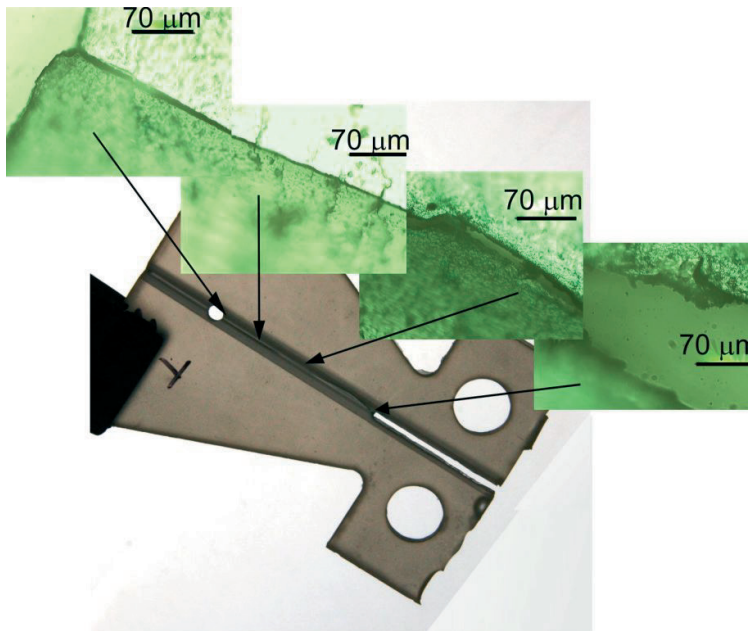


Fig. 3.5. Epoxy TDCB specimen with a crack and transmitted light microscopy images made in several places along the crack

Additional independent evaluation of the crack volume was conducted by capillary method using the same specimens. The matter of the latest method was weight monitoring of the specimen with the crack, which is filled with dyed ethanol using surface tension forces. Ethanol was used due to the liquid perfectly wetted epoxy. Alcohol was injected from a syringe into slightly unclamped crack. Excess of liquid after clamping was partly removed with paper absorber. Unfortunately, guaranteed wetting of crack's surface implies wetting of the groove surface too (Fig. 3.6). To separate ethanol quantity filled the crack, from that in the groove; kinetics curves of alcohol volatilization were

measured. If alcohol weight is presented in logarithmic axis for the same specimens, it is easy to see two kinetics intervals (Fig. 3.7). The first interval of quick volatilization is attributed to volatilization from the groove walls but another one to volatilization from the crack. Place of inflection of the curve corresponds weight of alcohol in the crack. Collected data allowed estimating average crack volume as  $0.8 \pm 0.2 \text{ mm}^3$ . The analogous results of measurement obtained by both methods gave the assessment of the HA quantity necessary for full filling of the crack of volume  $0.3 - 1.0 \text{ mm}^3$  for successful self-healing.



Fig. 3.6. Epoxy TDCB specimen with a crack filled by green dyed alcohol

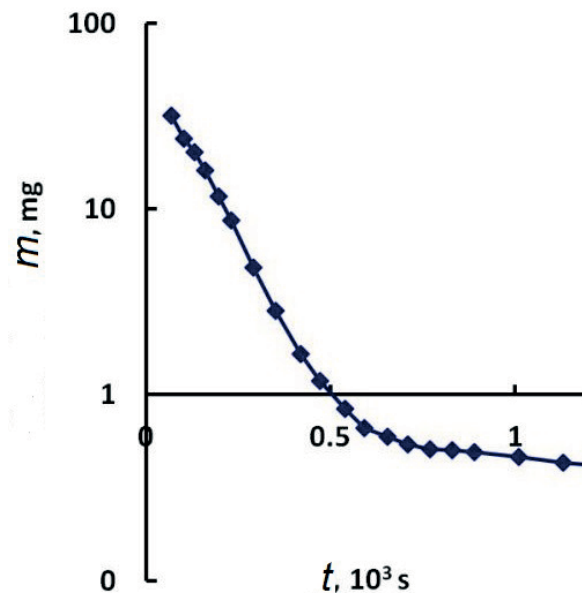


Fig. 3.7. Crack injected alcohol mass  $m$  vs. time  $t$  for a TDCB specimen

The second auxiliary task was to select suitable chemistry of the HA for the use in channels of the self-healing layer. To select potential HA the simulation of crack recovery via manual healing was sufficient procedure. The manual simulation of healing process

was carried out on six fractured epoxy TDCB specimens. The specimens were manufactured from bisphenol-A epoxy resin NM Laminering 275A cured by hardener NM Härdare 275 (Nils Malmgren AB). The specimens were tested in virgin and healed states. The healing efficiency was determined using (3.3). Two candidates were examined as possible HA i.e. ethyl cyanoacrylate glue (Fig. 3.8) and epoxy resin-hardener stoichiometric mixture (Fig. 3.9). The healing efficiency  $\eta$  with cyanoacrylate glue during 2 h at 20 °C was  $1.0 \pm 0.2$  but with epoxy mixture during 72 h at 20 °C was  $0.8 \pm 0.2$ . Despite the high healing rate and efficiency that were demonstrated in the preliminary experiments, the cyanoacrylate glue would show significant disadvantages when would be used as a HA. It is generally known, that cyanoacrylate rapidly polymerises in humid and alkali environment. This will cause problems with the shelf life of the HA in the hollow channels within the epoxy matrix, if amine hardeners have been used for matrix curing. At last, the self-healing process itself will need moist atmosphere, which reduces the versatility of the self-healing.

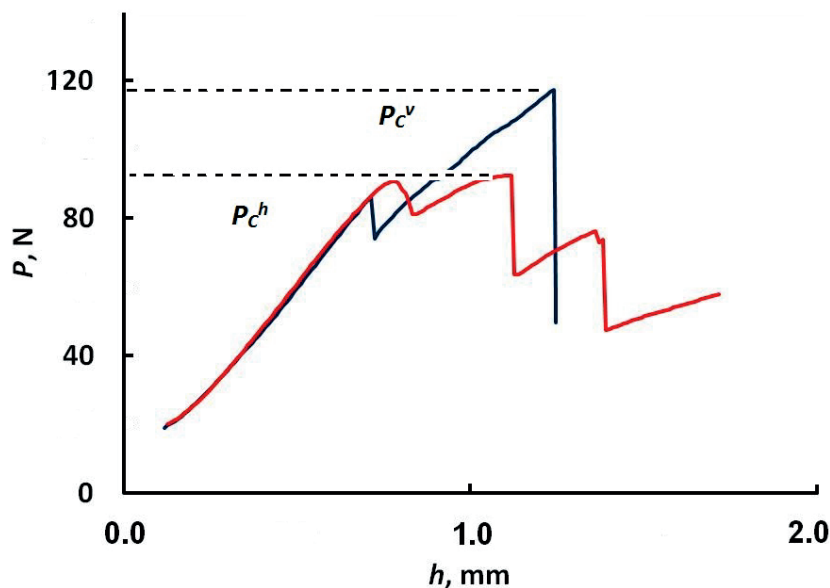


Fig. 3.8. Representative load  $P$  vs. displacement  $h$  curves of a TDCB specimen manually healed using ethyl cyanoacrylate glue

On the contrary, epoxy resins are important for healing chemistries because they can react with a wide variety of curing agents or hardeners at different temperatures and have affinity the epoxy based composites subjected to healing [140]. The positive result of manual healing allowed selecting the epoxy resin and hardener as HA for the following autonomous SH of TDCB specimens. The idea of further research was to use a two-part HA (the resin and hardener would be stored in channels separately). The base assumption was that acceptable polymerisation of components of HA will take place in real self-

healing conditions even if the mixing due to diffusion in the crack will not be in strictly stoichiometric proportion.

Thus, the conducted preliminary experimental research (crack volume determination and HA choice) served as a basis for development of practical self-healing layer on the base of meso-vascular system in epoxy matrix specimens of TDCB geometry.

The autonomously SH TDCB specimens were made from a room-temperature cured bisphenol-A-(epichlorhydrin) epoxy resin NM 275A and amine hardener NM 275B (Nils Malmgren AB, Sweden) mixed in a mass proportion 100 : 55 as recommended by the manufacturer. According to the technical data, the epoxy resin and hardener have the following characteristics, respectively: density 1.15 and 1.0 g/cm<sup>3</sup> at 20 °C; viscosity 2000 and 150 mPa·s at 25 °C.

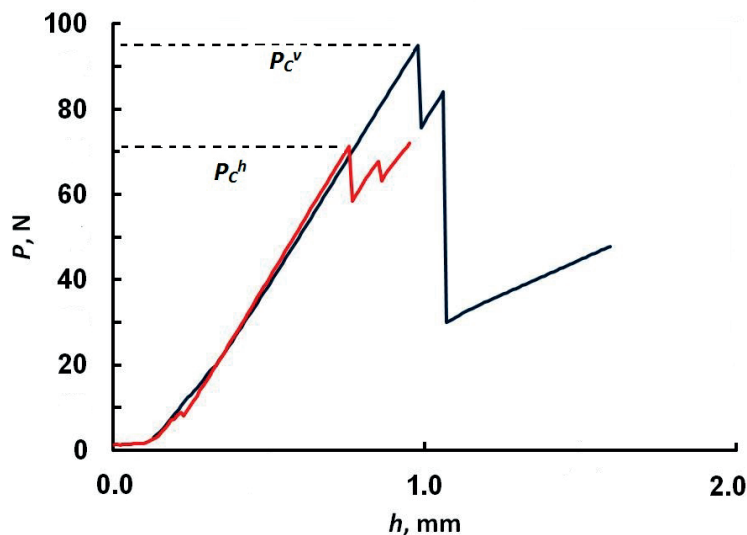


Fig. 3.9. Representative load  $P$  vs. displacement  $h$  curves of a TDCB specimen manually healed using resin and hardener stoichiometric mixture

A series of more than 10 TDCB specimens (Fig. 3.10) and basically proposed in [159] was poured in a closed silicone rubber mould, where five parallel-prestretched fragments of polytetrafluoroethylene (PTFE) tube of 0.9 mm diameter (TFT20028 Alpha Wire) were placed in a 5 mm distance from each other to form vascular channels. After the epoxy system curing during 15 hours at 50 °C, PTFE tubes were pulled-out from the TDCB specimens. According to the chart shown in Fig. 3.10, the hollow channels formed were filled with a two-part HA system comprising of epoxy resin NM 275A additionally containing 20 % vol. surfactant 4-nonylphenol (Acros Organics) to improve wettability and hardener NM 275B. After filling, the ends of channels were sealed. For a crack initiation, TDCB specimens were notched with a fine blade. A hole as a crack

propagation limiter was drilled through the groove at foundation part of a TDCB specimen (Fig. 3.10).

The upper bound for possible crack volume, which is necessary to fill by the HA is  $1 \text{ mm}^3$ , and the total amount of the agent stored in the layer of vascular channels is greater than  $100 \text{ mm}^3$  (the geometric evaluation). The fill factor of the crack  $\gamma \gg 1$ . Such HA reserve is a guarantee to ensure complete filling of the crack with released HA, as a prerequisite for a successful self-healing.

Fracture toughness of the TDCB specimens was determined using (3.4) with above mentioned geometry parameter values, particularly:  $m = 0.6 \text{ mm}^{-1}$  and  $\beta = b^{0.44} b_n^{0.56}$ <sup>1</sup>. Healing efficiency  $\eta$  was estimated as a ratio of fracture toughness  $K_{IC}$  determined for each TDCB specimen in virgin and healed state in accordance with (3.3).

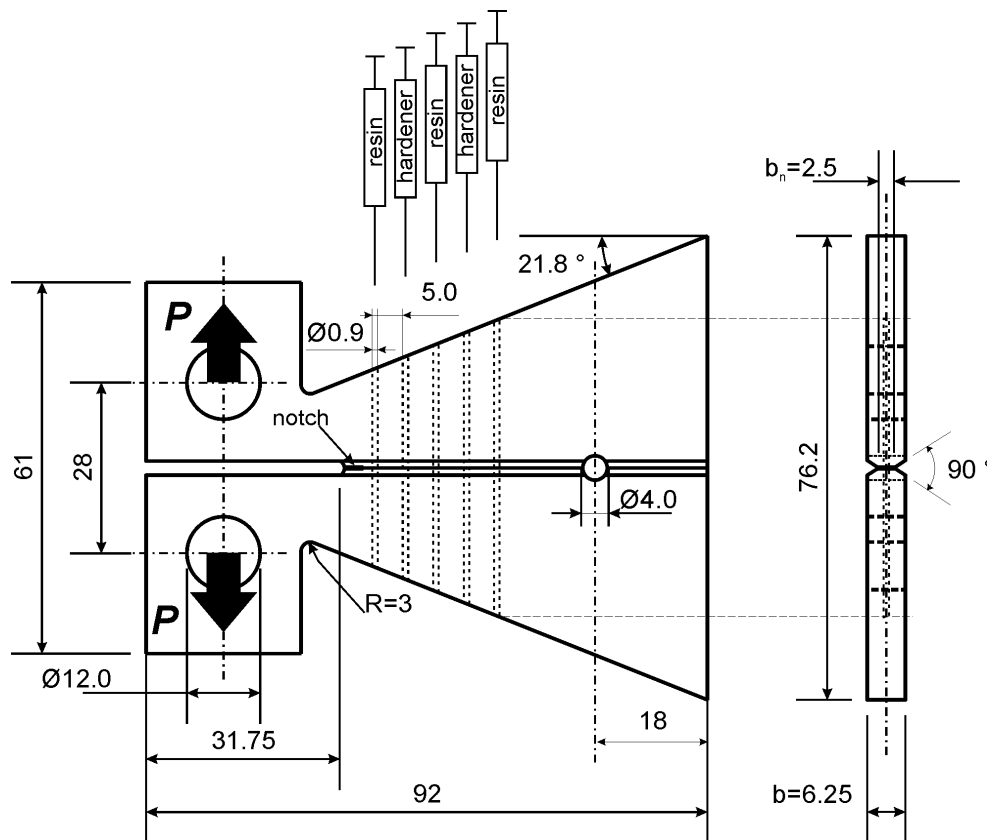


Fig. 3.10. TDCB specimen with 5 channels filled with two-part HA system

Virgin specimens with vascular system filled with the HA were subjected to fracture tests. under displacement control. The tests were carried out on the electro-mechanical testing machine Zwick 2.5 under displacement control, with speed 1 mm/min in three days after HA filling. The unloading occurred when a growing crack reached the limiter. Eight specimens survived the fracture test. Immediately after the tests, the top entries into the channels were unsealed to ensure a free flowing-out of the HA system

<sup>1</sup> The calculation of exponents of the formula was made using finite elements method by Dr. S. Tarasov.

inside a cracked region. Then, the specimens were kept at 50 °C during 24 h to cure the HA, which flowed out into the cracked region. View of a self-healed TDCB specimen is shown in Fig. 3.11.

After the first SH procedure, all these specimens were tested again. Six specimens were subjected to the second SH procedure and followed fracture tests. The representative relationship between applied load  $P$  and displacement  $h$  of the TDCB specimen ends is shown in Fig. 3.12. Values of fracture loads  $P_c^v$ ,  $P_c^h$  and,  $P_c^{hh}$  corresponding to crack initiation in a virgin, once, and twice healed states of the same specimen, are indicated in the ordinate.

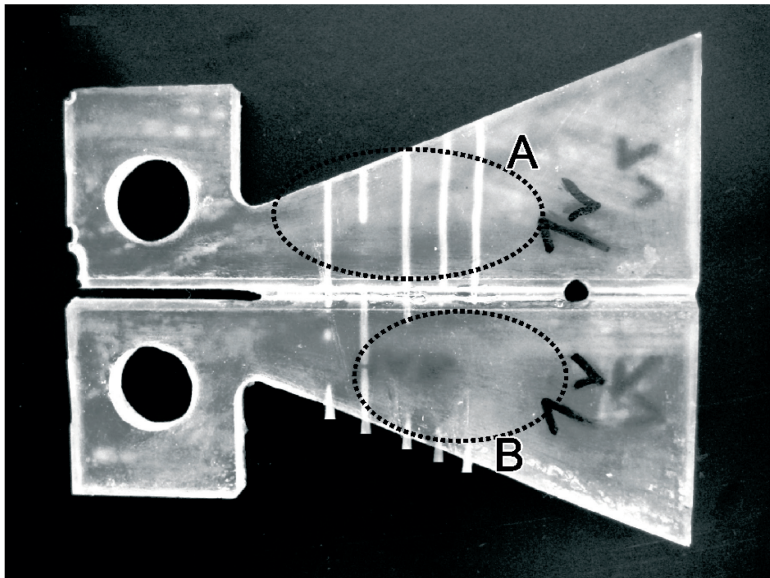


Fig. 3.11. TDCB specimen after self-healing: the channels in the upper part A are empty since the HA flowed out into the cracked region while the channels in zone B remain filled

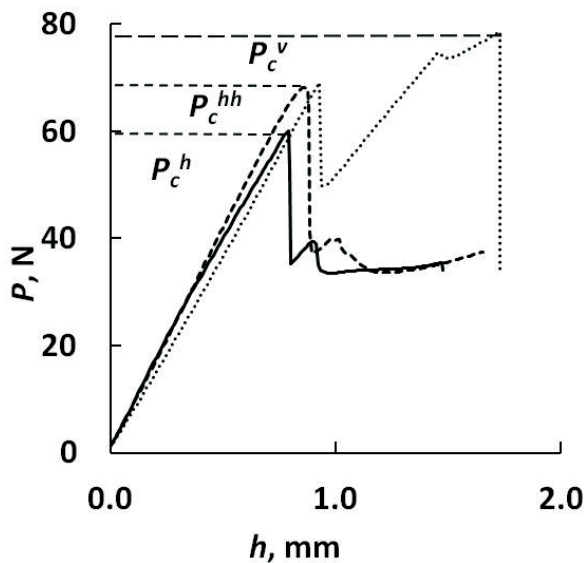


Fig. 3.12. Representative load vs. displacement curves of the virgin (dotted line), once healed (solid line), twice healed (dashed line) TDCB specimen

Experimental results obtained in fracture tests, including healing efficiencies  $\eta^h$  and  $\eta^{hh}$  of the specimens once and twice healed correspondingly, are summarized in Table 3.2.

The fracture tests demonstrated average HE  $\eta^h = 69 \pm 15$  %. The second healing increases efficiency  $\eta^{hh} = 93 \pm 29$  %. The revealed high dispersion of the HE reflects stochastic property of processes viz., fracture of specimen, mixture of released two-part HA, and subsequent cross-linking during fracture rebonding. Thus, variance increases from  $\eta^h$  to  $\eta^{hh}$  due to re-fracture and second self-healing. Mixing of the HA components (epoxy resin and hardener) along the whole length of cracked region has accidental character that usually would not provide the required stoichiometric ratio (100 : 55). As a result, HA does not get a degree of cross-linking in the space of crack as a native epoxy. If the previously healed substance had released in surplus quantity and by chance toughly cured, the second propagating crack could veer from the centre-line of the groove. It led to apparent increase in self-HE i.e. sometimes  $\eta^{hh} > 100$  % was observed, as well as in [100, 173]. Important, that experimental comparison of TDCB specimens with and without channels showed practically same average fracture toughness values  $K_{IC} = 1.20 \pm 0.23$  MPa·m<sup>1/2</sup>. This fact proved that system of vascular channels itself embedded into TDCB specimen does not degrade fracture toughness.

The results inspired the manufacture SH FRP composite with channel layer built-in between load-bearing glass-fibre-reinforcement yarns.

Table 3.2. Experimental data of TDCB specimens

No	$P_C^v$ , N	$P_C^h$ , N	$\eta^h$ , %	$P_C^{hh}$ , N	$\eta^{hh}$ , %	$K_{IC}^{virgin}$ , MPa·m <sup>1/2</sup>
1	54.6	40.3	74	22.2	41	1.08
2	68.4	34.8	51	55.5	81	1.07
3	43.1	41.0	95	70.3	163	0.82
4	75.0	42.7	57	54.6	73	1.29
5	80.4	44.9	56	–	–	1.54
6	65.7	58.0	88	71.6	109	1.07
7	78.5	60.1	77	72.4	92	1.31
8	72.9	37.4	51	–	–	1.31
Mean			69 ±15		93 ±29	1.18 ±0.17

### 3.2.2. Self-healing of FRP composite: development and experimental verification

The procedure that was proved by creating of SH system for epoxy resin, was applied for fabrication of the vascular channels layer filled with the two-part HA in FRP composite plates (Fig. 3.13). Thus, multiple sets of five PTFE tubes each were prestretched at 4 mm from each other. The sets were embedded into the manual stack between two layers of unidirectional constructive glass fibre yarns (500 g/m<sup>2</sup>) and aligned

with them. Two restrictive outer layers of plain glass fabric (AEROGLASS, 110 g/m<sup>2</sup>) were stacked on the top and the bottom of the yarns. Room temperature curable epoxy resin LH289 with hardener H289 (with stoichiometric ratio 100 : 33) was used as a binder (Havel Composites CZ s.r.o [109]). The stack with channels shapes was infused with epoxy resin using vacuum assisted resin transfer moulding (VARTM), which had been cost-effective manufacturing processes for composite components [174]. Thus, two series of plates (250 × 300 × 1.2 mm<sup>3</sup>) designated B and C were manufactured. A series of plates without vascular channels designated A was manufactured too. After curing, the PTFE tubes were easily removed. The specimens (250 × 23 × 1.2 mm<sup>3</sup>) with embedded five-channel layers into binder were cut from the plates B and C. The same size specimens were cut from the plate A. Likewise in TDCB study, epoxy resin NM 275A with additive of 20 % vol. surfactant 4-nonylphenol and hardener NM 275B were used as a HA system. Channels in the B-specimens were filled up only with the epoxy resin, while both components of HA system were used in the C-specimens. The resin was in the channels 1, 3, 5 and hardener was in channels 2 and 4. After filling, all channels were sealed with epoxy mastic. C-specimens were kept at the laboratory conditions during 1 – 3 weeks, 2 – 3 months, and 5 – 6 months. As result the FRP composite C-specimens were manufactured with additional autonomous SH function.

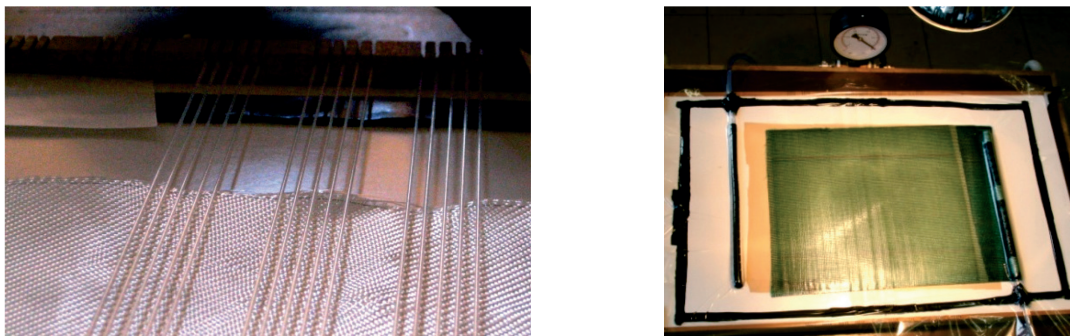


Fig. 3.13. Views of manual stacking of a plate preform with PTFE tubes (left) and VARTM process of plate manufacture (right)

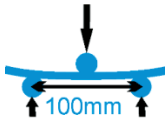
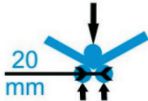
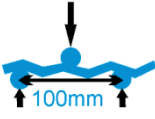
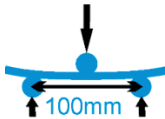
To evaluate the HE, the apparent static flexural modulus  $E^f$  was chosen as the mechanical characteristic  $F$  in (3.2):

$$E^f = \frac{Pl^3}{4bh^3w_{\max}}, \quad (3.7)$$

where  $b$  and  $h$  are width and thickness of flat specimen;  $l$  is span between the supports;  $P$  is applied load;  $w_{\max}$  is specimen deflection at the centre. The apparent modulus is quite sensitive to changes in the ratio of the elastic moduli of the matrix and reinforcement of the composite [171]. The changes in the ratio will take place both after damage and after

SH of the binder. The sequence of experiments to determine  $E^f$  included five principal steps, which are shown in Table 3.3. The steps 1, 3, and 5 consisted in the evaluation of the flexural modulus of all specimens of the series A, B, and C in virgin, damaged, and healed conditions respectively. Universal testing machine Zwick 2.5 was used for three-point flexure tests at constant crosshead rate of 1.2 mm/min and span  $l = 100$  mm. In the step 2, all samples were subjected to the procedure of mechanical damage tailored to rupture the specimen matrix and the channels. Multiple damages were performed ca. every 12 mm along the specimen length. The damages each were obtained in bending tests with span of 20 mm (Fig. 3.14). The loading continued up to the ultimate stress. The test was completing, when applied load reduced by ca. 30 % of maximum value in the load-displacement curve. Visual assessment verified the multiple breakages of the vascular channels and HA release in filled specimens. At least 20 % of the specimen area had the damages. It gave the assessment of the total volume of damaged composites more than 1000 mm<sup>3</sup>. In the step 4, all damaged specimens were subjected to a heat treatment at 50 °C during 24 h to heal them.

Table 3.3. Stages of sequence of experiments

Step 1	Step 2	Step 3	Step 4	Step 5
Determination of $E_{virgin}^f$	Multiple damaging of specimens	Determination of $E_{damaged}^f$	SH of specimens	Determination of $E_{healed}^f$
				
Three-point flexure tests with span of 100 mm or 20 mm (Zwick 2.5 at crosshead rate of 1.2 mm/min)			Finally, retention >3 weeks at 20 °C	Three-point flexure tests after SH and after retention

After these tests, specimens were subjected to more than 3 weeks long retention at 20 °C and repeatedly tested in three-point bending with span of 100 mm as in the step 5.

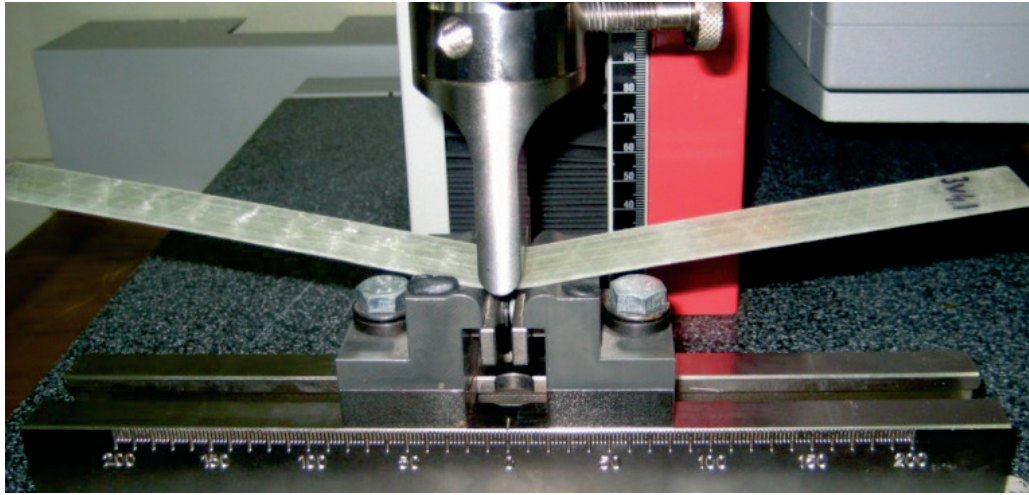


Fig. 3.14. Multiple damages in the specimens by three-point flexure loading with a short span

Efficiency of self-healing  $\eta$  was estimated in accordance with (3.2) as a ratio of changes of the flexural modulus:

$$\eta = \frac{E_{healed}^f - E_{damaged}^f}{E_{virgin}^f - E_{damaged}^f}. \quad (3.8)$$

The experimental data processed are summarized in Table 3.4. The results obtained in the three-point bending tests are presented in the numerators of this table. The specimens without channels (A) and with all channels filled up with only resin (B) served as reference specimens. The results indicate that creation of the vascular channels and their fill-up with resin or HA do not practically change modulus  $E_{virgin}$  in comparison with the reference specimens without channels.

Table 3.4. Elastic modulus and healing efficiency of flat specimens determined in static (numerators) and dynamic (denominators) flexural tests

Specimen series		$N$	$E_{virgin}$ , Pa	$\eta$ , %	
				24 h, 50 °C*	3 weeks or more, 0 °C**
A	Without channels	9	$24.4 \pm 0.6$	$9 \pm 7$	$10 \pm 4$
			$21.7 \pm 0.8$	$3 \pm 8$	–
B	Resin in channels	3	$25.5 \pm 1.6$	$14 \pm 7$	$15 \pm 5$
			$26.4 \pm 1.3$	$13 \pm 11$	–
C	HA in channels 1-3 weeks***	13	$25.2 \pm 2.0$ $23.3 \pm 2.0$	$36 \pm 6$	$52 \pm 7$
				$50 \pm 12$	–
	HA in channels 2-3 months	12		$22 \pm 6$	$26 \pm 7$
			$29 \pm 9$	–	
	HA in channels 5-6 months	6		$26 \pm 6$	$32 \pm 10$
				$35 \pm 8$	–

\* for heat treated specimens; \*\* for specimens after prolonged room retention; \*\*\* retention before damage;  $N$  is number of tested specimens.

There was awareness in the research that values of  $P$  and  $w_{\max}$  directly determined in tests are dependent on mutual arrangement of a load/support point position and local damages of a specimen. Thus, such integral characteristics as the apparent flexural modulus calculated using (3.7) and healing efficiency estimated by (3.8) could become dependent on distribution of local damages in a specimen. To confirm the validity of using the apparent flexural modulus for evaluation of healing efficiency for lengthwise inhomogeneous specimens, another experimental method was applied. Dynamic modulus of elasticity for virgin and healed specimens was determined by method of cantilever beam vibration [175]:

$$E = \frac{12m}{bh^3L} (2\pi f)^2 \left( \frac{l^2}{3.515625} \right)^2, \quad (3.9)$$

where  $m$  is mass of specimen;  $b$  and  $h$  are width and thickness of flat specimen;  $L$  and  $l$  are total and unclamped length of specimen;  $f$  is a frequency of the first natural mode of vibration.

Values of  $\eta$  calculated by (3.8), (3.9) using data of cantilever beam vibration tests for heat treated specimens are presented in the denominators of Table 3.4.

Firstly, the results obtained indicate that creation of the vascular channels and their fill-up with resin or HA does not practically change modulus  $E_{\text{virgin}}$  in comparison with the reference specimens of series A. Thus, elastic modulus determined in static tests is  $(24.4 \pm 0.6)$  GPa for specimens without channels and  $(25.2 \pm 2.0)$  GPa for specimens with HA in channels (Table 3.4) are sufficiently close. The values of elastic moduli obtained by both methods are close for lengthwise homogeneous specimens. The apparent static flexural and dynamic moduli of damaged and healed (lengthwise inhomogeneous) specimens more differed and have high dispersion. The objective reasons of the scatter of self-healing efficiency are similar to the reasons of the scatter of self-healing TDCB specimens.

Additional cause is irreproducibility of the total sample damage via the multiple discrete acts of damage affecting randomly not only the matrix of composite, but often reinforcing fibres in the specimens. In the experiment, it causes a high variation of the starting conditions before the self-healing for the different samples. The results more reflect achievable recovery of specimens in self-healing conditions close to the real performance and warn of high healing efficiency scatter, in comparison with the results of other more sophisticated and model experiments. Nevertheless, both estimations of the self-healing efficiency obtained using three-point bending and cantilever beam vibration methods are in good agreement in principle. Thus, static as well as dynamic flexural moduli of flat specimens may be successfully applied for qualitative and quantitative estimation of the healing efficiency.

The main conclusions about healing efficiency are based on comparison between the results of samplings with volume from 9 to 13 trials (specimen series A and C). These samplings provide in fact information about the order of estimated values and their variances. Experimental results reveal that reference A- and B-specimens do not recover their integrity. A small increase of  $\eta > 0$  (flexural tests) for heat treated specimens and then constancy of this value at the prolonged room retention (see Table 3.4) can be explained by polymerisation peculiarities of room-temperature curing epoxy binders used in this investigation. An exothermic nature of polymerisation of these binders, reduces the composition gel time, and causes its uneven curing and incomplete conversion of the epoxy groups [176]. Therefore, the additional heat treatment, which caused a greater degree of conversion of the epoxy groups in layered composite, has led to the observed increase of its elastic modulus and healing efficiency.

The experimental results testify that C-specimens with vascular channels filled with HA can be self-healed with a sufficiently high healing efficiency reached up to 36 % in static and 50 % in dynamic flexural tests for heat-treated specimens. Moreover, it is seen that C-specimens retained the high enough ability to self-healing at least six months after manufacturing. The efficiency reached 26 % and 35 % in the mentioned already tests. The process is time dependent and the efficiency  $\eta$  can increase (e.g. from ca. 36 % to 52 % in flexural tests) during the subsequent long-term SH retention of the samples at room temperature. The proposed technique for building-in the layer of vascular self-healing channels provides SH of large-scale damages.

### **3.3. Function of Self-Healing under Pressure**

The presence of SH channels reduces the volume fraction of reinforcement in the composite. This may not be desirable in terms of specific load-bearing capacity of SH composites, when compared with conventional composites [177]. Use of hollow glass micro-tubes as the vascular channels does not fully compensate the reduced strength. Filling of the SH vasculature with a liquid HA gives an additional weight, which is critical for high-performance load-bearing applications [155]. Consequently, the development is topical of such vascular channels layer for healing system, which allows overcoming aforementioned restrictions of traditional self-healing vascular channels and can restore specific load-bearing capacity.

This work is aimed for development and experimental proof of a novel concept of using high modulus pultruded carbon fibre-reinforced plastics (CFRP) micro-tubes as the vascular channels for HA and implementation of this approach for laminated GFRP panels.

### 3.3.1. Preparation of carbon FRP micro-tube layer

To check suitability of the micro-tube for a liquid delivery through it and this liquid storage, then to check capability to release the liquid into damaged GFRP upon impact a simple unidirectional glass-fibre specimen with one embedded micro-tube has been made. A model indentation test has been carried out on the specimen (Fig. 3.15) because carbon fibre micro-tube should behave stiffer and stronger than the surrounding codirectional glass fibre reinforcement under the tensile, compressive, or bending loading. These mentioned loadings damaging the specimen could leave undamaged the micro-tube without releasing of the liquid. Firstly, it has been revealed that the CFRP micro-tube, which is filled with a liquid dye and embedded into GFRP specimen, keeps the liquid as a vascular channel until its rupture. During the indentation, crumpling of the specimen laminas accompanies cracking of the micro-tube (the dashed line in Fig. 3.15) and release of the stored liquid. The green area in Fig. 3.15 illustrates as the dye fills microcracks as it could make a liquid healing agent. Although in the work, different non-destructive methods have not been used visual inspection, which is not particularly accurate, shows that the liquid dye cannot permeate all microcracks. There are matt areas on a large distance from the micro-tube Fig. 3.15. It is necessary to reckon with possible incomplete HA infiltration in real self-healing experiments. Nevertheless, a result of the indentation test has instilled confidence in the ability to use the micro-tubes as the vascular channels. The subsequent tasks were interrelated. They consisted of making of a CFRP micro-tube layer, its embedment, and the HE assessment of the realised vascular SH function in a composite.

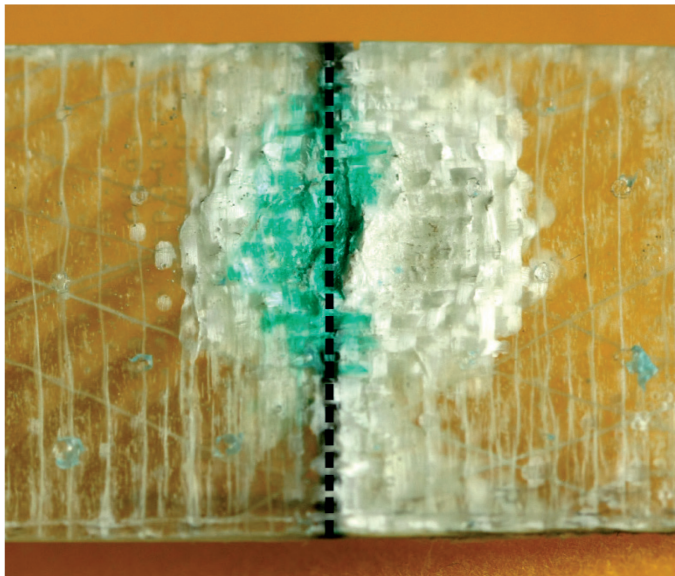


Fig. 3.15. A CFRP micro-tube embedded into GFRP releases liquid dye after indentation

Table 3.5. Physical and mechanical properties of DPP<sup>TM</sup> high performance micro-tubes [178]

Outer/ inner diameter, mm	1.0 / 0.5
Specific weight, g/m	0.80
T <sub>g</sub> (binder), °C	120
Average fibre fraction, %	63
Tensile strength (virgin fibre), MPa	4900
Tensile modulus (virgin fibre), GPa	230
Tensile strength (CFRP), MPa	2500
Tensile modulus (CFRP), GPa	140
Compression strength (CFRP), MPa	1600
Ultimate elongation, %	2

GFRP laminated panels for a specimen production were manufactured using room-temperature-cure two-component epoxy binder: Bisphenol-A-(epichlorhydrin) resin LH 288 (viscosity 500 – 900 mPa·s at 25 °C) and amine hardener H 284 with stoichiometric ratio 100 : 23 [109]. The epoxy gel time of 150 – 180 min. was sufficient for impregnation and hand lay-up stacking of reinforcement layers and placement of a CFRP micro-tube package between the layers. Unidirectional E-glass fibre yarns connected by network UD 500 [109] with a surface density of 500 g/m<sup>2</sup> were used as the reinforcement.

Laminated fiberglass panels with the micro-tube layer embedded were produced by vacuum bag moulding process. For this purpose, a bleeder fabric, perforated release film, and four layers of glass fibres impregnated with a binder were sequentially stacked on the working surface, with the layup sequence (0/90)<sub>2</sub>. Then, a planar package of five, closely adjacent to each other CFRP micro-tubes was stacked in the direction of 90°. The mutual arrangement of the micro-tubes with hard contact (without spacing) was fixed with adhesive tape at the ends of the package. Next four (90/0)<sub>2</sub> layers of fiberglass were laid-up on the stack with micro-tubes package. The general stack was covered by perforated release film and bleeder fabric. The ends of micro-tubes were sealed to prevent ingress of the binder during fiberglass manufacture. Pressing and curing of the planar composite panels were processed in a vacuum at a pressure 0.4 bar and temperature 40 °C for 20 hours. At first, composite panels were postcured at 95 °C for 24 hours and then at 50 °C for 24 hours.

Test specimens with dimensions  $L \times b \times h = 115 \times 15 \times 3.3$  mm (Fig. 3.16) were cut from the fiberglass panels with a diamond saw thus that specimen longitudinal  $x$ -direction corresponded with 0-direction of the initial panel. Two notches were made on two faces in the  $xy$ -plane of stacking parallel to  $y$ -axis up to the mid-thickness. The specimen corresponded to ASTM D 2733 [171], the average distance between notches was  $l = 6.7$  mm. The CFRP micro-tube layer had been placed only in the zone between notches. After machining, the waste material was removed out of the micro-tubes with acetone and distilled water. Then, the micro-tubes were purged with compressed air. Any

epoxy ingress in hollow micro-tubes during the laminate consolidation as well as any microcrack or debonding between the micro-tubes and the GFRP laminate due to residual cure stresses was not revealed when the open ends of micro-tubes in the specimens were inspected under a microscope.

The authors [13, 125, 177, 179] recommend placing a vascular system into the laminate solid with its minimal perturbation. Preferably, the transverse orientation of the micro-tubes should coincide with the orientation of the glass fibres in the surrounding composite layers and the more distant longitudinal layers should be curved as small as possible. In practice, embedded CFRP micro-tubes will have some influence on the entire complex of elastic and strength properties of fiberglass composite. The study of this issue will be of interest in the future for optimal design of self-healing structural members.

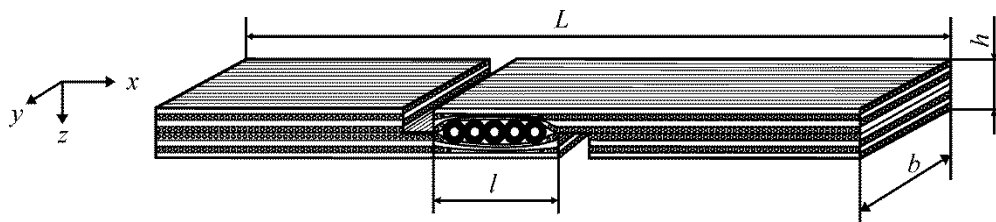


Fig. 3.16. The scheme of specimen for shear test with the CFRP micro-tube layer transversely positioned in the middle zone between notches

In this research, the examination procedure designed was multistep sequences of tests to evaluate HE using interlaminar shear strength as  $F$  in (3.2). The peculiarity was the comparison of the strength of different origin specimens due to their complete failure after each tensile test in the virgin (V), damaged (D), or healed states. The specimens were planned to heal in three ways. Different stages of experimental procedure and the defined strength characteristic are shown on the flowchart (Fig. 3.17).

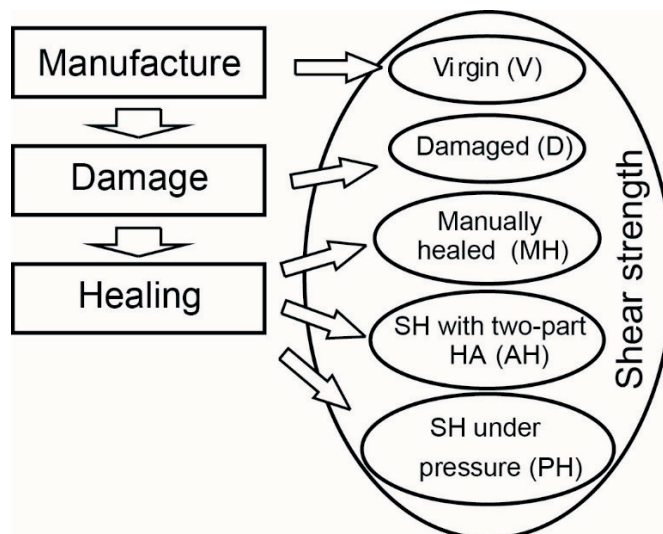


Fig. 3.17. A flowchart of the experimental study of laminated composite

Designed healing possibilities were manual healing (MH), autonomous self-healing with two-part HA (AH), and self-healing with one component HA under pressure (PH). The first way corresponded to a reference manual healing (MH) or repairing when all cracks and defects in the damaged binder were completely infiltrated by HA via immersing of specimen into a one-component HA. The maximal possible strength recovery could be obtained by this method. The second and third ways gave estimation of strength recovery that could be really achieved during an autonomous SH with the two-part HA (AH) or during a stimulated self-healing with the one-component HA (from outer reservoir) under little pressure (PH). In the second case, the amount of stored HA is limited with the internal volume of the vascular system; the mixing of the components has a random nature. In the first and third cases, the volume of HA is practically unlimited. Stoichiometric mixture of the one-component HA is prepared in advance, but has limited pot life before triggering of healing.

Damage of the specimen had to be such that micro-tubes of a used size would be broken also at the same time to trigger effective self-healing. In addition, the damage had been necessary to cause only in the zone with the vascular channels i.e. between the notches, while retaining the load-bearing capacity of the rest part of the specimen at the virgin level. The quasi-static indentation with a hydraulic press using cylindrical indenter could simulate impact damage [40] of the specimen in  $z$  direction but be performed only in the region between the notches. At this stage of research, when the effectiveness of the micro-tubes as the self-healing vascular channels was interested, there was no requirement to establish compliance between compression intensity and simulated impact energy. In practice, the quasi-static compression between a flat surface and a cylindrical indenter of 50 mm diameter was used (Fig. 3.18). The axis of the cylinder was parallel the notches of the specimen and the contact of the indenter and specimen was in the middle of the distance between notches. The press created 25 kN load for 2 min. The total damage volume estimation was equal to the volume of the sample between the notches (more than 300 mm<sup>3</sup>). This identical procedure was selected to create the damage to specimens. At these conditions, visual inspection demonstrated uniform crumpling and splitting of micro-tubes in longitudinal direction, formation of multiple crack networks within GFRP in the zone between notches and surrounding binder. No visible rupture of the load-bearing glass fibres was observed. Similarly, as McCombe et al. [180] it was assumed that all five embedded vascular channels were entirely damaged in each specimen. Correspondingly, amount of micro-tubes ready to release HA was equal in all the specimens.

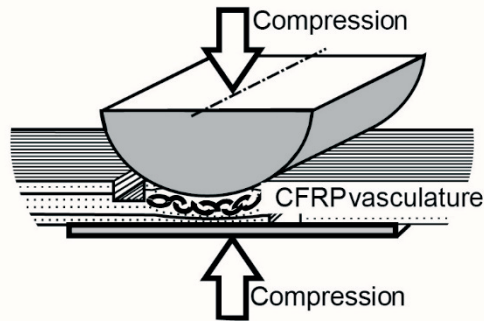


Fig. 3.18. The scheme of damage of the specimens with self-healing vascular channels

Specimens had to be tested in the virgin and damaged state remained with empty micro-tubes. It was assumed that the absence or presence of liquid in the micro-tubes did not affect the mechanical properties of the specimens [179], although Kling et al. [157] had noted that the liquid filling of the microvascular system HA markedly increased flexural strength of the specimens.

The HA for CFRP micro-tube layer was the same resin and hardener had used for GFRP panels manufacture. Filling up of the micro-tubes with HA was performed as follows.

1. MH-specimens (manually healed) were damaged, then immersed to half with open ends of micro-tubes into the liquid one-component HA (stoichiometric mixture of the resin and hardener prepared in advance). The HA infiltrated into the specimen cracks during approximately 20 min. The process arose mostly via crumpled micro-tubes due to capillary effect. Obviously, the HA penetrated also into the cracks along the wetted surface of the specimen. Then, the HA was cured in impregnated specimen.
2. AH-specimens (autonomously self-healed with the two-part HA) were filled with HA before the damage. Three micro-tubes (the 1-st, 3-rd, and 5-th) were filled with hardener immersing the specimen face into the liquid and using capillary action. Two alternated with them (the 2-nd and 4-th) micro-tubes were filled in the same manner with resin. All micro-tubes were sealed. Then, the specimens were damaged. The released HA components impregnated microcracks spontaneously, mixed in random proportions, and then cured.
3. PH-specimens (stimuli self-healed with the HA under pressure) were damaged, and then their micro-tubes were filled with the one-component HA from the outer reservoir under overpressure. In practice, micro-tubes were connected with a syringe, which served as the outer reservoir for HA. The piston of syringe was producing slight overpressure manually until the drops of HA appeared onto the opposite face of the specimen. Further, during the curing, the syringe maintained connected with the micro-tubes.

Curing of the released HA continued for 24 hours at 30°C.

The interlaminar shear strength tests were carried out at room temperature. Results for each group were averaged for five tested specimens. V- and D-specimens were heated for 24 hours at 30 °C before testing to have the same thermal history as specimens with HA. Healed specimens were tested just after HA curing. Specimens were stretched on a universal testing machine Zwick 2.5 at a constant grip displacement speed 2 mm/min. The specimen was placed between two steel guides to prevent bending of the specimen (Fig. 3.19). Unloading was carried when the maximum stress was overcome. The interlaminar shear strength was determined as an average value of the tangential stress  $\tau_m$  (3.6).

Although only the shear strength would be analysed quantitatively in this research to illustrate and qualitatively compare the specimen deformation diagrams the normalized elongation of the zone between notches (engineering strain but not true shear strain)  $\epsilon$  was used. Binder compliance in the shear zone between notches was on the order above that of the machine and other parts of specimen, where longitudinal reinforcement worked. Therefore, it was assumed that elongation of the shear zone between notches was approximately equal the displacement of the grips of testing machine. Caused by this inaccuracy should not influence the diagrams comparison of the same specimens.

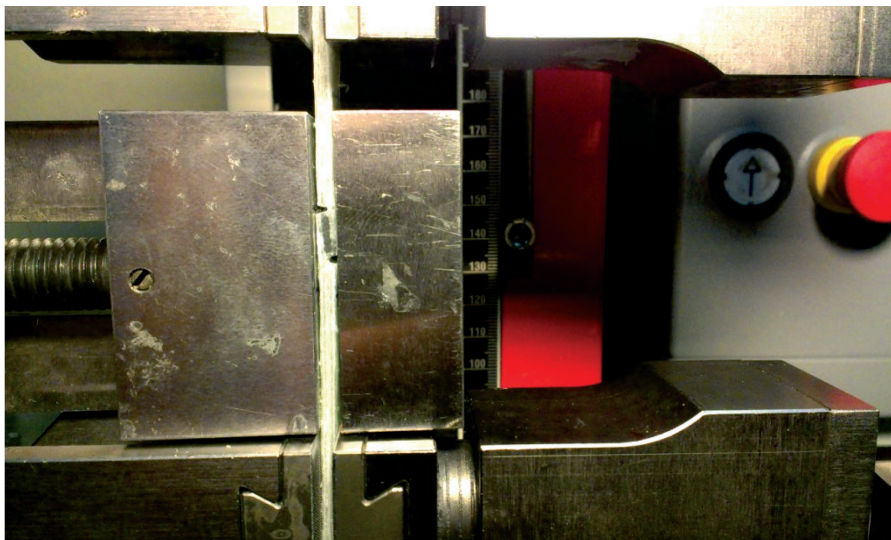


Fig. 3.19. Tensile tests of specimen with two notches

### 3.3.2. *Experimental determination of self-healing efficiency*

*The virgin V-specimens.* The deformation diagrams of interlaminar shear tests (spaced by 2 % along the abscissa) are given in Fig. 3.20. The average strength of the specimens is  $\tau_m = 8.7 \pm 1.0$  MPa. Besides, it has been visually observed that the crack

propagated from the notch has been stopped near the first CFRP micro-tube. This corresponds to the segment on the  $\tau$ - $\epsilon$  curves behind the first local maximum.

After the stress accumulation, the crack has deflected and rounded micro-tubes and spread over the boundary with load-bearing longitudinal fibres (Fig. 3.21). Norris et al. [181] has observed similar character of the shear crack propagation (Mode II) in the unidirectional epoxy fiberglass with transversely spaced hollow channels. This fracture mode testifies that the composite damage that is caused by shear along the  $x$ -axis perpendicular to the self-healing vasculature is not able to destroy this vascular system and trigger the self-healing. On the other hand, the embedment of CFRP micro-tube system does not weaken the symmetry plane of composite where they have been placed from the point of view of conducted shear testing. Crack deflection around the micro-tubes means that it is harder for the crack to propagate in shear zone, thereby increasing the fracture toughness in the symmetry plane of stacking [179, 182].

*The damaged D-specimens.* Fracture of the specimens during the interlaminar shear test has occurred mainly along the symmetry plane of the panel directly through the damaged CFRP micro-tubes (Fig. 3.22). It means that sufficiently crumpled and fractured micro-tubes with transversely oriented carbon reinforcement have been the most weakened place after the damage.

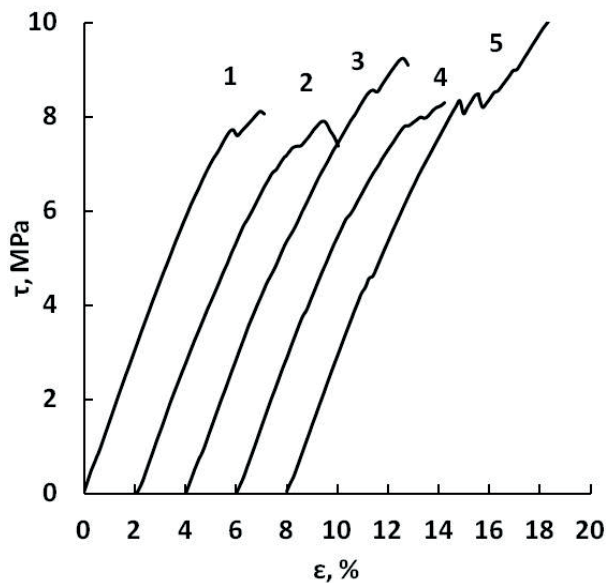


Fig. 3.20. Deformation diagrams of the virgin V-specimens

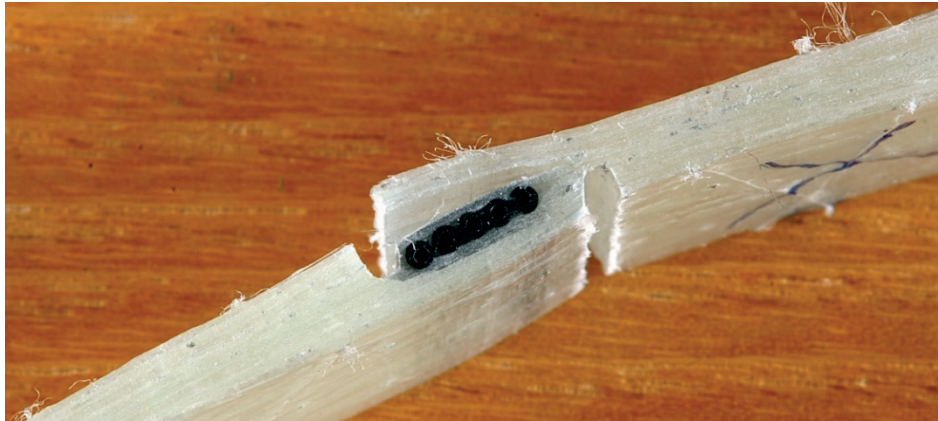


Fig. 3.21. Shear fracture of the virgin V-specimens: the crack deflects around the micro-tubes

The residual strength of the specimens has been reduced to  $\tau_m = 3.4 \pm 2.6$  MPa, which is approximately 40 % of the strength of the virgin specimens. In these experiments, the highest scatter of the strength (approximately 70 %) has been observed. Thus, damage to the specimens has been the least controlled process during the experiments.

Typical  $\tau$ - $\varepsilon$  curves have obtained during the tests of virgin, damaged, and three groups of healed specimens are shown in Fig. 3.23.



Fig. 3.22. Shear fracture of the damaged D-specimens: the crack propagates through the micro-tubes

*The manually healed MH-specimens* have shown the greatest recovery of the strength up to  $\tau_m = 7.2 \pm 1.0$  MPa (Fig. 3.24) that is about 83 % of the strength of the virgin specimens. The resulting value of the strength is the maximum attainable after the self-healing by the chosen methodology of damage and integrity testing. This reason of such conclusion is that infusion conditions of matrix cracks with HA of a stoichiometric composition (HA delivering not only through the micro-tubes, but also from the specimen

surface via microcracks) are approaching to ideal at atmospheric pressure. Nevertheless, full recovery of the strength has not been achieved.

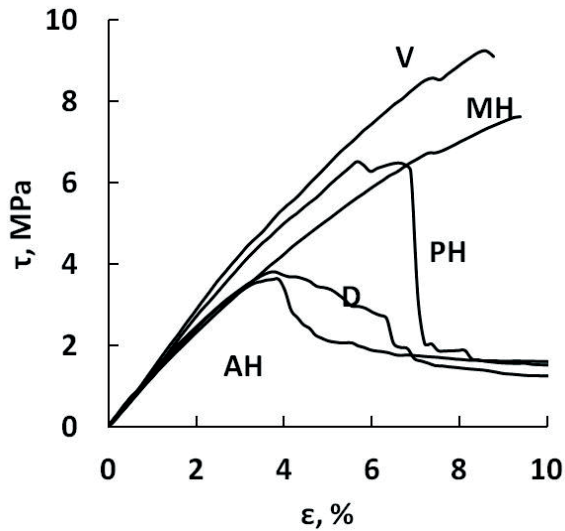


Fig. 3.23. Typical deformation diagrams of the virgin (V), damaged (D), manually healed (MH), self-healed with two-part HA (AH), and healed under pressure (PH) specimens

The sources of irreversible changes in MH specimens during experiment, which have impeded 100 % recovery of the shear strength, are several. (a) The damage degree of different specimens at the first stage of experiment has notable spread (Fig. 3.24) and is uncontrollable. It could affect the level of healing in a specimen because of random amount of crumpling of micro-tubes influences on the quantity of HA has released out of them. (b) Accidental deterioration of carbon and glass fibre reinforcement causes a partial and uncontrolled loss of the load-bearing capacity of some fibres in the shearing zone and near it. (c) During the healing process, presence of a certain amount of untreated micro-cracks could not be excluded too due to possibility of some micro-tube parts to be not crumpled, limited time of the HA infiltration, and the absence of extra pressure for process stimulation [103]. It leads to a not fully recovered binder of the composite. Although the HA infiltrates and treats first of all the cracks in CFRP micro-tube walls themselves the partial recovery could be due to different chemical formulae of HA and CFRP matrix. Tensile tests of MH-specimens have demonstrated that the shear crack has tended to propagate mostly through the interface of 0° and 90° layers in the middle of the specimen, as in the case of V-specimens. However, in some specimens it has passed through the damaged and not fully recovered CFRP micro-tubes also.

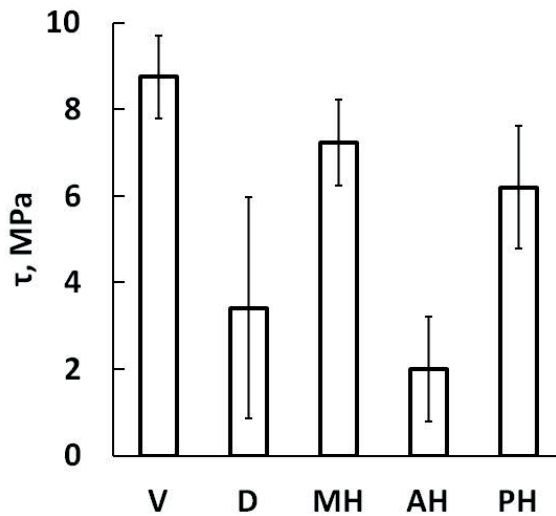


Fig. 3.24. Comparison of the interlaminar shear strength of virgin (V), damaged (D), manually healed (MH), self-healed with two-part HA (AH), and healed under pressure (PH) specimens (error bars reflect one standard deviation of data)

Aforementioned factors affect more-less the downward recovery of shear strength of other healed specimens but with the certain features.

*The autonomously self-healed AH-specimens.* Tests of the specimens with a fixed amount of beforehand stored two-part HA in sealed channels of 15 mm in length and 0.5 mm diameter have shown the strength close to that of the damaged specimens within the experimental error (Fig. 3.24). There is not any recovery in interlaminar shear strength by this healing. The crack has propagated in the plane of micro-tubes as it propagated in D-specimens.

The observable absence of self-healing in this case lies between two factors: inactive mixing of two parts of the two-part HA and scarcity of the HA for complete infiltration into a formed damage. The role of each factor may vary depending on the characteristics of the designed self-healing vascular channels and whole system. For example, in research of self-healing sandwich panels with remotely located channels of each HA component, Williams et al. [155] have attributed low healing efficiency to the first factor. In previous research we have shown, the two-part HA stocked in sufficient quantities in the vascular system allows recovering the damaged composite without any extra pressure. In this research, the vascular channels for self-healing have been in proximity to each other and the cause of failure is the second factor domination. Respectively improving the efficiency of self-healing samples has been expected when the amount of available HA augments. This has been confirmed by experiments with the next group of specimens.

The *PH-specimens* has demonstrated effective healing at which the recovered strength has reached  $\tau_m = 6.2 \pm 1.4$  MPa. In this case, the strength is the recovered mechanical characteristic, so substituting  $F$  for  $\tau_m$  in the HE formulae (3.1) or (3.2) has been ca.  $\eta = 71$  % or  $\eta = 52$  %. The HE does not concede to many of the referred results in Table 3.1 but the stiffness of this self-healing laminate in CFRP micro-tube direction could be higher than stiffness of the similar laminate with hollow glass channels. More than 70 % recovery of initial strength of V-specimens has matched  $\approx 85$  % of the recovered strength of the MH-specimens (Fig. 3.24). The mode of shear fracture has been like mode observed for MH-specimens. In most cases, the crack has propagated along the interface of micro-tubes with load-bearing layer. The principal difference of this case from the "repair" of the matrix in the MH-specimens consists of the similar HA delivering solely via the CFRP self-healing vascular channels. Small overpressure has been a tool for maximal infiltration of the one-component HA into the cracks at the beginning of healing but it has not allowed achieving the same degree of strength recovery as in the MH-specimens. Nevertheless, this group of specimens experimentally demonstrates the suitability of the CRFP micro-tube layer embedded into critical place (e.g. from the point of view the shear strength ensuring) of laminated load-bearing composite to impart vascular SH function and to get the highly efficient healing under the pressure.

A few the consistently superposed objective reasons has caused relatively high scatter of the residual strength values of the damaged and healed specimens in comparison with the values of the virgin specimens (Fig. 3.24). Among them are: (a) inhomogeneity of the composite with the embedded vascular channels; (b) scatter of the damage degree of the compared specimens; (c) stochastic nature of the self-healing process; (d) the chosen test method, where the interlaminar shear strength is evaluated [183]. Despite these objective complicating factors, the achieved high average value of the recovered strength for PH-specimens is evidence that it has been able successfully to implement stimulated self-healing using for the first time a system of CFRP micro-tubes in a GFRP laminate specimens.

### 3.4. Conclusions of the Section

Provision of additional bio-inspired function of vascular self-healing improves a reliability of load-bearing FRP composites through the autonomous or under pressure recoveries of the damaged matrix.

Analysis of current trends in self-healing helps to design two innovative meso-vascular SH layers. The layers are equipped with hollow channels and CFRP micro-tubes. Epoxy resin and amine hardener are selected to act as the liquid HA.

The layers are embedded into vulnerable places of the binder between load-bearing reinforcement layers. The removable flexible tubes in a shape of channel preforms, as

well as commercial pultruded micro-tubes are used as channels for delivery of a sufficient volume of liquid HA.

The multistep sequences of tests are designed to evaluate the efficiency of the vascular SH function. A choice of vulnerable places for the layer embedment, damage creation and testing of matrix-sensitive mechanical characteristics are all combined in the experiments.

The fractured TDCB epoxy specimens demonstrate the HE of approx. 70 % with two-part HA. The heat treatment of composite with hollow-channel layer helps to reach a HE of the autonomous SH function of approx. 36 %. The healing continues even after extended resting at room temperature. Then, the efficiency reaches more than 50 %. The sealed HA is capable to maintain the SH for at least six months. Under the pressure, SH function demonstrates the interlaminar shear strength recovery with HE of approx. 52 % in the glass FRP specimens using the CFRP micro-tube layer. Large-scale damages are healed in all cases, confirming the corresponding thesis.

## GENERAL CONCLUSIONS

The tasks specified for the set aim are fulfilled:

- Innovative layers are created: (1) visual indication layer of mechanical impact on the base of encapsulated two-component chemistry; (2) layers with two types of vascular SH for large volume damages of composite binder, i.e. on the base of hollow channels and carbon FRP micro-tubes.
- The indication layer with an epoxy coating that adjusts sensitivity is embedded as an outer layer above load-bearing reinforcement. The vascular SH layers are built into vulnerable places between load-bearing reinforcement yarns. The vacuum moulding methods are used for integration of the composites.
- The evaluation the efficiency of additional functions requires development of the special method of digital image analysis for quantification of the visual response, design of the model of threshold load, and preparation of the sequences of tests (pseudo-impact indentation, damages of the binder of FRP, testing of mechanical characteristics etc.).
- The proof of function efficiency was a capability of indication to be activated within seconds and a sensitivity correspondence to the values of pseudo-impacts endangering the epoxy binder. The estimated high healing efficiency (above 52 %) ensures the significant recovery of the mechanical properties of damaged composites.

Performed study corresponds to Technology Readiness Levels: TRL 1-2. The results **confirm the proposed theses** about the use smart layers for increasing a reliability, load-bearing capacity stability, role of polymer protective coating and sensitivity regulation, and self-healing efficiency.

The results enable the load-bearing composite development with an increased lifetime using:

- The visual indication layer with a predetermined sensitivity or layer's adaptation to the finished products for early detection of impacts and loadings that cause damages;
- Vascular SH function capable to recover large-scale (above 100 mm<sup>3</sup>) damages of the composite binder;
- Smart built-in layers which do not lead to a significant reduction of stiffness and strength characteristics of composite;
- Multiple bio-inspired functions to get smart structures.

## REFERENCES

- [1] D. Mathijsen, "Structural health monitoring: composite skins are getting a nervous system," *Reinforced Plastics*, vol. 59, no. 3, pp. 139-142, 2015.
- [2] J. Chilles, A. Croxford and I. P. Bond, "Design, application, and validation of embedded ultrasonic sensors within composite materials," *Proc. SPIE*, vol. 9437, p. 94370D (12pp), 2015.
- [3] W. Feng, S. H. Patel, M.-Y. Young, J. L. Zunino and M. Xanthos, "Smart polymeric coatings— recent advances," *Advances in Polymer Technology*, vol. 26, no. 1, pp. 1-13, 2007.
- [4] R. S. Trask, H. R. Williams and I. P. Bond, "Self-healing polymer composites: mimicking nature to enhance performance," *Bioinspiration & Biomimetics*, vol. 2, pp. 1-9, 2007.
- [5] A. T. Rhead and R. Butler, "Compressive static strength model for impact damaged laminates," *Composites Science and Technology*, vol. 69, no. 14, pp. 2301-2307, 2009.
- [6] D. D. L. Chung, "Damage detection using self-sensing concepts," *Proceedings of the Institution of Mechanical Engineers, Part G: Journal of Aerospace Engineering*, vol. 221, no. 4, pp. 509-520, 2007.
- [7] H. Razi and S. Ward, "Principles for achieving damage tolerant primary composite aircraft structures," in *Conference on fibrous composites in structural design, 11<sup>th</sup> DOD/FAA/NASA*, Fort Worth, Texas, 26–30 August, 1996.
- [8] J. Tomblin, T. Lacy, B. Smith, S. Hooper, A. Vizzini and S. Lee, "Review of Damage Tolerance for Composite Sandwich Airframe Structures. Final Report, DOT/FAA/AR-99/49," 1999. [Online]. Available: <http://www.tc.faa.gov/its/worldpac/techrpt/ar99-49.pdf>. [Accessed 01 Mar 2012].
- [9] J. S. Tomblin, K. S. Raju, J. Liew and B. L. Smith, "Impact damage characterization and damage tolerance of composite sandwich airframe structures. Final Report, DOT/FAA/AR-00/44," 2001. [Online]. Available: <http://www.tc.faa.gov/its/worldpac/techrpt/ar00-44.pdf>. [Accessed 29 Feb 2012].
- [10] H. R. Williams, R. S. Trask and I. P. Bond, "A probabilistic approach for design and certification of self-healing advanced composite structures," *Proceedings of the Institution of Mechanical Engineers, Part O: Journal of Risk and Reliability*, vol. 225, no. 4, pp. 435-449, 2011.
- [11] R. Dilger, H. Hickethier and M. D. Greenhalgh, "Eurofighter a safe life aircraft in the age of damage tolerance," *International Journal of Fatigue*, vol. 31, no. 6, pp. 1017-1023, 2009.
- [12] J. Eastham, "Detection of damage in materials". UK Patent GB 2194062 A, 24 Feb. 1988.
- [13] G. Williams, R. Trask and I. Bond, "A self-healing carbon fibre reinforced polymer for aerospace applications," *Composites Part A: Applied Science and Manufacturing*, vol. 38, no. 6, pp. 1525-1532, 2007.
- [14] S. J. Garcia, "Effect of polymer architecture on the intrinsic self-healing character of polymers," *European Polymer Journal*, vol. 53, pp. 118-125, 2014.
- [15] K. Diamanti and C. Soutis, "Structural health monitoring techniques for aircraft composite structures," *Progress in Aerospace Sciences*, vol. 46, no. 8, pp. 342-352, 2010.

- [16] A. Todoroki, M. Ueda and Y. Hirano, "Strain and Damage Monitoring of CFRP Laminates by Means of Electrical Resistance Measurement," *Journal of Solid Mechanics and Materials Engineering*, vol. 1, no. 8, pp. 947-974, 2007.
- [17] T. Villmow, S. Pegel, A. John, R. Rentenberger and P. Pötschke, "Liquid sensing: smart polymer/CNT composites," *Materials Today*, vol. 14, pp. 340-345, 2011.
- [18] R. Guzman de Villoria, N. Yamamoto, A. Miravete and B. L. Wardle, "Multi-physics damage sensing in nano-engineered structural composites," *IOP Science Nanotechnology*, vol. 22, no. 18, p. 185502 (7pp.), 2011.
- [19] H. R. Williams, R. S. Trask, P. M. Weaver and I. P. Bond, "Minimum mass vascular networks in multifunctional materials," *Journal of The Royal Society Interface*, vol. 5, no. 18, pp. 55-65, 2008.
- [20] D. A. Tibaduiza, L. E. Mujica, J. Rodellar and A. Güemes, "Structural damage detection using principal component analysis and damage indices," *Journal of Intelligent Material Systems and Structures*, vol. 27, no. 2, pp. 233-248, 2016.
- [21] D. S. Forsyth, R. W. Gould and J. P. Komorowski, "Double Pass Retroreflection versus Visual Inspection of Impact Damage in Composites," *RTO MEETING PROCEEDINGS- NORTH ATLANTIC TREATY ORGANIZATION RESEARCH AND TECHNOLOGY ORGANIZATION RTO MP*, vol. 10, p. 18 (6pp.), 1998.
- [22] D. E. Cooney, "Approach for Indicating the Occurrence of a Mechanical Impact on a Material, such as Low-Ductility Composite Material". US Patent US 7647809 B1, 19 01 2010.
- [23] R. Luterbacher, T. Coope, R. Trask and I. Bond, "Self-healing cross-ply laminates – encouraging test results," *JEC MAGAZINE COMPOSITES*, no. 104, pp. 41-43, 2016.
- [24] C. Dry, "Self-repairing composites for airplane components," *Proc. SPIE*, vol. 6932, p. 693212 (13pp.), 2008.
- [25] V. K. Wadhawan, "Smart Structures and Materials," *Resonance – Journal of Science Education*, vol. 10, no. 11, pp. 27-41, 2005.
- [26] R. J. Martin-Palma, C. G. Pantano and A. Lakhtakia, "A novel technique for making highly efficient biomimetic devices," *SPIE Newsroom. DOI: 10.1117/2.1200809.1297*, 2008.
- [27] J. Baghdachi, "Smart Coatings," in *Smart Coatings II, ACS Symposium Series*, T. Provder and J. Baghdachi, Eds., Washington, DC, American Chemical Society, 2009, pp. 3-24.
- [28] A. V. Singh, A. Rahman, N. S. Kumar, A. S. Aditi, M. Galluzzi, S. Bovio, S. Barozzi, E. Montani and D. Parazzoli, "Bio-inspired approaches to design smart fabrics," *Materials & Design*, vol. 36, pp. 829-839, 2012.
- [29] N. Zhao, Z. Wang, C. Cai, H. Shen, F. Liang, D. Wang, C. Wang, T. Zhu, J. Guo, Y. Wang, X. Liu, C. Duan, H. Wang, Y. Mao, X. Jia, H. Dong, X. Zhang and J. Xu, "Bioinspired Materials: from Low to High Dimensional Structure," *Advanced Materials*, vol. 26, no. 41, pp. 6994-7017, 2014.
- [30] C. C. Ciang, J.-R. Lee and H.-J. Bang, "Structural health monitoring for a wind turbine system: a review of damage detection methods," *Measurement Science and Technology*, vol. 19, no. 12, p. 122001 (20pp.), 2008.
- [31] [Online]. Available: <http://www.eplcompositesolutions.co.uk/composite/bruisableComposites.asp>. [Accessed 23 May 2012].

- [32] [Online]. Available: <http://www.theengineer.co.uk/issues/26-october-2009/composite-design-shows-bruise-damage/>. [Accessed 14 Jan. 2013].
- [33] R. Bond, S. Underwood, D. E. Adams and J. J. Cummins, "Structural health monitoring-based methodologies for managing uncertainty in aircraft structural life assessment," *Structural Health Monitoring*, vol. 13, no. 6, pp. 621-628, 2014.
- [34] C. M. Dry and N. R. Sottos, "Passive smart self-repair in polymer matrix composite materials," *Proc. SPIE*, vol. 1916, pp. 438-444, 1993.
- [35] C. Dry, "Procedures developed for self-repair of polymer matrix composite materials," *Composite Structures*, vol. 35, no. 3, pp. 263-269, 1996.
- [36] R. P. Wool, "Self-healing materials: a review," *Soft Materials*, vol. 4, pp. 400-418, 2008.
- [37] D. Y. Wu, S. Meure and D. Solomon, "Self-healing polymeric materials: A review of recent developments," *Prog. Polym. Science*, vol. 33, pp. 479-522, 2008.
- [38] T. C. Mauldin and M. R. Kessler., "Self-healing polymers and composites," *International Materials Reviews*, vol. 55, pp. 317-346, 2010.
- [39] H. Fischer, "Self-repairing material systems—a dream or a reality?," *Natural Science*, vol. 2, pp. 873-901, 2010.
- [40] B. J. Blaiszik, S. L. B. Kramer, S. C. Olugebefola, J. S. Moore, N. R. Sottos and S. R. White, "Self-Healing Polymers and Composites," *Annual Review of Materials Research*, vol. 40, pp. 179-211, 2010.
- [41] Z. Y. Zhang and M. O. W. Richardson, "Visualisation of barely visible impact damage in polymer matrix composites using an optical deformation and strain measurement system (ODSMS)," *Composites Part A: Applied Science and Manufacturing*, vol. 36, no. 8, pp. 1073-1078, 2005.
- [42] M. Leong, L. C. T. Overgaard, I. M. Daniel, E. Lund and O. T. Thomsen, "Interlaminar/interfiber failure of unidirectional glass fiber reinforced composites used for wind turbine blades," *Journal of Composite Materials*, vol. 47, no. 3, pp. 353-368, 2012.
- [43] M. R. Jahanshahi, J. S. Kelly, S. F. Masri and G. S. Sukhatme, "A survey and evaluation of promising approaches for automatic image-based defect detection of bridge structures," *Structure and Infrastructure Engineering*, vol. 5, no. 6, pp. 455-486, 2009.
- [44] M. R. Jahanshahi and S. F. Masri, "Adaptive vision-based crack detection using 3D scene reconstruction for condition assessment of structures," *Automation in Construction*, vol. 22, pp. 567-576, 2012.
- [45] R. Matsuzaki, M. Kawasaki and A. Todoroki, "Uncertainty Visualization of Estimated Damage Using Kriging Model: Application to Time-Domain Reflectometry Sensing," *Journal of Nondestructive Evaluation*, vol. 34, no. 3, pp. 23-33, 2015.
- [46] A. Todoroki, K. Yamada, Y. Mizutani, Y. Suzuki and R. Matsuzaki, "Impact damage detection of a carbon-fibre-reinforced-polymer plate employing self-sensing time-domain reflectometry," *Composite Structures*, vol. 130, no. 0, pp. 174-179, 2015.
- [47] A. Todoroki, K. Ohara, Y. Mizutani, Y. Suzuki and R. Matsuzaki, "Lightning strike damage detection at a fastener using self-sensing TDR of composite plate," *Composite Structures*, vol. 132, pp. 1105-1112, 2015.

- [48] M. D. Rein, O. Breuer and H. D. Wagner, "Sensors and sensitivity: Carbon nanotube buckypaper films as strain sensing devices," *Composites Science and Technology*, vol. 71, no. 3, pp. 373-381, 2011.
- [49] M. A. Nasir, H. Akram, Z. M. Khan, M. Shah, S. Anas, Z. Asfar and S. Nauman, "Smart sensing layer for the detection of damage due to defects in a laminated composite structure," *Journal of Intelligent Material Systems and Structures*, 2014.
- [50] A. Todoroki, "Self-sensing composites and optimization of composite structures in Japan," *International Journal of Aeronautical and Space Sciences*, vol. 11, no. 3, pp. 155-166, 2010.
- [51] S. Gungor and C. E. Bakis, "Anisotropic networking of carbon black in glass/epoxy composites using electric field," *Journal of Composite Materials*, vol. 49, no. 5, pp. 535-544, 2015.
- [52] S. Gungor and C. E. Bakis, "Indentation damage detection in glass/epoxy composite laminates with electrically tailored conductive nanofiller," *Journal of Intelligent Material Systems and Structures*, vol. 27, no. 5, pp. 679-688, 2016.
- [53] S. Laflamme, M. Kolloosche, J. J. Connor and G. Kofod, "Soft capacitive sensor for structural health monitoring of large-scale systems," *Structural Control and Health Monitoring*, vol. 19, no. 1, pp. 70-81, 2012.
- [54] S. Egusa and N. Iwasawa, "Piezoelectric paints as one approach to smart structural materials with health-monitoring capabilities," *Smart Materials and Structures*, vol. 7, no. 4, p. 438, 1998.
- [55] Y. Zhang, "Piezoelectric paint sensor for real-time structural health monitoring," *Proc. SPIE*, vol. 5765, pp. 1095-1103, 2005.
- [56] S. Rattanachan, Y. Miyashita and Y. Mutoh, "Fabrication of piezoelectric laminate for smart material and crack sensing capability," *Science and Technology of Advanced Materials*, vol. 6, no. 6, pp. 704-711, 2005.
- [57] B. G. McLachlan and J. H. Bell, "Pressure-sensitive paint in aerodynamic testing," *Experimental Thermal and Fluid Science*, vol. 10, no. 4, pp. 470-485, 1995.
- [58] Y. L. Sant and M.-C. Mérienne, "Surface pressure measurements by using pressure-sensitive paints," *Aerospace Science and Technology*, vol. 9, no. 4, pp. 285-299, 2005.
- [59] B. J. Basu, N. Vasantharajan and C. Raju, "A novel pyrene-based binary pressure sensitive paint with low temperature coefficient and improved stability," *Sensors and Actuators B: Chemical*, vol. 138, no. 1, pp. 283-288, 2009.
- [60] Q. Zhou, B. Liu, L. Gao, L. Chen and M. Shi, "Pressure Measurement on Suction Surface of a Single Vane Using Pressure-sensitive Paint," *Chinese Journal of Aeronautics*, vol. 22, no. 2, pp. 138-144, 2009.
- [61] C. Weder, "Mechanoresponsive Materials," *J. Mater. Chem.*, vol. 21, pp. 8235-8236, 2011.
- [62] C. Weder, (2013) Mechanochromic Polymers," in *Encyclopedia of Polymeric Nanomaterials*, [Online]. [https://link.springer.com/referenceworkentry/10.1007/978-3-642-36199-9\\_6-4](https://link.springer.com/referenceworkentry/10.1007/978-3-642-36199-9_6-4)
- [63] A. Pucci and G. Ruggeri, "Mechanochromic polymer blends," *J. Mater. Chem.*, vol. 21, pp. 8282-8291, 2011.
- [64] A. Pucci, R. Bizzarri and G. Ruggeri, "Polymer composites with smart optical properties," *Soft Matter*, vol. 7, no. 8, pp. 3689-3700, 2011.

- [65] X. Jin, M. Götz, S. Wille, Y. K. Mishra, R. Adelung and C. Zollfrank, "A Novel Concept for Self-Reporting Materials: Stress Sensitive Photoluminescence in ZnO Tetrapod Filled Elastomers," *Advanced Materials*, vol. 25, no. 9, pp. 1342-1347, 2013.
- [66] C. G. Schäfer, M. Gallei, J. T. Zahn, J. Engelhardt, G. P. Hellmann and M. Rehahn, "Reversible Light-, Thermo-, and Mechano-Responsive Elastomeric Polymer Opal Films," *Chemistry of Materials*, vol. 25, no. 11, pp. 2309-2318, 2013.
- [67] B. A. Beiermann, S. L. B. Kramer, J. S. Moore, S. R. White and N. R. Sottos, "Role of Mechanophore Orientation in Mechanochemical Reactions," *ACS Macro Letters*, vol. 1, no. 1, pp. 163-166, 2012.
- [68] A.-D. N. Celestine, B. A. Beiermann, P. A. May, J. S. Moore, N. R. Sottos and S. R. White, "Fracture-induced activation in mechanophore-linked, rubber toughened PMMA," *Polymer*, vol. 55, no. 16, pp. 4164-4171, 2014.
- [69] N. Bruns, K. Pustelny, L. M. Bergeron, T. A. Whitehead and D. S. Clark, "Mechanical Nanosensor Based on FRET within a Thermosome: Damage-Reporting Polymeric Materials," *Angewandte Chemie*, vol. 121, no. 31, pp. 5776-5779, 2009.
- [70] S.-Y. Cho, J.-G. Kim and C.-M. Chung, "A fluorescent crack sensor based on cyclobutane-containing crosslinked polymers of tricinnamates," *Sensors and Actuators B: Chemical*, vol. 134, no. 2, pp. 822-825, 2008.
- [71] Y.-K. Song, K.-H. Lee, W.-S. Hong, S.-Y. Cho, H.-C. Yu and C.-M. Chung, "Fluorescence sensing of microcracks based on cycloreversion of a dimeric anthracene moiety," *J. Mater. Chem.*, vol. 22, pp. 1380-1386, 2012.
- [72] Y.-K. Song, K.-H. Lee, D.-M. Kim and C.-M. Chung, "A microcapsule-type fluorescent probe for the detection of microcracks in cementitious materials," *Sensors and Actuators B: Chemical*, vol. 222, pp. 1159-1165, Jan. 2016.
- [73] W. Li, C. C. Matthews, K. Yang, M. T. Odarczenko, S. R. White and N. R. Sottos, "Autonomous Indication of Mechanical Damage in Polymeric Coatings," *Advanced Materials*, vol. 28, pp. 2189-2194, 2016.
- [74] T. J. Kucharski and R. Boulatov, "The physical chemistry of mechanoresponsive polymers," *J. Mater. Chem.*, vol. 21, pp. 8237-8255, 2011.
- [75] B. D. Credico, G. Griffini, M. Levi and S. Turri, "Microencapsulation of a UV-Responsive Photochromic Dye by Means of Novel UV-Screening Polyurea-Based Shells for Smart Coating Applications," *ACS Applied Materials & Interfaces*, vol. 5, no. 14, pp. 6628-6634, 2013.
- [76] L. D. Stephenson and A. Kumar, "Technology Demonstration of Self-Healing Coatings for In-Place Management of Lead-Based Paint Hazards," 2003. [Online]. Available: <http://acwc.sdp.sirsi.net/client/search/asset/1002459>. [Accessed 12 Jan 2015].
- [77] S. A. Odom, A. C. Jackson, A. M. Prokup, S. Chayanupatkul, N. R. Sottos, S. R. White and J. S. Moore, "Visual Indication of Mechanical Damage Using Core-Shell Microcapsules," *ACS Applied Materials & Interfaces*, vol. 3, no. 12, pp. 4547-4551, 2011.
- [78] J. W. C. Pang and I. P. Bond, "'Bleeding composites'—damage detection and self-repair using a biomimetic approach," *Composites: Part A*, vol. 36, pp. 183-188, 2005.

- [79] J. W. C. Pang and I. P. Bond, "A hollow fibre reinforced polymer composite encompassing self-healing and enhanced damage visibility," *Composites Science and Technology*, vol. 65, pp. 1791-1799, 2005.
- [80] M. Samadzadeh, S. H. Boura, M. Peikari, S. M. Kasiriha and A. Ashrafi, "A review on self-healing coatings based on micro/nanocapsules," *Progress in Organic Coatings*, vol. 68, no. 3, pp. 159-164, 2010.
- [81] S. H. Boura, M. Peikari, A. Ashrafi and M. Samadzadeh, "Self-healing ability and adhesion strength of capsule embedded coatings — Micro and nano sized capsules containing linseed oil," *Progress in Organic Coatings*, vol. 75, no. 4, pp. 292-300, 2012.
- [82] Y.-K. Song, Y.-H. Jo, Y.-J. Lim, S.-Y. Cho, H.-C. Yu, B.-C. Ryu, S.-I. Lee and C.-M. Chung, "Sunlight-Induced Self-Healing of a Microcapsule-Type Protective Coating," *ACS Applied Materials & Interfaces*, vol. 5, no. 4, pp. 1378-1384, 2013.
- [83] H. Jin, C. L. Mangun, D. S. Stradley, J. S. Moore, N. R. Sottos and S. R. White, "Self-Healing Thermoset Using Encapsulated Epoxy-Amine Healing Chemistry," *Polymer*, vol. 53, no. 2, pp. 581-587, Jan 2012.
- [84] L. Yuan, G. Liang, J. Q. Xie, L. Li and J. Guo, "Preparation and characterization of poly(urea-formaldehyde) microcapsules filled with epoxy resins," *Polymer*, vol. 47, no. 15, pp. 5338-5349, 2006.
- [85] E. Campos, J. Branquinho, A. S. Carreira, A. Carvalho, P. Coimbra, P. Ferreira and M. H. Gil, "Designing polymeric microparticles for biomedical and industrial applications," *European Polymer Journal*, vol. 49, no. 8, pp. 2005-2021, 2013.
- [86] T. Nesterova, K. Dam-Johansen, L. T. Pedersen and S. Kiil, "Microcapsule-based self-healing anticorrosive coatings: Capsule size, coating formulation, and exposure testing," *Progress in Organic Coatings*, vol. 75, pp. 309-318, 2012.
- [87] Y. Zhao, W. Zhang, L.-p. Liao, S.-j. Wang and W.-j. Li, "Self-healing coatings containing microcapsule," *Applied Surface Science*, vol. 258, no. 6, pp. 1915-1918, 2012.
- [88] X. Liu, H. Zhang, J. Wang, Z. Wang and S. Wang, "Preparation of epoxy microcapsule based self-healing coatings and their behavior," *Surface and Coatings Technology*, vol. 206, pp. 4976-4980, 2012.
- [89] T. Szabó, L. Molnár-Nagy, J. Bognár, L. Nyikos and J. Telegdi, "Self-healing microcapsules and slow release microspheres in paints," *Progress in Organic Coatings*, vol. 72, no. 1-2, pp. 52-57, 2011.
- [90] T. Nesterova, K. Dam-Johansen and S. Kiil, "Synthesis of durable microcapsules for self-healing anticorrosive coatings: A comparison of selected methods," *Progress in Organic Coatings*, vol. 70, no. 4, pp. 342-352, 2011.
- [91] S. Kainuma, J.-H. Ahn, Y.-S. Jeong and H. Takahashi, "Evaluation on estimation in characteristics of fatigue crack using micro-encapsulated dye mixing paint," *Engineering Failure Analysis*, vol. 25, pp. 1-12, 2012.
- [92] S. Vidinejevs, A. N. Aniskevich, A. Gregor, M. Sjöberg and G. Alvarez, "Smart polymeric coatings for damage visualization in substrate materials," *Journal of Intelligent Material Systems and Structures*, vol. 23, no. 12, pp. 1371-1377, 12 Aug 2012.
- [93] G. Argy, A. Cheymol and H. Hervet, "Process and device for revealing impact(s) received by a substrate". US Patent US 5242830, 7 Sep. 1993.

- [94] B. E. Koene and M. E. Rogers, "Method for detecting damage". Patent WO 2006/105290 A2, 5 Oct. 2006.
- [95] M. Shigyo, "Pressure measuring film for measuring pressure in small contact area". US Patent 6742472 B1, 2004.
- [96] T. Danowski and T. Daly, "Stress indicating materials". US Patent US 2008/0083286 A1, 10 Apr. 2008.
- [97] M. R. Turner and D. A. Johnson, "Polymer composite materials". GB Patent GB 2469735 A, 27 Oct. 2010.
- [98] P. Brassier and P. Peres, "Evaluation method for monitoring the effects of an impact on a structural composite material part". US Patent US 2007/0050153 A1, 1 Mar. 2007.
- [99] G. A. Rush, "Impact indicator for athletic helmets". US Patent 6332226 B1, 2001.
- [100] Y. C. Yuan, M. Z. Rong, M. Q. Zhang, J. Chen, G. C. Yang and X. M. Li, "Self-Healing Polymeric Materials Using Epoxy/Mercaptan as the Healtant," *Macromolecules*, vol. 41, pp. 5197-5202, 2008.
- [101] C. Thies, "Microencapsulation," 2004. [Online]. Available: <http://dx.doi.org/10.1002/0471440264.pst198>. [Accessed 02 May 2012].
- [102] R. M. Christensen, *Mechanics of composite materials*, New York: Wiley-Interscience, 1979.
- [103] M. Ali and S. C. Joshi, "Impact Damage Resistance of CFRP Prepreg Laminates with Dispersed CSP Particles into Ply Interfaces," *International Journal of Damage Mechanics*, vol. 21, no. 8, pp. 1106-1127, 2012.
- [104] D. Zeleniakiene, V. Leisis, P. Griskevicius, O. Bulderberga and A. Aniskevich, "A Numerical Simulation of Mechanical Properties of Smart Polymer Composite with Microcapsules for Damage Sensing Applications," in *ECCM17 – 17th European Conference on Composite Materials, Munich, Germany, 26-30th June, 2016*.
- [105] P. W. Chen, J. Brignoli and A. R. Studart, "Mechanics of thick-shell microcapsules made by microfluidics," *Polymer*, vol. 55, pp. 6837-6843, 2014.
- [106] A. C. Jackson, J. A. Bartelt, K. Marczewski, N. R. Sottos and P. V. Braun, "Silica-Protected Micron and Sub-Micron Capsules and Particles for Self-Healing at the Microscale," *Macromolecular Rapid Communications*, vol. 32, no. 1, pp. 82-87, 2011.
- [107] M. P. Stevens, *Polymer Chemistry: An Introduction*, 3 ed., Oxford University Press, Inc, 1999.
- [108] A. H. Conner, "Urea–formaldehyde adhesive resins," in *Polymeric Materials Encyclopedia*, vol. 11, J. C. Salamone, Ed., CRC, 1996, pp. 8497-8501.
- [109] "Havel Composites CZ s.r.o.," [Online]. Available: <http://www.havel-composites.com/>. [Accessed 01 Jun. 2011].
- [110] M. Dale, L. A. Carlsson and B. A. Acha, "Impact force analysis during low-velocity impact of woven carbon/vinylester," *Journal of Composite Materials*, vol. 46, no. 25, pp. 3163-3172, 2012.
- [111] G. Caprino, A. Langella and V. Lopresto, "Prediction of the first failure energy of circular carbon fibre reinforced plastic plates loaded at the centre," *Composites Part A: Applied Science and Manufacturing*, vol. 34, no. 4, pp. 349-357, 2003.
- [112] V. Lopresto and G. Caprino, "Macroscopic behaviour and fracture modes of CFRP panels transversely loaded at the centre," in *ECCM 11 – 11th European conference on composite materials, Rhodes, Greece; May 31–June 3, 2004*.

- [113] M. Quaresimin, M. Ricotta, L. Martello and S. Mian, "Energy absorption in composite laminates under impact loading," *Composites Part B: Engineering*, vol. 44, no. 1, pp. 133-140, 2013.
- [114] D. Whisler and H. Kim, "Effect of impactor radius on low-velocity impact damage of glass/epoxy composites," *Journal of Composite Materials*, vol. 46, no. 25, pp. 3137-3149, 2012.
- [115] J. D. Krehbiel, J. Lambros, J. A. Viator and N. R. Sottos, "Digital Image Correlation for Improved Detection of Basal Cell Carcinoma," *Experimental Mechanics*, vol. 50, no. 6, pp. 813-824, 2010.
- [116] Z. Kalnroze and A. Aniskevich, "Measuring the biaxial deformations of thin films in long-term mechanical tests," in *XIV International Conference MCM-2006: Mechanics of Composite Materials, Riga, Latvia, May 29- June 2, 2006*.
- [117] J. R. M. d'Almeida, M. H. P. Mauricio and S. Paciornik, "Evaluation of the cross-section of lignocellulosic fibers using digital microscopy and image analysis," *Journal of Composite Materials*, vol. 46, no. 24, pp. 3057-3065, 2012.
- [118] K. L. Johnson, *Contact mechanics*, Cambridge University Press, 1985.
- [119] A. Smith, S. J. Wilkinson and W. N. Reynolds, "The elastic constants of some epoxy resins," *Journal of Materials Science*, vol. 9, pp. 547-550, 1974.
- [120] V. V. Vasiliev and E. V. Morozov, "Mechanics and Analysis of Composite Materials," in *1 Composite materials – Mechanical properties*, Oxford, Elsevier Science, 2001.
- [121] C. A. Rogers, "Workshop summary," 1988. [Online]. Available: [www.dtic.mil/dtic/tr/fulltext/u2/a218528.pdf](http://www.dtic.mil/dtic/tr/fulltext/u2/a218528.pdf). [Accessed 25 Jul 2013].
- [122] N. K. Guimard, K. K. Oehlenschlaeger, J. Zhou, S. Hilf, F. G. Schmidt and C. Barner-Kowollik, "Current Trends in the Field of Self-Healing Materials," *Macromolecular Chemistry and Physics*, vol. 213, no. 2, pp. 131-143, 2012.
- [123] A. Mačanovskis, A. Krasņikovs, I. Spruģe, G. Šahmenko and A. Lukašenoks, "Mechanical Properties and Self-Healing Effect of Concrete Containing Capillary Hydro Insulation Admixture," *Construction Science*, vol. 18, no. 1, pp. 17-21, 2016.
- [124] Y. M. Malinskii, V. V. Prokopenko, N. A. Ivanova and V. A. Kargin, "Investigation of self-healing of cracks in polymers. I. Effect of temperature and crosslinks on self-healing of cracks in polyvinyl acetate," *Polymer Mechanics*, no. 2, pp. 240-244, 1970.
- [125] C. J. Norris, G. J. Meadway, M. J. O'Sullivan, I. P. Bond and R. S. Trask, "Self-Healing Fibre Reinforced Composites via a Bioinspired Vasculature," *Advanced Functional Materials*, vol. 21, no. 19, pp. 3624-3633, 2011.
- [126] J. A. Syrett, C. R. Becer and D. M. Haddleton, "Self-healing and self-mendable polymers," *Polymer Chemistry*, vol. 1, pp. 978-987, 2010.
- [127] S. D. Bergman and F. Wudl, "Mendable polymers," *J. Mater. Chem.*, vol. 18, pp. 41-62, 2008.
- [128] S. R. White, N. R. Sottos, P. H. Geubelle, J. S. Moore, M. R. Kessler, S. R. Sriram, E. N. Brown and S. Viswanathan, "Autonomic healing of polymer composites," *Nature*, vol. 409, pp. 794-797, February 2001.
- [129] M. R. Kessler, "Self-healing: A new paradigm in materials design," *Proceedings of the Institution of Mechanical Engineers, Part G: Journal of Aerospace Engineering*, vol. 221, no. 4, pp. 479-495, 2007.

- [130] D. Therriault, R. F. Shepherd, S. R. White and J. A. Lewis, "Fugitive Inks for Direct-Write Assembly of Three-Dimensional Microvascular Networks," *Advanced Materials*, vol. 17, no. 4, pp. 395-399, 2005.
- [131] A. Bejan, S. Lorente and K.-M. Wang, "Networks of channels for self-healing composite materials," *Journal of Applied Physics*, vol. 100, no. 3, p. 033528, 2006.
- [132] R. S. Trask and I. P. Bond, "Biomimetic self-healing of advanced composite structures using hollow glass fibres," *Smart Materials and Structures*, vol. 15, pp. 704-710, 2006.
- [133] Y. Yang, X. Ding and M. W. Urban, "Chemical and Physical Aspects of Self-Healing Materials," *Progress in Polymer Science*, Vols. 49-50, pp. 34-59, 2015.
- [134] M. Scheiner, T. J. Dickens and O. Okoli, "Progress towards self-healing polymers for composite structural applications," *Polymer*, vol. 83, pp. 260-282, 2016.
- [135] K. Urdl, A. Kandelbauer, W. Kern, U. Müller, M. Thebault and E. Zikulnig-Rusch, "Self-healing of densely crosslinked thermoset polymers— a critical review," *Progress in Organic Coatings*, vol. 104, pp. 232-249, 2017.
- [136] F. Awaja, S. Zhang, M. Tripathi, A. Nikiforov and N. Pugno, "Cracks, microcracks and fracture in polymer structures: Formation, detection, autonomic repair," *Progress in Materials Science*, vol. 83, pp. 536-573, 2016.
- [137] J. F. Patrick, M. J. Robb, N. R. Sottos, J. S. Moore and S. R. White, "Polymers with autonomous life-cycle control," *Nature*, vol. 540, no. 7633, pp. 363-370, 2016.
- [138] D. G. Bekas, K. Tsirka, D. Baltzis and A. S. Paipetis, "Self-healing materials: A review of advances in materials, evaluation, characterization and monitoring techniques," *Composites Part B: Engineering*, vol. 87, pp. 92-119, 2016.
- [139] R. Wang, H. Li, W. Liu and X. He, "Surface Modification of Poly(urea-formaldehyde) Microcapsules and the Effect on the Epoxy Composites Performance," *Journal of Macromolecular Science, Part A*, vol. 47, no. 10, pp. 991-995, 2010.
- [140] R. P. Ollier, M. E. Penoff and V. A. Alvarez, "Microencapsulation of epoxy resins: Optimization of synthesis conditions," *Colloids and Surfaces A: Physicochemical and Engineering Aspects*, vol. 511, pp. 27-38, 2016.
- [141] M. Raimondo, L. Guadagno, C. Naddeo, P. Longo, A. Mariconda and A. Agovino, "New structure of diamine curing agent for epoxy resins with self-restoration ability: Synthesis and spectroscopy characterization," *Journal of Molecular Structure*, vol. 1130, pp. 400-407, 2017.
- [142] E. N. Brown, S. R. White and N. R. Sottos, "Retardation and repair of fatigue cracks in a microcapsule toughened epoxy composite – Part II: In situ self-healing," *Composites Science and Technology*, vol. 65, no. 15-16, pp. 2474-2480, 2005.
- [143] E. N. Brown, S. R. White and N. R. Sottos, "Fatigue crack propagation in microcapsule-toughened epoxy," *Journal of Materials Science*, vol. 41, no. 19, pp. 6266-6273, 2006.
- [144] A. S. Jones, J. D. Rule, J. S. Moore, N. R. Sottos and S. R. White, "Life extension of self-healing polymers with rapidly growing fatigue cracks," *Journal of The Royal Society Interface*, vol. 4, no. 13, pp. 395-403, 2007.
- [145] G. O. Wilson, J. S. Moore, S. R. White, N. R. Sottos and H. M. Andersson, "Autonomic Healing of Epoxy Vinyl Esters via Ring Opening Metathesis Polymerization," *Advanced Functional Materials*, vol. 18, no. 1, pp. 44-52, 2008.

- [146] K. S. Toohey, N. R. Sottos, J. A. Lewis, J. S. Moore and S. R. White, "Self-healing materials with microvascular networks," *Nature Materials*, vol. 6, pp. 581-585, 2007.
- [147] K. S. Toohey, C. J. Hansen, J. A. Lewis, S. R. White and N. R. Sottos, "Delivery of Two-Part Self-Healing Chemistry via Microvascular Networks," *Adv. Funct. Mater.*, vol. 19, pp. 1399-1405, 2009.
- [148] C. J. Hansen, W. Wu, K. S. Toohey, N. R. Sottos, S. R. White and J. A. Lewis, "Self-Healing Materials with Interpenetrating Microvascular Networks," *Advanced Materials*, vol. 21, pp. 4143-4147, 2009.
- [149] R. S. Trask and I. P. Bond, "Bioinspired engineering study of Plantae vasculae for self-healing composite structures," *Journal of The Royal Society Interface*, vol. 7, pp. 921-931, 2010.
- [150] A. P. Esser-Kahn, P. R. Thakre, H. Dong, J. F. Patrick, V. K. Vlasko-Vlasov, N. R. Sottos, J. S. Moore and S. R. White, "Three-Dimensional Microvascular Fiber-Reinforced Composites," *Advanced Materials*, vol. 23, no. 32, pp. 3654-3658, 2011.
- [151] A. R. Hamilton, N. R. Sottos and S. R. White, "Pressurized vascular systems for self-healing materials," *Journal of The Royal Society Interface*, vol. 9, no. 70, pp. 1020-1028, 2012.
- [152] A. M. Coppola, P. R. Thakre, N. R. Sottos and S. R. White, "Tensile properties and damage evolution in vascular 3D woven glass/epoxy composites," *Composites Part A: Applied Science and Manufacturing*, vol. 59, pp. 9-17, 2014.
- [153] J. F. Patrick, K. R. Hart, B. P. Krull, C. E. Diesendruck, J. S. Moore, S. R. White and N. R. Sottos, "Continuous Self-Healing Life Cycle in Vascularized Structural Composites," *Advanced Materials*, vol. 26, no. 25, pp. 4302-4308, 2014.
- [154] S. M. Bleay, C. B. Loader, V. J. Hawyes, L. Humberstone and P. T. Curtis, "A smart repair system for polymer matrix composites," *Composites Part A: Applied Science and Manufacturing*, vol. 32, no. 12, pp. 1767-1776, 2001.
- [155] H. R. Williams, R. S. Trask and I. P. Bond, "Self-healing sandwich panels: Restoration of compressive strength after impact," *Composites Science and Technology*, vol. 68, pp. 3171-3177, 2008.
- [156] S. Zainuddin, T. Arefin, A. Fahim, M. V. Hosur, J. D. Tyson, A. Kumar, J. Trovillion and S. Jeelani, "Recovery and improvement in low-velocity impact properties of e-glass/epoxy composites through novel self-healing technique," *Composite Structures*, vol. 108, pp. 277-286, 2014.
- [157] S. Kling and T. Czigány, "Damage detection and self-repair in hollow glass fiber fabric-reinforced epoxy composites via fiber filling," *Composites Science and Technology*, vol. 99, pp. 82-88, 2014.
- [158] R. S. Trask, C. J. Norris and I. P. Bond, "Stimuli-triggered self-healing functionality in advanced fibre-reinforced composites," *Journal of Intelligent Material Systems and Structures*, vol. 25, no. 1, pp. 87-97, 2014.
- [159] E. N. Brown, N. R. Sottos and S. R. White, "Fracture Testing of a Self-Healing Polymer Composite," *Experimental Mechanics*, vol. 42, no. 4, pp. 372-379, December 2002.
- [160] W. Beres, A. K. Koul and R. Thamburaj, "A tapered double-cantilever-beam specimen designed for constant-K testing at elevated temperatures," *Journal of testing and Evaluation*, vol. 25, pp. 536-542, 1997.

- [161] E. N. Brown, "Use of the tapered double-cantilever beam geometry for fracture toughness measurements and its application to the quantification of self-healing," *J. Strain Analysis*, vol. 46, pp. 167-186, 2011.
- [162] R. J. Lemmens, Q. Dai and D. D. Meng, "Side-Groove Influenced Parameters for Determining Fracture Toughness of Self-Healing Composites Using a Tapered Double Cantilever Beam Specimen," *Theoretical and Applied Fracture Mechanics*, vol. 74, pp. 23-29, 2014.
- [163] J. D. Rule, N. R. Sottos and S. R. White, "Effect of microcapsule size on the performance of self-healing polymers," *Polymer*, vol. 48, pp. 3520-3529, 2007.
- [164] M. M. Caruso, B. J. Blaiszik, S. R. White, N. R. Sottos and J. S. Moore, "Full Recovery of Fracture Toughness Using a Nontoxic Solvent-Based Self-Healing System," *Adv. Funct. Mater.*, vol. 18, pp. 1898-1904, 2008.
- [165] Y. C. Yuan, M. Z. Rong, M. Q. Zhang and G. C. Yang, "Study of factors related to performance improvement of self-healing epoxy based on dual encapsulated healant," *Polymer*, vol. 50, pp. 5771-5781, 2009.
- [166] E. L. Kirkby, V. J. Michaud, J.-A. E. Månson, N. R. Sottos and S. R. White, "Performance of self-healing epoxy with microencapsulated healing agent and shape memory alloy wires," *Polymer*, vol. 50, pp. 5533-5538, 2009.
- [167] J. C. Prichard and P. J. Hogg, "The role of impact damage in post-impact compression testing," *Composites*, vol. 21, no. 6, pp. 503-511, 1990.
- [168] M. Salvo, P. Lemoine, M. Ferraris and M. Montorsi, "Joining of Carbon-Carbon Composites for Thermonuclear Fusion Applications," *J. Am. Ceram. Soc.*, vol. 80, no. 1, pp. 206-212, 1997.
- [169] L. Pan and B. Zhang, "Damping and Mechanical Properties of Cured Composite Laminates with Embedded Perforate Viscoelastic Layer," *J. Mater. Sci. Technol.*, vol. 25, no. 4, pp. 543-546, 2009.
- [170] O. Strekalova, S. Vidinejevs and A. Aniskevich, "GFRP Composite with Integrated Damage Indication Layer," in *XVIII International Conference on Mechanics of Composite Material, June 2-6, 2014, Riga, Latvia* Book of abstracts.
- [171] Y. M. Tarnopol'skii and T. Y. Kincis, Static test methods for composites. Translation of 3rd Russian edition, New York: Van Nostrand Reinhold Co, 1985, p. 301.
- [172] D. F. Adams, "A comparison of shear test methods," September 2005. [Online]. Available: <http://www.compositesworld.com/articles/a-comparison-of-shear-test-methods>. [Accessed 13 March 2014].
- [173] M. W. Keller, S. R. White and N. R. Sottos, "A Self-Healing Poly(Dimethyl Siloxane) Elastomer," *Adv. Funct. Mater.*, vol. 17, pp. 2399-2404, 2007.
- [174] X. Ma, Y. Gu, Y. Li, M. Li and Z. Zhang, "Interlaminar properties of carbon fiber composite laminates with resin transfer molding/prepreg co-curing process," *Journal of Reinforced Plastics and Composites*, vol. 33, pp. 2228-2241, 2014.
- [175] J. F. Hunt, "Cantilever-beam dynamic modulus for thin fiberboard composite products. Part 2, Property comparison with bending modulus," 2009.
- [176] L. V. Chursova, A. E. Roskutin, G. Y. M. and N. N. Panina, "Cold cure binder for construction industry," *Adhesives. Sealants. Technology (in Russian)*, no. 5, pp. 40-44, 2012.

- [177] A. Kousourakis, M. K. Bannister and A. P. Mouritz, "Tensile and compressive properties of polymer laminates containing internal sensor cavities," *Composites Part A: Applied Science and Manufacturing*, vol. 39, no. 9, pp. 1394-1403, 2008.
- [178] "vDijk Pultrusion Products (DPP)," [Online]. Available: <http://www.dpp-pultrusion.com/en/>. [Accessed 27 Oct. 2014].
- [179] A. Kousourakis and A. P. Mouritz, "The effect of self-healing hollow fibres on the mechanical properties of polymer composites," *Smart Materials and Structures*, vol. 19, no. 8, p. 085021, 2010.
- [180] G. P. McCombe, J. Rouse, R. S. Trask, P. J. Withers and I. P. Bond, "X-ray damage characterisation in self-healing fibre reinforced polymers," *Composites Part A: Applied Science and Manufacturing*, vol. 43, no. 4, pp. 613-620, 2012.
- [181] C. J. Norris, I. P. Bond and R. S. Trask, "Interactions between propagating cracks and bioinspired self-healing vasculae embedded in glass fibre reinforced composites," *Composites Science and Technology*, vol. 71, no. 6, pp. 847-853, 2011.
- [182] A. Kousourakis, A. P. Mouritz and M. K. Bannister, "Interlaminar properties of polymer laminates containing internal sensor cavities," *Composite Structures*, vol. 75, pp. 610-618, 2006.
- [183] M. Godani, M. Gaiotti and C. M. Rizzo, "Interlaminar shear strength of marine composite laminates: tests and numerical simulations," *Composite Structures*, vol. 112, pp. 122-133, 2014.

## **ACKNOWLEDGEMENTS**

I would like to express my deepest gratitude to my supervisor Dr. Andrey Aniskevich, for his invaluable support and inspiration, constructive dialogs, and critics during the discussions of the results.

I am grateful Professor Sergei Sapozhnikov and Dr. Andre Gregor for interesting discussions rich of fresh ideas.

I would like to thank Dr. Vladimir Kulakov for thoughtful discussion of the dissertation, Mr. Viktor Novikov for decisive contribution in composite specimens' manufacture using vacuum moulding methods and colleagues from the Institute for Mechanics of Materials University of Latvia for their support.